COLORIMETRIC ASSAYS FOR THE DETECTION OF SINGLE NUCLEOTIDE POLYMORPHISM BASED ON PLASMONIC NANOPARTICLES

MARIA SANROMAN IGLESIAS

Motivation of the Thesis

Human blood is a chemically rich medium, crowded with clinically relevant biomolecules that have the potential of becoming biomarkers for the most relevant disease of the XXI century - cancer. The detection of biomarkers in blood is a task that concerns not only scientists working in the field of biomedicine, but also a broad scientific community covering research fields within physics, chemistry and engineering. Thus, only by joining forces from different disciplines and introducing interdisciplinary approaches, we can develop feasible methods for biomarkers detection, thereby allowing the emergence of future biosensing technologies.

The present thesis emerged with this optimistic vision in mind. We aimed at using available tools in materials chemistry, colloid chemistry in particular, to face a specific problem relevance in current biomedicine – discrimination of mutations in DNA sequences that are associated with lung and breast cancer. By finding a common ground (and first of all a common language), a close scientific relationship was established between the Bionanoplasmonics Laboratory (CIC biomaGUNE) and the Oncology Area (Biodonostia Institute). Long sessions of stimulating scientific discussions allowed us to extract in mid 2013 the overarching aim of the present thesis, which reads as follows:

The present thesis seeks to develop a colloidal colorimetric assay based on plasmonic nanoparticles for rapid detection (~10 min) of single nucleotide polymorphism in long, double-stranded DNA sequences (>100 pair bases), in the concentration range below 1 nM, in physiological media.

It should be clarified here that not all of the proposed objectives were successfully met. For example, the detection of DNA mutations in physiological media remains unresolved at the time of writing the thesis; which was presumably due to the chemical complexity of human plasma (presence of proteins) hindering the detection of DNA sequences through aggregation of plasmonic nanoparticles. This is probably a task that remains for younger colleagues.

Of course, the complexity of the proposed objective required a reductionist approach. Our studies were strategically conveyed to face one experimental parameter of the assay at a time, thus providing a topic for each chapter.

In Chapter 2, gold nanoparticles of different sizes were synthesized and functionalized with DNA sequences, and subsequently used for the selective hybridization with the target single stranded DNA. The best sensitivity (10 pM) and rapid selectivity within 10 minutes were achieved for larger nanoparticles with a diameter of 63 nm. By studying the effect of particle size, the minimum number of target DNA (match and mismatch) was established to induce the colorimetric detection.

The detection of mutations in long, single-stranded DNA sequences is the subject of Chapter 3. An assay based on gold nanoparticles (65 nm) stabilized with DNA was capable of discriminating single nucleotide polymorphism in long biological sequences (up to 140 bases), related to lung cancer. Pre-incubation of AuNPs and the target sequence allowed us to progressively untie the secondary structure of the target DNA fragment.

In Chapter 4, an amplification-free methodology was proposed for the detection of single base mutation in binary mixtures containing double-stranded DNA sequences, both wild-type and mutated, by using aggregating gold nanoparticles as the only transducer. A blocking strategy was developed by the combination of high-temperature denaturation and subsequent selective blocking of the denatured antisense strands, thereby allowing specific nanoparticle aggregation.

This Ph.D. thesis is expected to represent an advancement in the use of metal nanoparticles for biosensing of relevant DNA sequences. Various improvements and approaches have been proposed to facilitate the detection of different biomolecules with no need for complex procedures and expensive instrumentation.

Chapter 1. Introduction

1.1 Cancer, Biomarkers and Sensing Approaches

Cancer is a leading cause of death and accounted for about 8.8 million deaths in 2015[1]. Its origin is linked to genetic mutations that accumulate stepwise, triggering a network of processes responsible of carcinogenesis[2]. The analysis of tumor-linked substances is increasingly used for diagnosis and prognosis purposes. Biomolecules that carry the chemical information relevant for cancer diagnosis are known as *biomarkers*, which are described as follows: "a substance or activity that can be objectively measured and evaluated as an indicator for a normal biological process, pathogenic process, or pharmacological response to a therapeutic intervention". Thus, cancer biomarkers are present in tumor tissues or serum and encompass a wide variety of molecules, including DNA, mRNA, enzymes, metabolites, transcription factors, and cell surface receptors[3]. The research field of cancer biomarkers aims at developing reliable and cost-effective detection and monitoring strategies for cancer risk indication, early cancer detection, and tumor classification.

Standard clinical protocols for the evaluation of oncogenic mutations through biomarkers are usually based on tissue biopsy, which consists of sampling cells from the human body. This procedure constitutes a significant barrier for monitoring of oncogenic mutations. In addition, it can potentially introduce clinical risks for the patient, is costly, and patient compliance with this procedure is variable, given its invasive nature as well as discomfort. A number of technical limitations have also been associated with this approach[4], the most important of which is the difficulty in accounting for tumor cells heterogeneity, so biopsies often suffer from sample bias[5]. Another important technical limitation relates to difficult tumor sampling from some cancer types, resulting in inadequate amounts of tissue for genetic testing. In the case of advanced or metastatic non-small cell lung cancers (NSCLC) as many as 31% of cases do not have accessible tissue[6].

The above-mentioned limitations have prompted the development of new methods for the harvesting of cancer biomarkers in a simpler and more convenient way, compared to tissue biopsy. The science of non-invasive monitoring of diseases has greatly advanced since the first report on cell-free DNA in body fluids by Mandel and Metais in 1948[7], which set the milestone of the "liquid biopsy". The core advancement was based on the observation that the levels of circulating DNA were higher in individuals with cancer than in healthy ones, opening the possibility to screen the presence of the disease through a simple blood test. Thus, liquid biopsy has emerged as a potential complement of the traditional biopsy for early cancer diagnosis,[4] in which biological fluids are sampled to monitor the level of cancer biomarkers available in the chosen medium. It is commonly agreed that, liquid biopsy on blood samples can provide the genetic landscape of all cancerous lesions (primary and metastases), as well as offering the opportunity to systematically track genomic evolution.

Nowadays, a vast number of biomarkers in blood are classified with potential implications for cancer diagnosis and treatment. These include circulating tumor cells (CTCs)[8], circulating membranous structures (microvesicles, exosomes) containing molecular biomarkers[9], circulating cell-free nucleic acids[4], RNA, microRNA[10] and proteins (**Figure 1.1**)[11]. In this context, circulating cell-free DNAs (released from both normal and tumor cells) and circulating tumor DNA (ctDNA, i.e., DNA released only from tumor cells) offer a number of advantages that have attracted enormous attention over the last 5 years.

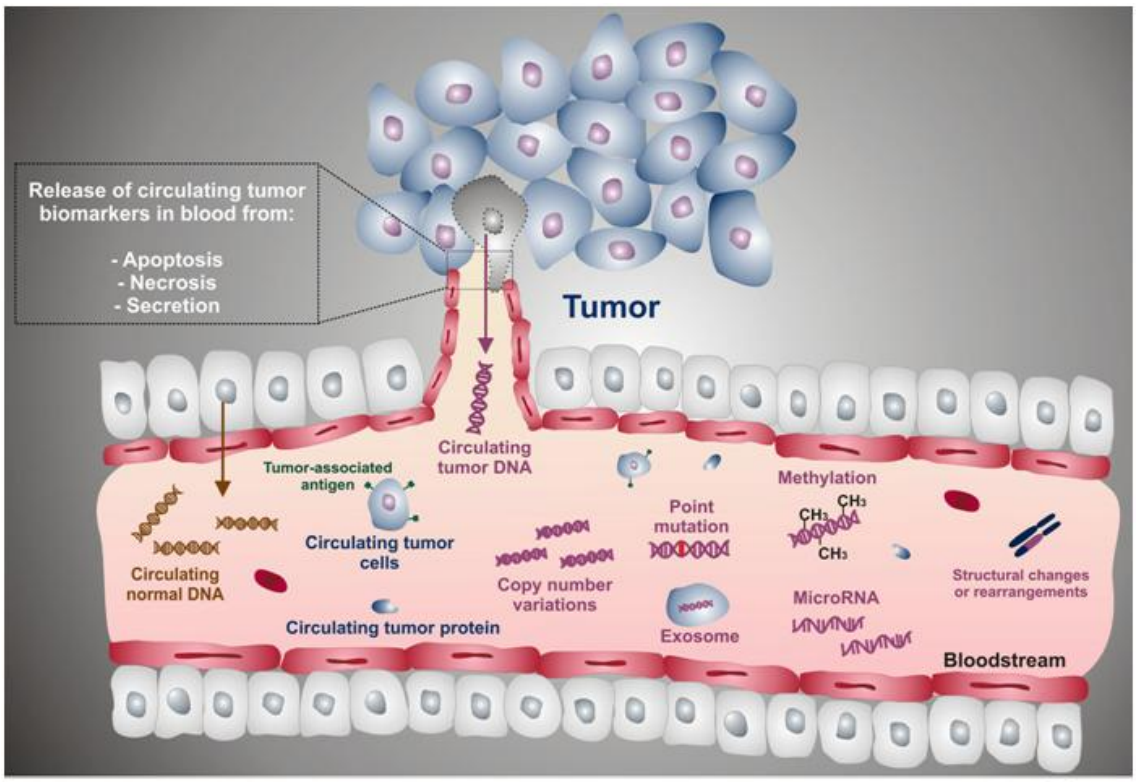

Figure 1.1. Schematic representation of tumor-linked molecular markers, cells, and membranous structures circulating in the blood. Cancer cells release tumor biomarkers in blood through various physiological events, such as apoptosis, necrosis, and secretion. Adapted from [12].

1.1.1 Circulating Tumor and Circulating Cell-Free DNA - Characteristics

All cells, including tumor cells and non-malignant cells, shed circulating cell-free DNA (ccfDNA), into the circulatory system[13]. Circulating tumor DNA (ctDNA), on the other hand, is a subclass of ccfDNA which is shed exlusively from tumor cells into the circulatory system (**Figure 1.2**). There are several mechanisms ruling the release of DNA from tumor cells into blood: (1) secretion from tumor cells as free DNA or in cell-derived vesicles - exosomes; (2) secretion from phagocytized tumor cells; (3) release via cell death through apoptosis and necrosis[13–17]. The ctDNA is distinguished from ccfDNA by the presence of somatic mutations, making up only a small fraction (often only <1%) in solid malignancies[18–20]. In hematological malignancies (e.g., leukemia) the blood contains higher percentages of ccfDNA derived from cancer cells. The contributing fraction of ctDNA to the total ccfDNA increases with increasing tumor

burden[21] and, therefore, the amount recovered may vary greatly among patients. Importantly, the fragment size of ccfDNA ranges in length from few hundreds to few thousands of base-pairs. The ctDNA fragments of about 145–180 bp are supposed to be generated from cell apoptosis, whereas longer fragments (up to 10 kbp) are generated from cell necrosis[13,18,19,22–25].

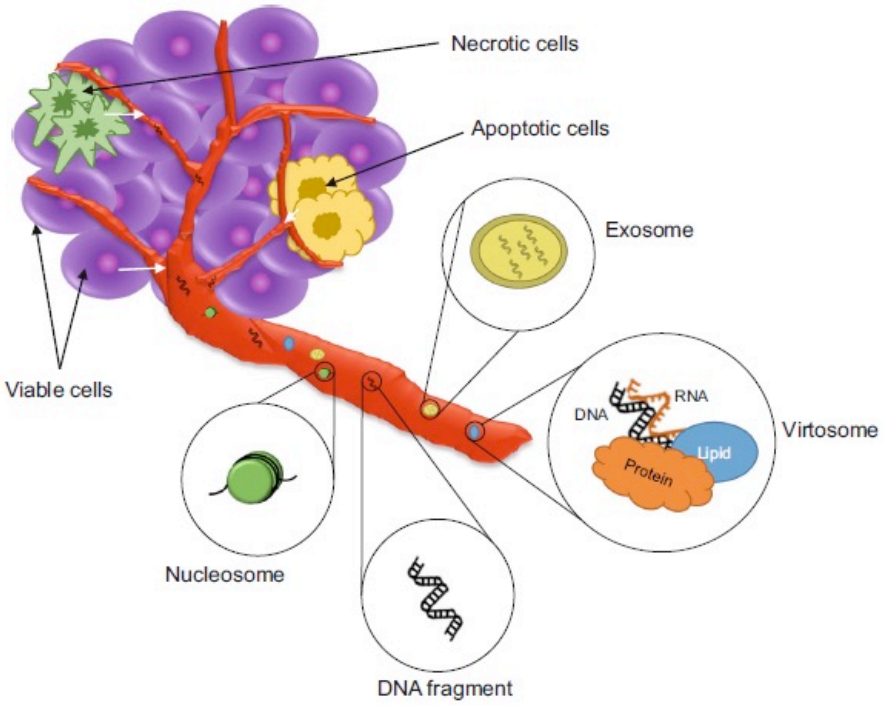

Figure 1.2. Circulating cell-free DNA can be released into the bloodstream, either through cell death, i.e. apoptosis (yellow) or necrosis (green), or by viable cells (purple). Circulating cell-free DNA can be present in the form of unbound DNA, nucleosomes, vesiclebound DNA, or virosomes. Adapted from [14].

Cancer detection that is based on monitoring ccfDNA and ctDNA in plasma is considered technically challenging because of their low concentration. Typically, median ccfDNA concentrations lower than 20 ng/mL are found in plasma obtained from cancer patients, whereas healthy individuals show even lower median concentrations (< 7 ng/mL in plasma) which overlaps with the concentration ranges for cancer patients[26,27]. Additional challenges are related to the fact that ctDNA is a fraction of the total ccfDNA in cancer patients, with percentages depending on cancer type and progression stage[28]. In general, mean numbers of mutated DNA fragments

(ctDNA) per mL ranging from few units to 10^4 have been found in plasma of cancer patients, accounting for few units percent of ccfDNA. Overall, the knowledge over quantitative characteristics of the circulating cell-free DNA in real samples (length, concentration) is essential in the design of biosensors because of the limiting values that one needs to approach.

1.1.2 Single Nucleotide Polymorphism

Single nucleotide polymorphism (SNP) is one of the most common forms of genetic variation in the human genome and it is the single nucleotide variation in a genetic location, occuring at a frequency of 1 in every 1000 bases, approximately[29]. Nowadays, a total of 1.42 million single base mutations have been identified[30]. The variations in coding regions of the gene may modify the sequences of aminoacids and in fact modify the role of the corresponding protein (**Figure 1.3**)[31]. Taking into account the importance of SNP, it emerges as a next generation genetic biomarker in the field of prognosis and clinical diagnosis. Especially important is the presence of SNP in ctDNA since it offers a valuable indication of the probability of cancerous disease.

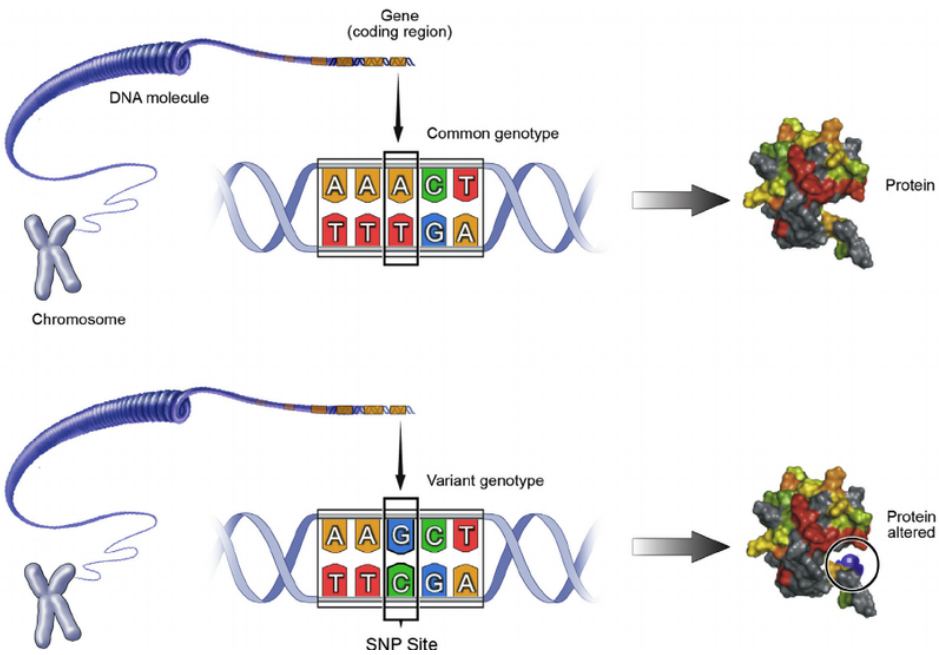

Figure 1.3. Single nucleotide polymorphisms are genetic mutations where the DNA sequences of many individuals vary by a single base that leads to the modified sequence of an aminoacid, causing thus a malfunction of the corresponding protein.

Table 1.1 displays the most relevant single-nucleotide polymorphisms that are currently being exploited as biomarkers for cancer detection, and some of them being the model biomarkes in the present thesis. SNPs that relate to lung cancer are currently considered as the most emergent biomarkers, because of the high mortality among patients diagnosed with this type of cancer. The emergence of non-small cell lung cancer (NSCLC), leads to overexpression of the epidermal growth factor receptor (EGFR), a transmembrane protein that, upon activation, binds the corresponding epidermal growth factor. The binding of ligands induces a conformational change that leads to unregulated activation of an enzyme (tyrosine kinase) that in turns results in uncontrolled cell division[32]. It has been found that EGFR-mutated lung tumors correlate with a specific mutation (L858R) at relatively high frequency (43%)[33]. Therefore, the EGFR gene is a prime biomarker candidate for the development of targeted therapeutics. Hence, its detection through plasmonic nanoparticles will be exploited in the context of this thesis.

Another important SNP relates to breast cancer, which is the most frequently diagnosed cancer and the leading cause of cancer death in females worldwide. Breast cancer 1 gene (BRCA1) induces the formation of proteins that act as a tumor suppressor. These proteins help preventing cells from growing and dividing too rapidly in an uncontrolled way. The appearance of mutations in the BRCA1 gene induces the production of an abnormally short version of the BRCA1 protein. As a result, there is no sufficient protein to help repair the damaged DNA or to fix mutations. It is worth mentionining that in total over 1800 mutations have been identified in this particular gene and many of these mutations were related with an increased risk of breast cancer.

Cancer	Biomarker (Gene Mutation)	Reference
Prostate	Androgen Receptor AR c.2105T>A (L702H)	[34]
	AR c.2632A>G (T878A)	[35]
Breast	Serine/Threonine-Protein Kinase AKT1 c.49G>A (E17K)	[36]
	Human Epidermal Receptor Growth Factor 2 HER2 (ERBB2) c.2264T>C (L755S)	[37]
	Phosphatidyl 3-Kinase PIK3CA c.1633G>A (E545K)	[38]
Lung	Epidermal Growth Factor Receptor EGFR c.2573T>G (L858R)	[33]
	Kirsten Rats Sarcoma Virus Gene KRAS c.34G>T (G12C)	[39]
Bladder	Fibroblast Growth Factor Receptor 3 FGFR3 c.742C>T (R248C)	[40]
	FGFR3 c.746C>G (S249C)	[41]
Epithelial Ovarian	Serine/Threonine-Protein Kinase BRAF c.1799T>A (V600E)	[42]
	Phosphatidyl 3-Kinase PIK3CA c.3140A>G (H1047R)	[43]
Thyroid	Serine/Threonine-Protein Kinase BRAF c.1799T>A (V600E)	[44]
Colorectal	Signal Transduction Protein SMAD4 c.1082G>A (R361H)	[45]

Table 1.1. The most relevant cancer biomarkers.

The last years of intense studies led to the development of state-of-the-art analytical techniques for the genotyping of known SNP and for detection of new and unknown SNPs. Although DNA sequencing is considered as a conventional method[46], its long operation times and the complex procedures render the use of this technique non optimal. Conformation changes[47], mass spectroscopy[48], polymerase chain reaction (PCR)[49], and DNA hybridization[50] are considered as alternative approaches. But still, low throughput and low specificity limit their wider application. Although recent alternatives such as DNA microarrays and denaturing high performance liquid chromatography have been developed for analysis of single base mutations[51,52], these methods need expensive facilities and fluorescent tags. Thus, rapid, simple, and specific technology is urgently needed for high throughput analysis.

1.2 Biosensors

1.2.1 Historical Overview and General Definition

The term biosensor is defined by the International Union of Pure and Applied Chemistry (IUPAC) as a "*device that uses specific biochemical reactions mediated by isolated enzymes, immunosystems, tissues, organelles, or whole cells to detect chemical compounds usually by electrical, thermal, or optical signals*"[53]. This definition has evolved through the years on the basis of intense studies, since the development of the first biosensor by L. C. Clark in 1956, who suggested a probe for measuring oxygen in blood. Later in 1962, the enzyme electrode was described, consisting of an oxygen probe and two dialysis membranes carrying a small portion of the aqueous solution of glucose oxidase in between them. The strategy of electrochemical detection of oxygen or hydrogen peroxide allowed the detection of glucose in biological samples[54].

Since then, important progress in the field of biosensors has been made, both in technology and applications. Between 1980 and 2000, the development of biosensors has gone hand in hand with the progress in the characterization of biochemical compounds (see next section). Biochemicals have been involved in sensitive biological elements and the transducer in the final assembling of the biosensor. A progressive shift is being made toward transduction systems of biosensors, which ensure feasability due to the recent progress in the fields of biotechnology, nanotechnology and bioelectronics[55].

1.2.2 Components of Biosensors

From a compositional point of view, a biosensor consists of a biological sensing element, a physico-chemical transducer and a detecting system (**Figure 1.4**). In such a configuration, the measurement of the target analyte(s) is achieved by selective transduction of a parameter of the biomolecule-analyte reaction into a quantifiable signal. In addition, it has been shown that such a configuration is able to meet the

desired characteristics of biosensors: sensitive, fast, cost-effective, low-reagent-consumption and ease-of-use.

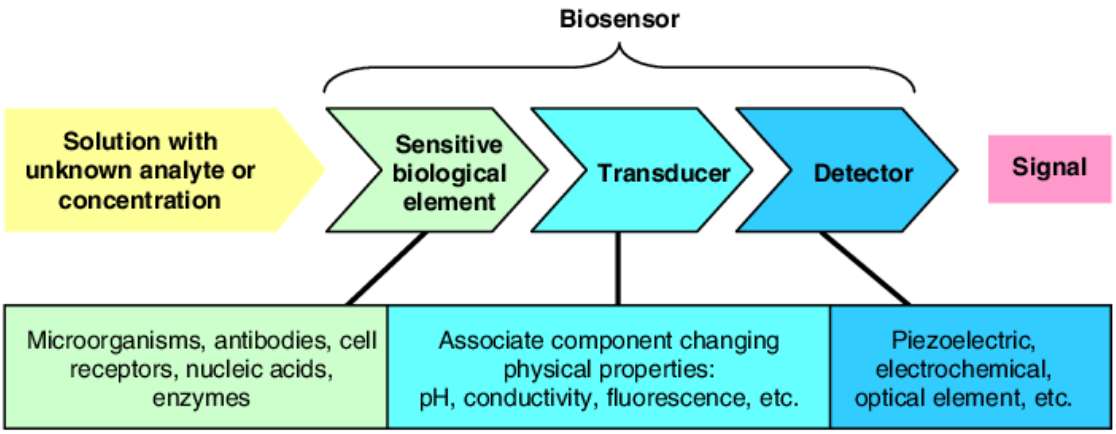

Figure 1.4. Schematic representation of a biosensor.

1.2.2.1 Sensitive Biochemical Elements

The sensitive biochemical elements are classified into enzyme and affinity types. The enzyme type relates to the system involving enzymatic reactions while the affinity type includes immunosensors and DNA sensors. The main difference in their behavior is related to the signal nature; enzyme sensors belong to the kinetic methods of analysis. The signal reflects the rate of substrate conversion, which is high in the first minutes of the reaction and then decreases. Affinity biosensors, on the other hand, exploit reversible biochemical interactions like antigen–antibody or DNA–protein. They reach maximal response corresponding to the equilibrium state. The difference in time response of these two classes of biochemical elements dictates the design of the whole sensor, covering the aspect of mass transfer as the flow rate in flow-injection analysis or solution stirring in batch conditions. It should be mentioned that the more complicated the biochemical component, the more variational the response it shows, so that the term ‘‘equilibrium’’ is hardly applicable to biological cells. In most cases, a signal that is independent on time is classified as stationary. **Figure 1.5** displays the classification of biosensors according to the biochemical component.

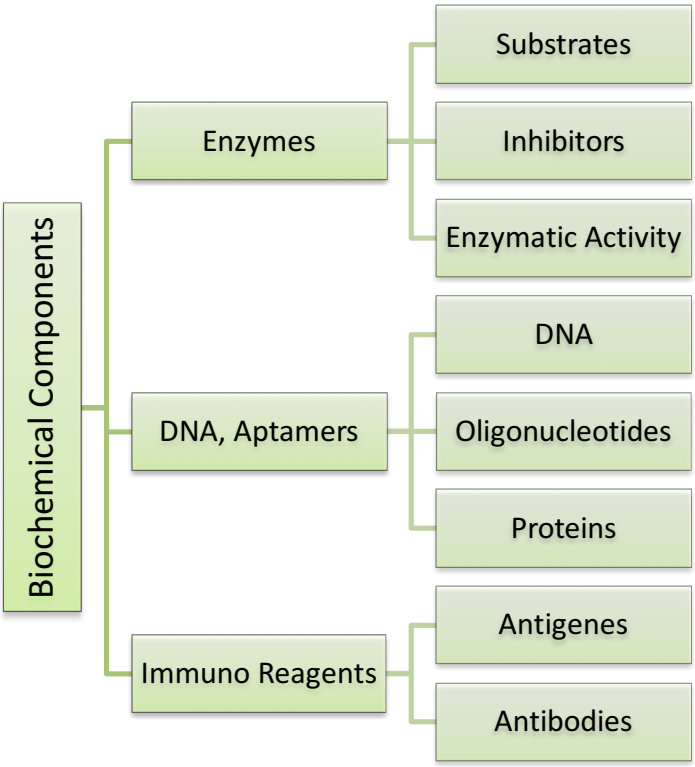

Figure 1.5. Biochemical components used in biosensor design.

Enzymatic biosensors, also called enzyme sensors, take advantage of the properties of the enzymes implemented in the surface layer of a transducer. In some cases, the number of individual enzymes can be specified (bi-enzymatic, tri-enzymatic sensors) but only in the case where alternative constructions of biosensors exist. Thus, glucose can be determined with enzymatic sensors including glucose oxidase, which catalyzes the oxidation of a substrate to gluconic acid. Meanwhile,the bi-enzyme sensor involves peroxidase as an auxiliary enzyme, intended for the simplification of the signal measurement[56]. Tri-enzyme sensors are described for the detection of starch[57], ATP[58] and lactate[59].

Stability and specificity of the molecular recognition systems (e.g antibody/antigen) serves as a fundamental bassis for the development of immunosensors that rely on the affinity between an immobilized ligand on solid-state devices, in which the immunochemical reaction is coupled to a transducer[60].

The DNA sensor (genosensors) has been exploited for its inherent physicochemical stability and suitability to discriminate different organism strains. These biosensors involve elements derived from DNA, i.e., natural oligonucleotide sequences (DNA probes) or aptamers. The biosensors based on such sequences are intended to detect the DNA fragments specific for appropriate genes[61]. Aptamers also consist of nucleotides but have no analogy in the native DNA structure.

Listed below are the principal advantages of DNA biosensors[62,63]:

1) Hybridization in solution. DNA can be detected in liquid phase reaction by recording the changes of sound, light, electricity signals, etc.
2) Real-time detection of DNA. In combination with microfluidic chips, it is possible to monitor the dynamic reaction process of DNA in real-time.
3) DNA dynamic detection in vivo. DNA sensors provide the possibility for studying dynamic processes of nucleic acid metabolism transfer in vivo.
4) Multiplex detection. Several DNA samples can be detected at the same time by the development of multi-functional or intelligent DNA sensors.
5) High sensitivity. DNA sensors can directly detect the target materials. If these sensors are combined with polymerase chain reaction (PCR) or other amplification techniques, a great improvement of the sensitivity can be achieved.
6) High specificity. A DNA sensor is based on the principle of complementary combination.
7) Clean and safe. It does not need isotopic labeling, and avoids harmful substances.

Most of the recently reported DNA sensors exhibit hybridization times between 10 and 120 min, which are low as compared to traditional overnight hybridization (20 h), but still too long for practical implementation for in point-of-care devices. The time required for the hybridization process (hybridization time) and the sensitivity of the assay is in itself a pair of contradictory elements. The decrease of the hybridization time in the premise of ensuring adequate sensitivity remains as a major challenge in the field of DNA-based biosensors.

Deoxyribozymes (DNAzymes) are single-stranded oligonucleotides that exert catalytic activity similar to that of enzymes[64]. Although the first DNAzyme was synthesized in 1994, they have recently been introduced in the biosensor assembly for the specific detection of organic species. DNAzymes are synthesized using the protocols developed for aptamers and are commonly intended for the hydrolysis of phosphodiester bonds or for mimicking peroxidase activity[65].

Whole cells, whether microorganisms or cultured tissues of multicellular organisms, have an intermediate rank between biomolecules (proteins and nucleic acids) and biological tissues. Due to a rather simple and cost-effective culture, microorganisms are used as an an inexpensive source of appropriate enzyme activity[66]. The application of microbial biosensors is closely related to the main microbiological technologies producing starch, saccharides, ethanol, organicacids, etc.

1.2.2.2 Transducing and Detection Systems

An important component in biosensor design is the transduction system, which makes use of a physical change accompanying the reaction and defines the detection system: electrochemical (amperometric, conductimetric, impedance and potentiometric biosensors) or optical (colorimetric, fluorimetric, IR). While electrochemical biosensors offer high specificity, low limit of detection and relative freedom from matrix interference, optical biosensors exhibit low signal-to-noise ratio and low reagent volume requirements, are immune to electromagnetic interferences and capable of performing remote sensing, while providing multiplexed detection within a single device[22]. Some advantages of this type of biosensors are its high sensitivity, ease of operation, high accuracy and wide detection capacity. **Figure 1.6** shows the general classification of biosensors according to the type of transducer.

Except for test strips, or indicating tubes with visual detection of color change[67], optical biosensors did not receive adequate interest until very recently. This type of sensors shows important advantages compared to other sensing methodologies, including better stability in aggressive environments, ability of providing label-free measurements combined with their potential for multiplexing and

miniaturization. Among the different optical sensing platforms, those based on the use of plasmonic materials meet many of these benefits, and as a consecuence, are considered to be key components for the creation of advanced biosensing platforms. The most extensively employed optical biosensors are those based on surface plasmon resonances (SPR), which provide a tunable control over the dynamic biochemical interactions that affect the total reflectance of the laser emission in an ultra-thin gold layer modified with biochemical receptor molecules. These commercially available systems are rather expensive and limted to research laboratories for biochemical studies[68]. However, optical nanobiosensors can be also devised using nanostructured metals, rather than thin films, the home pregnancy test being an excellent example of how nanoparticles can be used in diverse fields like clinical diagnosis.

Recent progress in the development of advanced techniques such as reflectance Fourier-transform infrared spectroscopy (FTIR) and surface enhanced Raman spectroscopy (SERS), which can be used on a solid interface, increased the interest in optical biosensors[69]. This is particularly true for the use of nanoparticles and nanopore materials (artificial ion channels) that offer opportunities for an enormous increase in sensitivity that is of great importance for single DNA detection.

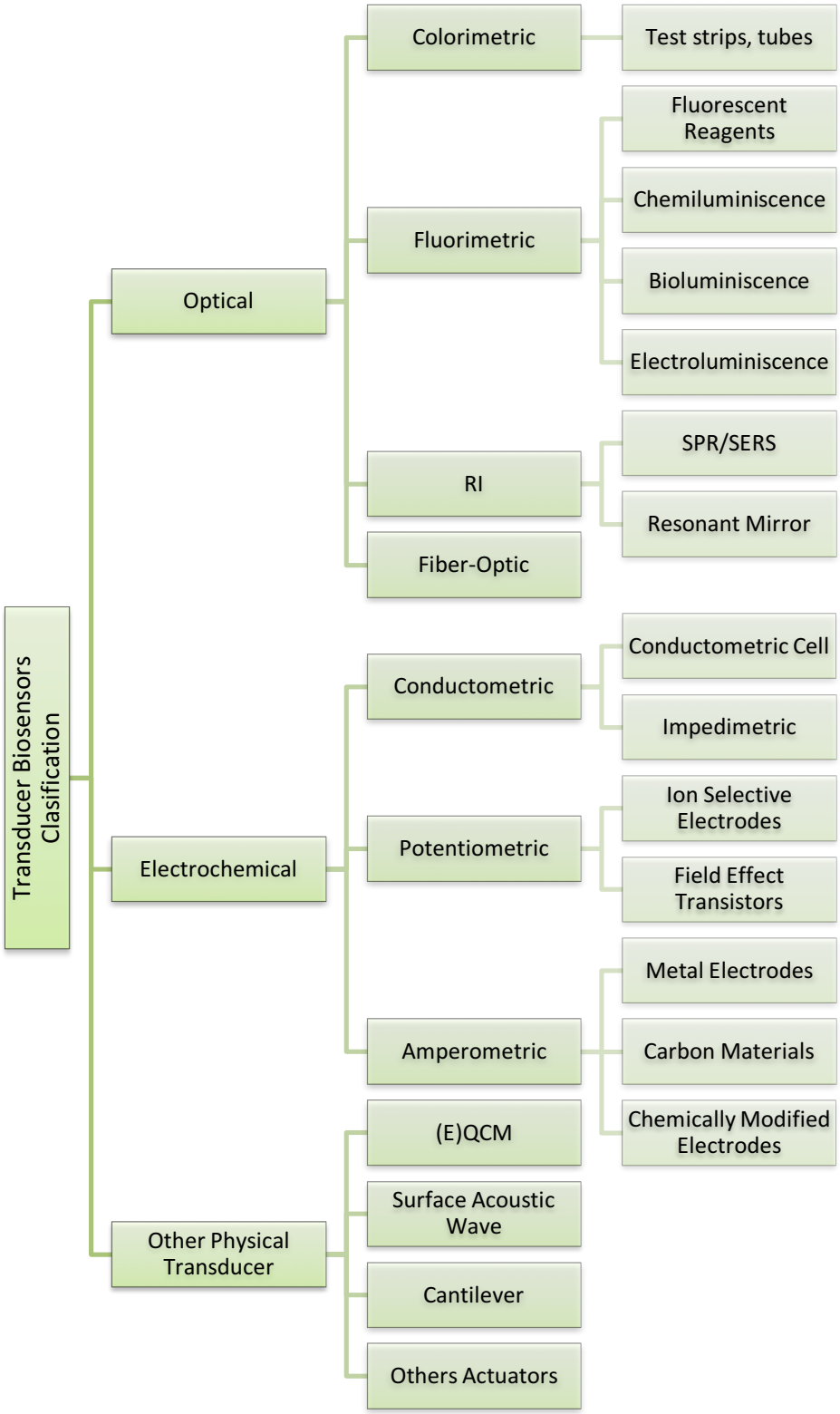

Figure 1.6. Classification of biosensors according to transducer/signal transduction principles.

1.2.2.3 Characteristics of Biosensors

In analitycal chemistry, the validation of a given method is a crucial step in demonstrating that the results are close enough to the unknown value of the analyte. A method can be validated by its figure of merit, which includes concepts related to the method and to the analyte (i.e. sensitivity, selectivitiy, limit of detection and signal-to-noise ratio) and concepts concerning the final results (i.e. traceability, uncertainty, representativity).

1.2.2.4 Sensitivity and Selectiviy

The sensitivity toward a given analyte is defined as the slope of the analytical calibration curve. Therefore, the sensitivity of an analytical method increases when a small change in analyte concentration induces a significant change in the response of the sensor. Selectivity, on the other hand, is defined as the ratio of the slopes of the calibration lines of the analyte of interest and the interferences. Therefore, a method is selective when the response of the analyte can be differentiated from other responses - only the analyte of interest contributes to the measured signal.

1.2.2.5 Limit of Detection

The limit of detection (LoD) is the concentration derived from the smallest signal that can be detected with an acceptable degree of uncertainty for a given analytical procedure. Such a lowest amount is the signal corresponding to n times the standard deviation, s, of the blank above the mean blank value. The LoD can be used as a figure of merit to describe the ability of a biosensor to discriminate the signal from the noise level, thus defining the signal-to-noise ratio, i.e. the distance between the analytical signal of the analyte and the instrumental noise.

1.2.2.6 Repeatibility and Reproducibility

According to the IUPAC, repeatability and reproducibility refer to the closeness of the agreement between the results of successive measurements of the same measurement and carried out in the same (repeatability) or different (reproducibility) conditions related to operator, apparatus, laboratories and/or intervales of time analysis.

1.3 Nanoparticles

Wet-chemistry methods for the synthesis of nanoparticles have been widely developed during the last three decades, resulting in the possibility of preparing nanoparticles in the size range 1-100 nm, with a broad variety of shapes and surface chemistry. The physical properties of these new materials resemble neither those of the bulk metal nor those of molecular compounds, but they strongly depend on the size, which is related to a significant increase of the fraction of surface atoms per unit volume. The ratio of surface atoms to interior atoms changes dramatically if one successively divides a macroscopic object into smaller parts. For example, for a cube of iron of 1 cm^3, the percentage of surface atoms would be only 10^{-5} %. When the cube is divided into smaller cubes with an edge of 10 mm, the percentage of surface atoms will increase to 10%. In a cube of iron of 1 nm^3, every atom would be a surface atom. **Figure 1.7** shows how the percentage of surface atoms changes with the diameter of palladium clusters. Such an increase in the ratio of surface atoms to interior atoms in nanostructures and nanomaterials might illustrate why variations in the size range of nanostructures are expected to lead to great changes in the physical and chemical properties of the materials. For example, metallic nanoparticles have lower melting temperatures as compared with their bulk forms, when the particle size decreases below 100 nm. The lowering of the melting point is in general explained by the fact that the surface energy increases with a decreasing size. The melting point of bulk gold is 1337 K and decreases rapidly for nanoparticles with sizes below 5 nm, as shown in **Figure 1.7**. Such a size dependence has also been found in other materials such as copper, tin, indium, lead, and bismuth, in the form of particles and films.

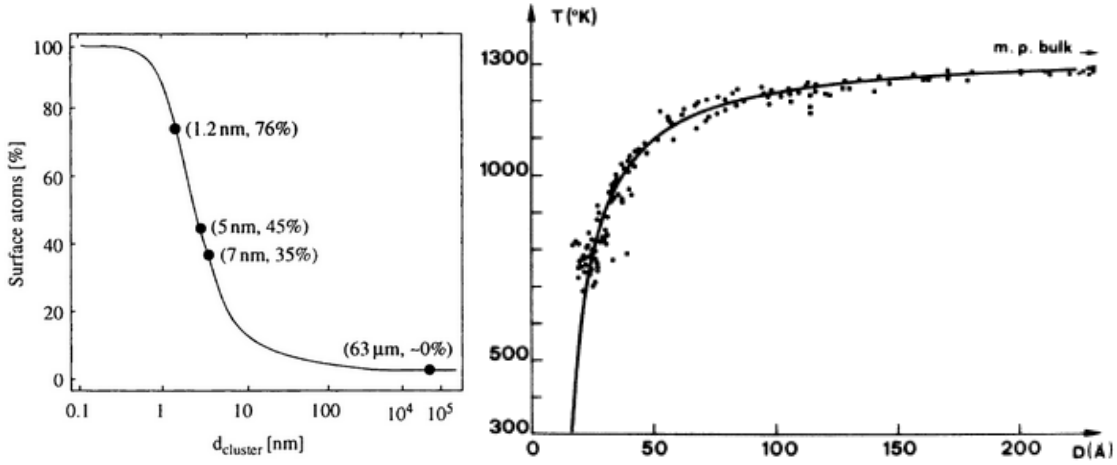

Figure 1.7. (Left) The percentage of surface atoms changes with the diameter of palladium clusters. Adapted from [70]. (Right) The melting point of bulk gold is 1337 K and decreases rapidly for NP with diameter below 5 nm. Experimental data (dots) and results of a least-squares fit (solid line).

1.3.1 Noble Metal Nanoparticles

The high surface-to-volume ratio in metal nanoparticles also affects their optical properties, making this material a promising candidate for a variety of applications. However, it has not been until recent years that the optical properties of metal nanoparticles have been fully exploited. For centuries, gold, silver, and copper nanoparticles have been used in stained glass to produce colored drinking cups (Lycurgus cup, **Figure 1.8**a)[71] or stained glass windows (Canterbury cathedral, **Figure 1.8**b). Michael Faraday was the first who ascribed the colors of stained glass or in solution to metal nanoparticles (**Figure 1.8**c).

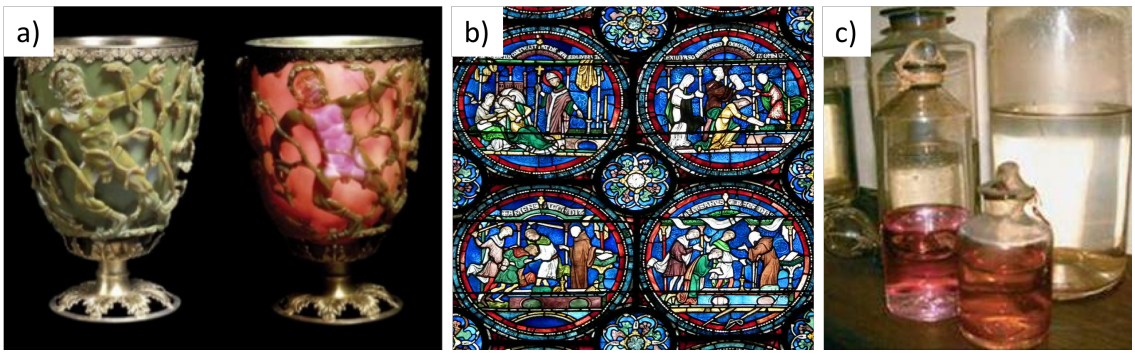

Figure 1.8. a) The Lycurgus Cup at the British Museum in London. b) Stained glass window at Canterbury cathedral. c) Faraday's gold colloidal solutions at the Royal Society in London.

In his article published in 1857, Faraday concluded[72]: "I think that in all these cases the ruby tint is due simply to the presence of diffused finely-divided gold." Approximately 50 years later, in 1908, Gustav Mie explained the appearance of the colors theoretically. He applied Maxwell's equations in spherical coordinates to a small sphere in a homogeneous environment[73,74]. The theory showed that the total extinction cross-section comprises contributions from the scattering and absorption cross-sections, i.e. the extinction cross-section, $\sigma_{ext}=\sigma_{abs}+\sigma_{scat}$ (absorption cross-section + scattering cross-section).

1.3.2 Optical Propertie of Noble Metal Nanoparticles

Today it is well known that the intense colors of metal colloids arise from surface plasmons. Surface plasmons exhibit unique characteristics due to the oscillation of conduction electrons near the metal surface, upon excitation by incident light. At the nanometer range, metallic nanoparticles possess high surface area to volume ratios and show distinctly different optical properties compared to their bulk and molecular counterparts[75,76]. Surface plasmons strongly confined on the surface of metallic nanoparticles are termed localized surface plasmon resonances (LSPR)[77]. When the incident electromagnetic field interacts with the metal nanoparticle, the conduction electrons oscillate collectively and coherently, in resonance with the light frequency, with respect to the nanoparticle lattice, due to the coulombic attraction between electrons and metallic nuclei (**Figure 1.9**). This collective oscillation of

electrons in resonance with the incident light frequency creates an LSPR on the metal nanoparticle surface.

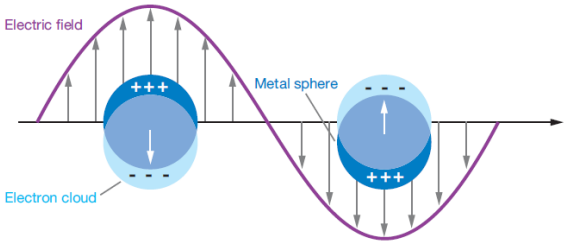

Figure 1.9. Schematic diagram illustrating a localized surface plasmon. A dipole is induced, which oscillates in phase with the electric field of the incoming light. Adapted from [78].

As mentioned above, the surface plasmon resonance of spherical particles with radius R was predicted by Mie theory, through expressions for the extinction cross section. When the size of the nanoparticles is significantly smaller than the wavelength of light ($\lambda \gg 2r$, where r is the radius of the nanoparticle), the exact condition for LSPR can be solved using the Mie theory or a simple oscillator model[79], as the extinction cross-section is expressed by,

$$\sigma_{ext} = 9\left(\frac{\omega}{c}\right)(\varepsilon_{diel})^{\frac{3}{2}}V\frac{\varepsilon''_{metal}}{(\varepsilon'_{metal}+2\varepsilon_{diel})^2+(\varepsilon''_{metal})^2} \qquad Eq\ (1.1)$$

where V is the volume of the particle, $\frac{4}{3}\pi R^3$, ω is the angular frequency of the exciting light, c is the velocity of light, ε_{diel} is the dielectric function of the medium surrounding the NP, and ε', ε'' are the real and imaginary parts of the dielectric function of the nanoparticle, respectively, i.e. $\varepsilon=\varepsilon'+i\varepsilon''$. The origin of the strong color changes displayed by small particles lays in the denominator of Eq (1.1), which predicts the existence of a maximum when $\varepsilon'=-2\varepsilon_{diel}$.

1.3.3 The Effect of Size and Aggregation on the Optical Properties of Gold Nanoparticles – the pillars of colorimetric sensors.

Since the LSPR can be excited by incident light, the plasmon can also re-radiate its energy into the far field as scattering, with the size of the particle determining the relative contribution of absorption or scattering. **Figure 1.10**a-c shows the spectra for spherical gold colloids of 13, 46 nm 63 nm in diameter, respectively. In general, light absorption dominates the extinction spectrum for particles of relatively small radius (<20 nm), while light scattering becomes progressivelly the dominant process for larger nanoparticles. Overall, with increasing the size of the nanoparticle, the contribution of absorption and scattering components strongly enhances the total cross-section (compare the three plots in **Figure 1.10**), rendering larger particles convenient for optical biosensors. As the particles increase in size, the LSPR are usually shifted towards higher wavelengths (535 and 540 nm are the LSPR maxima in the case of particles with a diameter of 46 and 63 nm, respectively).

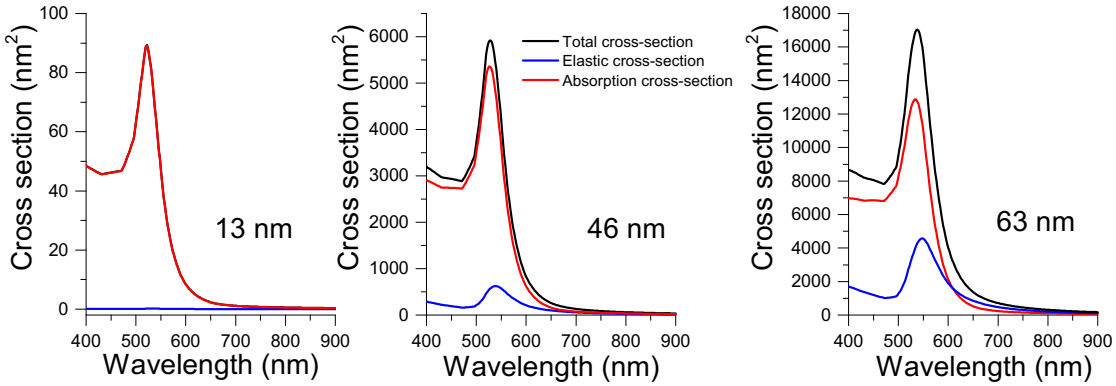

Figure 1.10. Calculated optical coefficients for a spherical gold particle with radius of 13, 46 and 63 nm. (ext. stands for extinction, abs. for absorption and sca. for scattering). The Cross-section spectra were calculated via online widget tools available at http://garciadeabajos-group.icfo.es.

The extremely intense and highly confined electromagnetic fields induced by the LSPR provide a highly sensitive probe to detect small changes in the dielectric environment around the nanocrystal, which is particularly attractive for sensing applications. Depending on the origin of LSPR maximum change, it is possible to

distinguish two types of sensors: aggregation sensors and refractive index sensors. The first group is based on the drastic color change induced by the aggregation of nanoparticles due to near-field electromagnetic coupling. In general, for two metal NPs, the resonance peak red-shifts when the interparticle separation distance decreases below the particle diameter (**Figure 1.11** left)[80].

On the other hand, the redshift of the LSPR induced by an increase of the refractive index around metal surface is the basis of the refractive index sensors (**Figure 1.11** right). Local refractive index changes such as those induced by biomolecular interactions at the surface of the nanostructures can be monitored via the LSPR band shift.

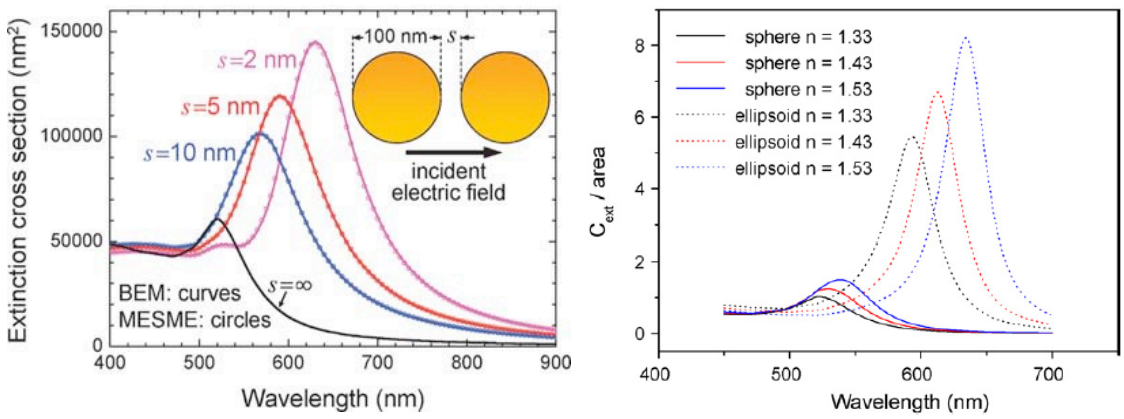

Figure 1.11. (Left) Theoretical Extinction cross-section spectra of gold dimers for different distances between the spheres surfaces. Adapted from [81]. (Right) The redshift of the extinction cross-section spectra of 20 AuNP and ellipsoids with aspect ratio 2 upon changes in the refractive index of the medium. Adapted from [82].

Other appealing sensing schemes can be devised taking advantage of the extremely large electromagnetic fields created in the so-called “hot spots”, which occur within nanoparticle aggregates or at sharp edges and tips in single nanoparticles. Within these regions, the cross-section of inelastic optical processes can be amplified by many orders of magnitude, giving rise to surface enhanced Raman scattering (SERS), surface enhanced fluorescence (SEF) and other related phenomena.

1.3.4 Synthesis of Gold Nanoparticles (AuNPs)

In 1857, Michael Faraday reported for the first time a synthetic method for metal nanoparticles by the reduction of a metal salt by white phosphorus, in carbon disulfide[72]. The preparation of AuNPs with controlled sizes and shapes has attracted much attention during the second half of the XXth century. A significant advancement was made by Turkevich in 1951[83], who proposed the so-called citrate reduction method (see **Figure 1.12** for a typical TEM image of colloidal gold prepared by Turkevich's method), which was improved by Frens in 1973[84]. Then, Mulvaney proposed the synthesis of AuNPs stabilized by thiols in 1993[85], and Brust and Schiffrin reported a biphasic method to produce thiol-stabilized AuNPs[86]. During the last two decades, these methods were progressively improved, providing today a wide range of available nanoparticles for a variety of applications.

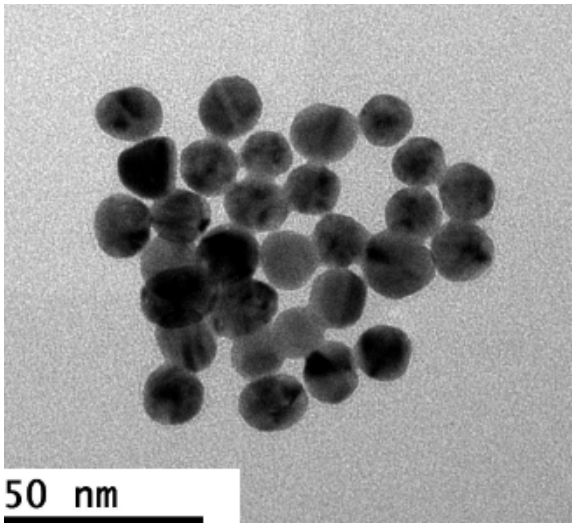

Figure 1.12. Gold nanospheres. TEM image of ≈13 nm AuNPs obtained through Turkevich's method.

Nowadays, we can distinguish two main mechanisms for the synthesis of metal nanoparticles: nucleation and growth method and autocatalytic reduction on preformed nanoparticles, also called seeded-growth (**Figure 1.13**).

Figure 1.13. Two mechanisms for the synthesis of metallic NPs. In the nucleation and growth mechanism metal ions are reduced to zero-valent nuclei by a strong reducing agent, followed by growth into nanoparticles. In the seeded growth, a reducing agent gets oxidized on a seed surface, facilitating the mild reduction of metal ions on the surface to produce particles with the desired size or shape. Adapted from [87].

The model of nucleation and growth was exploited by Faraday to prepare solutions containing ‘‘finely dispersed metals’’. In this approach, dispersed nanoparticles are produced by the reduction of a metal salt by a strong reducing agent. Organic molecules present in solution adsorb onto the surface of the particles, providing colloidal stability and thus preventing aggregation and sedimentation. Subsequent advancements by Turkevich and Frens allowed additional control on the size of the particles, through the molar ratio between the stabilizing/reducing agent and the metal precursor[84]. By that time, LaMer proposed a general model for the synthesis of monodispersed colloids[88], which found general acceptance in the synthesis of noble metal nanoparticles. Briefly, to obtain monodispersed particles one should increase the nucleation rate so that after the first nucleation no additional nuclei are formed and a saturation point is reached at which individual precursors only deposit on existing particles, the growth process. Since the saturation point is achieved faster at high concentration of the metal precursor, this approach permits the synthesis of large amounts of particles without loss of quality.

The first autocatalytic approach for selective reduction of gold on spherical seeds of the same metal was proposed by Turkevich[83]. In this approach, citrate-stabilized nanoparticles were used as seeds that catalyzed $HAuCl_4$ reduction by hydroxylamine hydrochloride exclusively on the surface of seeds. As a result, spherical nanoparticles were obtained, with fine control over the final diameter. The size prediction was defined by the following equation: $D_f = D_n((Au_n + Au_g)/Au_n)^{1/3}$ where D_f

is the final diameter, D_n is the diameter of the seed, Au_n the amount of metallic gold in the seed particles and Au_g is the amount of gold in the growth medium[89]. In other words, this expression defines the final particle diameter by changing the molar ratio between metal precursor and seeds. Another advantage of this approach is the control over the final concentration of nanoparticles, which is strictly related to the amount of seeds.

1.3.5 Surface Chemistry

The surface functionalization of NPs causes changes in the properties to fit targeted applications. The modification of the metal surface with functional molecules and polymers (**Figure 1.14**)[90] has different tasks to fulfill:

- stabilize the nanoparticles to control the growth of the initial particles and determine their shape during the growth process;
- provide functional groups at the surface for further derivatization;
- enhance the NPs stability in various solvents to extend their applications;
- modify the electronic, optical, spectroscopic and chemical properties to provide a plethora of controllable nanotools;
- alter the capability to assemble the particles in specific arrays or the ability to target desired chemical, physical, or biological environments;
- improve the mechanical and chemical performance of the nanoparticle surface, e.g., protection against oxidation.

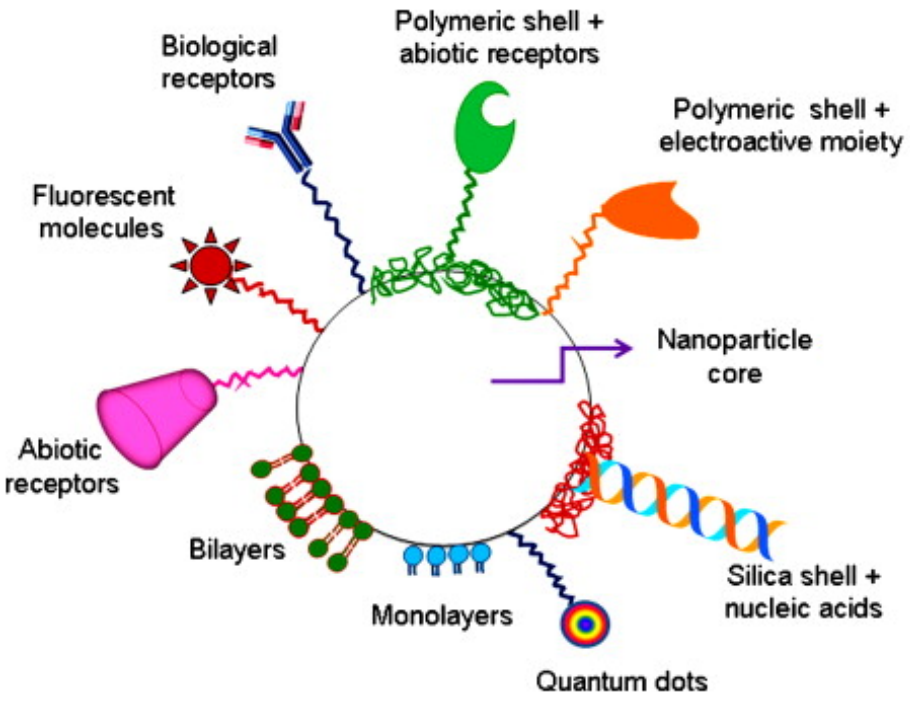

Figure 1.14. Gold nanostructures can be conjugated with a wide varietey of functional moieties. Adapted from [91].

1.3.6 Spherical Nucleic Acids

Among the variety of biomolecules that can be incorporated onto the surface of plasmonic nanoparticles, DNA is a unique system in the detection of cancer-related biomarkers which is vital in meeting the objective of the present thesis. In 1996, the group of Mirkin and coworkers[92] reported for the first time the use of 13 nm AuNPs functionalized with thiol-capped short single-stranded DNA (ssDNA). Two batches of AuNPs were functionalized with non-complementary DNA oligonucleotides capped with thiol groups. When the complementary sequence was added to the solution, the NPs aggregated, inducing a color change from red (for dispersed AuNPs in solution) to purple/blue (for aggregates). These aggregates dehybridized cooperatively with an increase of the temperature displaying narrow melting transitions compared to the free DNA (**Figure 1.15**)[93]. DNA attached to the surface of the nanoparticle ensures the behavior of the particles and their stability in complex media. Usually, a construct between the nanoparticle and the DNA sequence requires a binding group (mostly thiol groups), a spacer group and the single-stranded DNA sequence. The spacer

provides the freedom of DNA probes in its environment. In general, the spacer is formed by a single or double-stranded DNA sequence. Gold nanoparticles capped with a dense monolayer of radially distributed DNA exhibit properties that differ from the DNA that they derive from. Nanoparticles functionalized with a radial DNA shell have higher binding constants than free oligonucleotides[94], present cooperative binding and thus sharp melting transitions[95] (**Figure 1.15**). Therefore, such structures received its own name -spherical nucleic acids (SNA) - in which DNA strands are highly oriented.

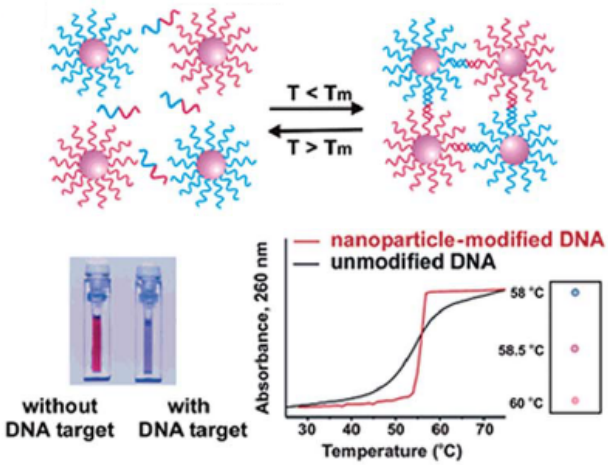

Figure 1.15. Schematic representation of the strategy for colorimetric DNA detection using DNA conjugated AuNPs. The addition of a complementary target to DNA oligonucleotide-functionalized AuNPs leads to aggregation, resulting in a color change from red to blue. The aggregates dehybridized in a very narrow temperature range, in comparison with free DNA. Adapted from [93].

Although the protocols for binding DNA to the surface of gold nanoparticles are well established[92], there are some important issues during the ligand exchange process that may affect not only the colloidal stability of the nanoparticles but also the proper performance of the DNA shell. For example, during the incubation step, apart from Au-S binding, non-specific binding of the DNA sequences can also occur. These unspecific interactions between gold and DNA are mediated by amine groups in the purine and pyrimidine rings of the nucleotides[96,97]. Therefore, the choice of a proper sequence for the DNA spacer is critical to avoid unspecific interactions. A spacer formed by the oligonucleotide timine has been found to present by far the lowest unspecific binding affinity[98].

Another important parameter is the extent of grafting density that defines the unspecific interactions between the DNA strands and the gold surface. To cover the surface of the particles with short oligonucleotides, a conventional ligand exchange process is usually applied, involving Au-S bond formation and leading to a limited number of DNA strands attached to the metallic core. Electrostatic repulsion of negatively charged DNA strands prevents dense packing, leading to limited colloidal stability. A great improvement was the introduction of a salt aging process. The progressive increase of the concentration of sodium ions (0.15 M) screened electrostatic repulsion between neighboring strands, promoting higher densities of oligonucleotides on the surface of the nanoparticles (**Figure 1.16**). In general, the salt concentration in the salt aging process is proportional to the DNA density on the particle surface until steric hindrance inhibits further adsorption. Of course, the maximum surface coverage of DNA strands depends on the particle size and shape. For spherical particles, in general, smaller particles can support a higher oligonucleotide density than larger particles because the radius of curvature is greater, which provides a deflection angle between neighboring oligonucleotides. This deflection angle produces additional space in the volume surrounding the DNA strands, and decreases as the particle size increases.

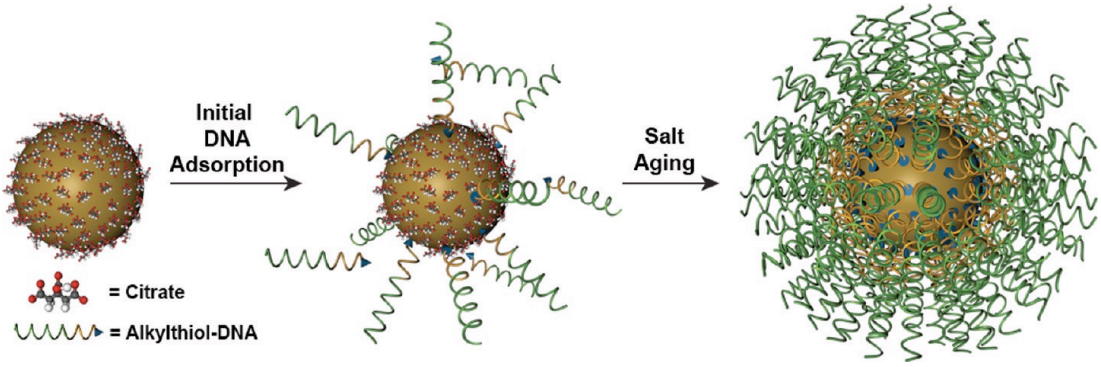

Figure 1.16. Preparation of spherical nucleic acids. Particles stabilized with citrate are incubated with alkylthiol-functionalized oligonucleotides in water. Subsequently, incubating the nanoparticles in aqueous solution with successively higher concentrations of salt and surfactant, a high-density shell of DNA strands is formed. Adapted from [99].

1.3.7 Colorimetric Biosensing based on Nanoparticles Aggregation

Historically, colloidal aggregation is the core feature of sensitive label-free assays that can even be visualized with a ‘‘naked’’ eye. Early biosensing experiments for detection of a variety of biomolecules (e.g., proteins) employed the change of color that emerged during the aggregation of gold nanoparticles. As a result, the detection of DNA strands through selective particle aggregation, became a powerful colorimetric biosensing strategy (**Figure 1.15**). Currently, there are three types of mechanisms for the colorimetric detection of DNA strand through colloidal aggregation: (A) aggregation of unmodified nanoparticles in the presence of dsDNA and salt, (B) aggregation through selective DNA crosslinking and, (C) aggregation without selective crosslinking of DNA. **Figure 1.17** describes schematically the three detection mechanisms.

The first method is based on the assumption that ssDNA molecules have higher affinity toward gold surface than dsDNA.[100] The adsorption of ssDNA on gold surface prevents the aggregation at elevated salt concentrations that would usually screen their electrostatic repulsion. Therefore, colloidal samples that contain dsDNA in solution irreversibly aggregate when the salt concentration is increased, while solutions with ssDNA remain stable (**Figure 1.17A**).

The second method involves the mixing of two type metal nanoparticle, each grafted with a different and non-complementary thiol-terminated single-stranded DNA. Addition of a third oligonucleotide, which is complementary to both immobilized ssDNA (one at each end), induces aggregation through hybridization between the complementary oligonucleotides. Aggregation is then accompanied by a color change of the colloidal solution, from red to purple-blue. The aggregation can be reversed by simply changing the ionic strength of the solution or raising the temperature above the melting point of DNA, thus inducing dehybridization. Such a color change in the colloidal solution allowed for differentiation between complementary strands and strands with one or more mutations (**Figure 1.17B**)[93,101].

The third method involves nanoparticles aggregation through the formation of dsDNA but without crosslinking events. The increase in ionic strength causes extensive aggregation of gold nanoparticles stabilized with ssDNA. The aggregation is prevented in the presence of a complementary target that binds the ssDNA anchored to the gold surface (**Figure 1.17B**)[102,103]. Among these three strategies described above, the self-assembly through a complementary target is the most exploited approach, which is due to a rather lower risk of giving a false positive.

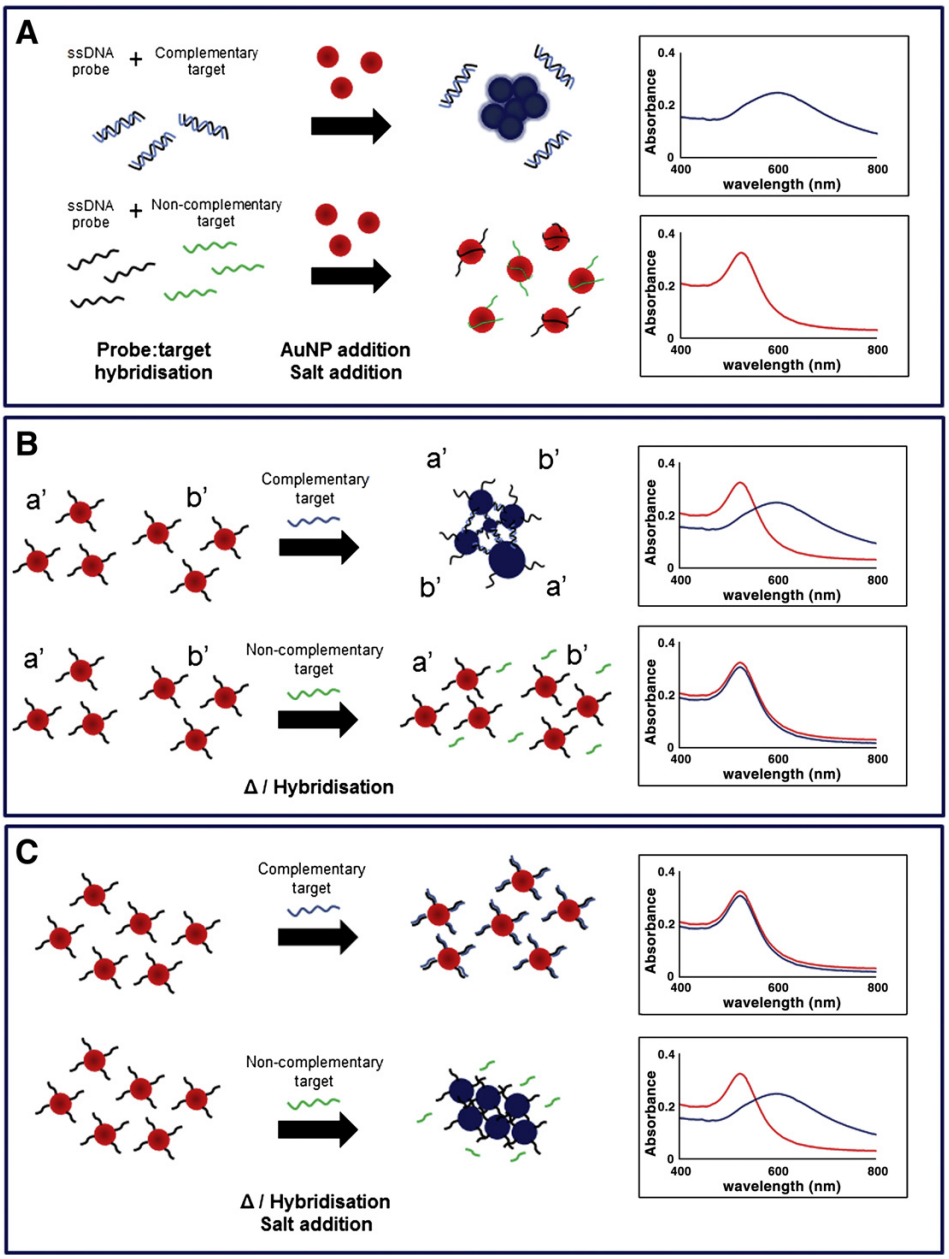

Figure 1.17. AuNP based colorimetric assays. a) colorimetric assay based on naked AuNPs: the presence of ssDNA stabilizes AuNPs against salt-induced aggregation, whereas double-strand DNA does not; b) crosslinking hybridization assay: hybridization brings both AuNP-DNA probes in close vicinity, leading to aggregation and color change; c) non-crosslinking hybridization assay: an increase in ionic strength causes AuNP-DNA probes aggregation (blue solution), which is prevented by the presence of the complementary target. Adapted from [104].

1.4 Detection of Single Base Mutation based on the Aggregation of AuNPs: State-of-Art

The aim of this section is to review the most relevant examples on colorimetric assays for detection of SNP using gold nanoparticles. The reviewed works will be organized according the three methods describd in the previous section, namely: (Type A) assay based on the use of unmodified AuNPs, (Type B) crosslinking hybridization assay, and (Type C) non-crosslinking hybridization assay. The performance of each example will be disscused taking into account parameters such as the *time* required for the detection process, the *sensitivity* (i.e., LoD) and the single base mismatch *selectivity*. In addition, the emphasis will be put on the length of the target sequence, and the diameter of the NPs employed.

Over two decades ago, Mirkin and co-workers reported for the first time the colorimetric detection of a DNA target (24-30 bases) carrying a single nucleotide polymorphism, using an assay based on aggregating gold nanoparticles[105]. However, the small particle size, 13 nm, limited the colorimetric LoD sensitivity and single-base mutation selectivity to 60 nM. Since then, various strategies were reported, which are briefly summarized in this section. **Table 1.2** lists relevant examples dealing with various methodologies for the colorimetric detection of single nucleotide polymorphism by aggregating nanoparticles without any amplification system or use of any enzyme.

Reference	DNA Target / Length	Limit of Detection	NPs Diameter
Colorimetric assay based on unmodified AuNPs (Type A)			
Rothberg and Li	24 bases	4.3 nM	13 nm
Plaxco and coworkers	27 bases	1.25 pM	20 nm
Chakrabarti and Klibanov	12 bases	-	13 nm
Zhu et al.	14 bases	250 nM	13 nm
Lee and coworkers	20 bases	10 ng/µL	18 nm
Zhou and coworkers	41 bases	5 nM	13 nm
Colorimetric assay with crosslinking (Type B)			
Mirkin and coworkers	30 bases	60 nM	13 nm
Guo et al.	22 bases	1 pM	43 nm
Charrier and coworkers	22 bases	47.6 nM	13 nm
Duan et al.	34 bases	1 nM	10 nm
Graham and coworkers	14 bases	100 nM	13 nm
Colorimetric assay without crosslinking (Type C)			
Maeda and coworkers	15 bases	500 nM	13 nm
Baptista and coworkers	-	117 nM	13 nm
Lee and coworkers	12, 21 and 42 bases	100 nM	18 nm

Table 1.2. Colorimetric detection based on gold nanoparticles for the detection of single nucleotide polymorphism in relevant DNA sequences.

The Type A methods in which the pre-functionalization of the nanoparticles is exluded has been exploited by Rothberg and Li[100]. In their method, single-stranded DNA (ssDNA) or duplex DNA (dsDNA) was added to citrate-stabilized gold nanoparticles, followed by the addition of salt, leading to the selective aggregation in the presence of dsDNA in the nanoparticle mixture. The principle of this methods is based on the assumption that the binding of dsDNA toward the gold surface is much less efficient than ssDNA because the bases in dsDNA are buried in the helical structure. The bases in ssDNA, on the other hand, are more accessible toward the gold surface, thereby stabilizing the nanoparticles in the presence of high concentration of salt. Therefore, a red to purple color change upon salt addition indicated the presence of target DNA. This assay involved the use of 13 nm gold nanoparticles that allowed the visual detection of single base mismatches with impressive limit of detection down to 4.3 nM.

A new method improving the sensitivity of the label-free colorimetric approach was developed by Plaxco and coworkers who used 20 nm NPs and polyelectrolytes instead of salt (**Figure 1.18**)[106]. In this work, ssDNA or dsDNA was added to citrate-stabilized gold nanoparticles, followed by addition of cationic conjugated polyelectrolyte. However, the working principle of this assay was oposited as in the previous example. That is, the addition of polyelectrolyte to the ssDNA/nanoparticle mixture caused aggregation of ssDNA-decorated nanoparticles because of the interaction between ssDNA and polyelectrolytes. Opositely, the addition of polyelectrolyte to the dsDNA/nanoparticle mixture did not induce nanoparticle aggregation because the interaction of dsDNA with polyelectrolytes was weaker than that of ssDNA. Althouth the sensitivy was improved (1.25 pM) the selectivity remained low since this method could discriminated only three or more mismatched bases.

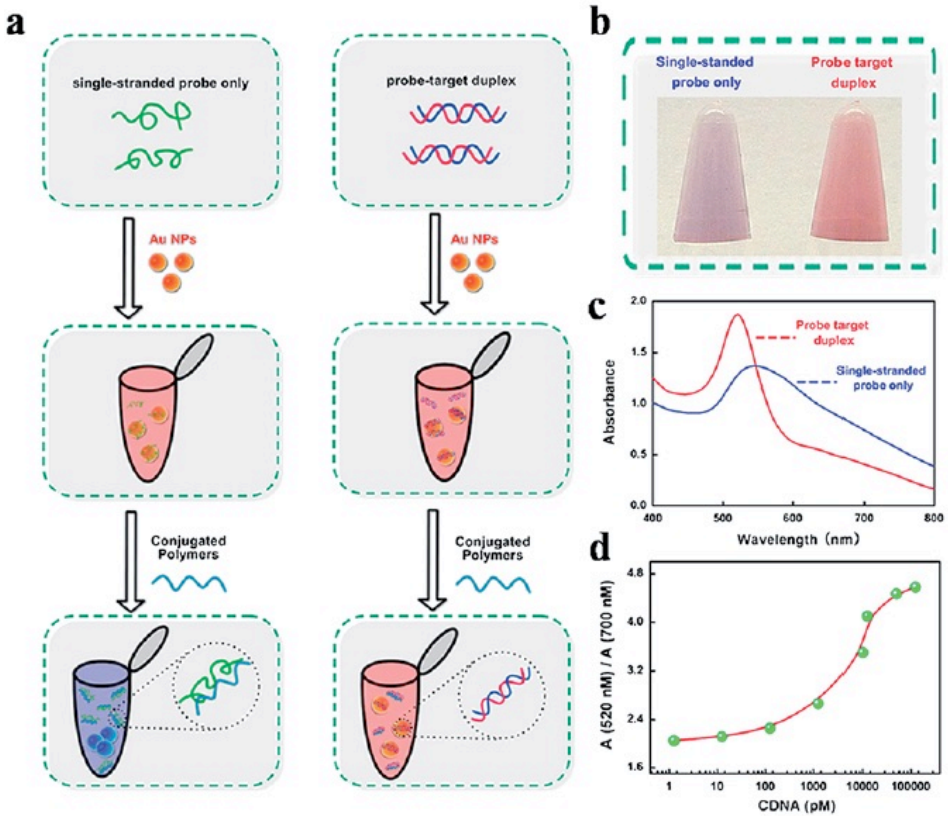

Figure 1.18. Schematic representation of a colorimetric assay for DNA detection using unmodified AuNPs. (a) Scheme of the addition of positively charged polyelectrolyte to a mixture of ssDNA and AuNPs, leading to color change, while no color change occurs in the case of dsDNA. (b) Photographs of colloidal solutions of AuNPs in the presence of ssDNA (blue) and dsDNA (red). (c) Extinction spectra of AuNPs with double-stranded and single-stranded DNA. (d) Plot of target DNA concentration vs. the A_{520}/A_{700} ratio, showing the possibility of determining the target concentration. Adapted from [106].

Alternatively, peptide nucleic acid (PNA) can also be use as effective coagulant of citrate-stabilized gold nanoparticles. Chakrabarti et al.[107] have demonstrated that PNA-stabilized AuNPs agglomerated in aqueous solutions in the presence of salt because of the charge neutrality of PNA. The addition of target ssDNA (12 bases) to the aggregated solution of AuNP@PNA resulted in the redispersion of NPs, which was due to the binding of negatively charged DNA strands to neutral PNA on the nanoparticle surface NPs. The specificity of the PNA-DNA complex allowed for colorimetric discrimination of SNP in DNA sequence. In similar works, Kanjanawarut et al.[108,109] confirmed that the addition of PNA to citrate-stabilized AuNPs (13 nm) induces aggregation of NPs through PNA binding to the gold surface. The presence of

complementary target DNA (22 bases, 1μM) prevented aggregation of the NPs due to the formation of PNA-DNA complex. The incorporation of the single base mismatch into the DNA allowed for visual discrimiantion of the mutation in the analyte DNA.

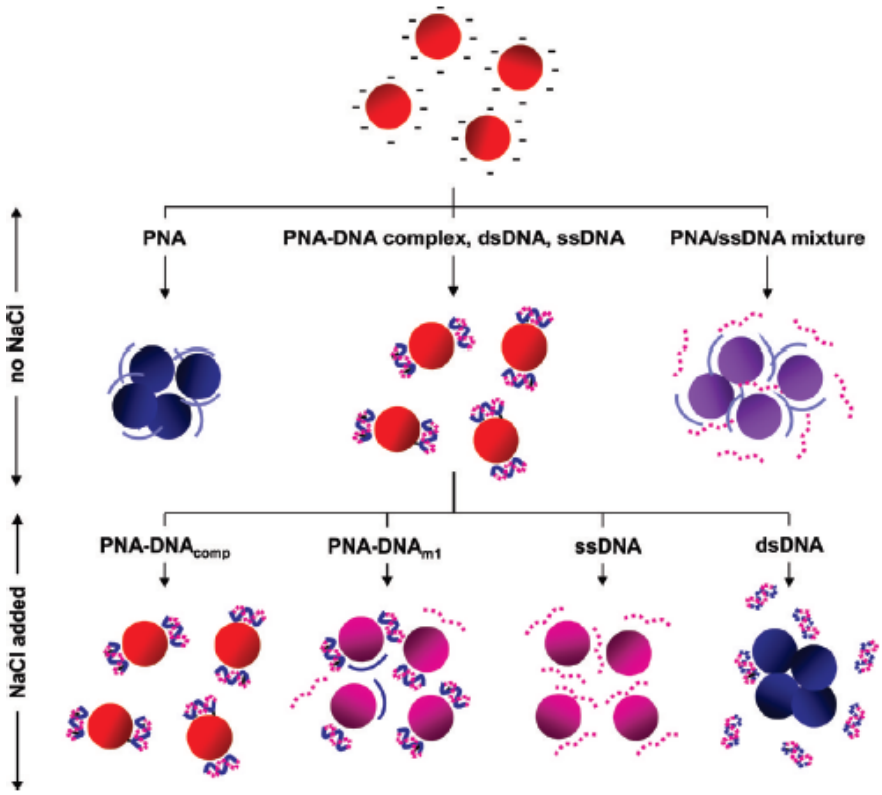

Figure 1.19. Schematic illustration of how different nucleic acids (PNA, PNA-DNA complexes, ssDNA, dsDNA, and PNA/DNA mixture) affect AuNP intrinsic stability and AuNP stability against salt. Adapted from [108].

A mixture of single-stranded triplex-forming oligonucleotide (TFO), double-stranded DNA and citrate-stabilized AuNPs (13 nm), was proposed by Zhu et al. to discriminate SNP[110]. The TFO sequences interacted with AuNPs through nitrogen-containing bases, thus protecting AuNPs from salt-induced aggregation. The addition of duplex DNA to the mixture led to the triplex DNA formation, consequently exposing the particles to the high ionic strength environment, thus causing aggregation. The color transition from red to blue indicated the formation of triplex DNA. The

introduction of a mutation into the TFO sequence prevented the triplex DNA formation, and thus particle aggregation at a given salt concertation.

The detection of mutations in the epidermal growth factor receptor (EGFR) of non-small cell lung cancer cells using selective AuNPs aggregation (18 nm) was studied by Lee and coworkers[111]. Mutations in exon 19 and exon 21 of EGFR gene were detected in non-amplified genomic DNAs that were isolated from both the lung cancer cell lines and the cancer tissues of non-small cell lung cancer patients. At the optimal salt concentration, the addition of the mutant DNA that was hybridized with the complementary probe of 20 bases into the suspension of unmodified gold nanoparticles caused the substantial aggregation of the AuNPs and color change of the solution. Gold nanoparticles, however, did not exhibit significant aggregation, and the solution color remained unchanged with the addition of the wild-type DNA that was hybridized with the probe. In the eight specimens from non-small cell lung cancer patients, deletion mutant in exon 19 and the L858R point mutation in exon 21 were detected in a concentration of 10 ng/μL.

A colorimetric biosensing strategy to discriminate single-nucleotide mutation in DNA with high selectivity using unmodified AuNPs as indicators was reported by Zhou and coworkers[112]. In the AuNPs-based colorimetric strategy, binary DNA probes were produced by splitting the DNA probe in the middle for sensitive differentiation of single-base mismatch (**Figure 1.20**). Upon the addition of target DNA to the solution of binary DNA probes and 13 nm citrate-protected AuNPs, hybridization between target DNA and binary DNA probes reduced the ability to protect AuNPs from salt-induced aggregation, leading to color change. Whereas the presence of a single base mismatch did not induce the AuNPs aggregation and the solution remained stable. Regarding assay performance, this approach presented a detection limit of 5 nM.

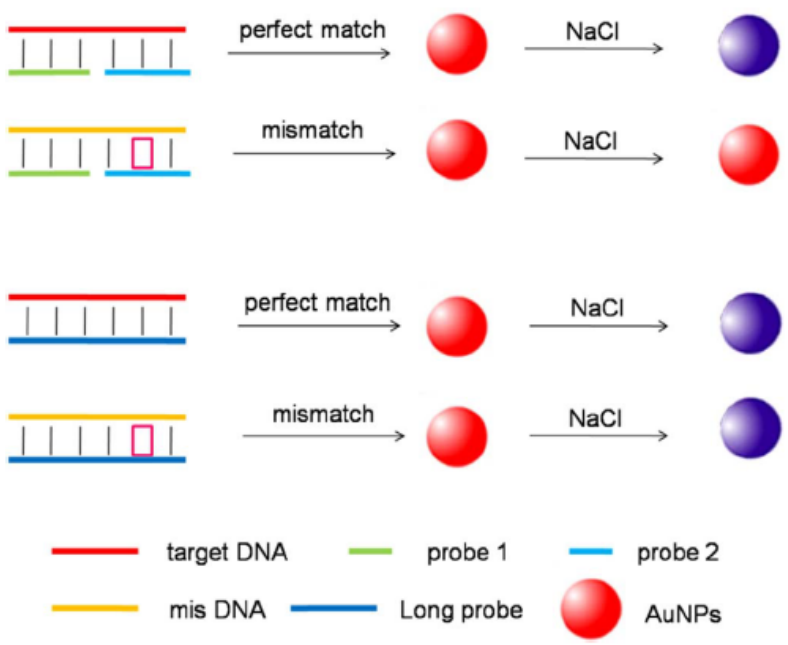

Figure 1.20. Schematic illustration of AuNPs-based colorimetric system using binary DNA probes for sensitive discrimination of single-base mismatches. Adapted from [112].

The examples covering the Type A methods (based on the use of unmodified AuNPs) present a good sensitivity but their main drawback is the high risk of of false positives. So, other possibility for the detection of DNA sequences and the discrimination of SNP is based on colorimetric assays with crosslinking. The most relevant approaches are explained below. An assay for SNP detection through oriented nanoparticle aggregation in the presence of DNA target have developed by Guo et al.[113]. Upon target binding, the 43 nm AuNPs were asymmetrically functionalized with DNA probes formed into a Y-shaped DNA duplex, which pulls the two linked NPs to a minimum separation distance (**Figure 1.21**a). The extinction spectra of the oriented sensor exhibited a sharp peak at 600 nm, indicating the formation of AuNP dimers (**Figure 1.21**b), whereas the non-oriented version exhibited a broad band after target binding (**Figure 1.21**c). This approach allowed for the detection of DNA sequences with only one base variation in targets with a length of 22 bases. With this method, the limit of detection was improved 10,000 times, up to 1 pM, and the dynamic range of

detection was more than two orders of magnitude wider compared with the non-oriented nanoparticle aggregation version.

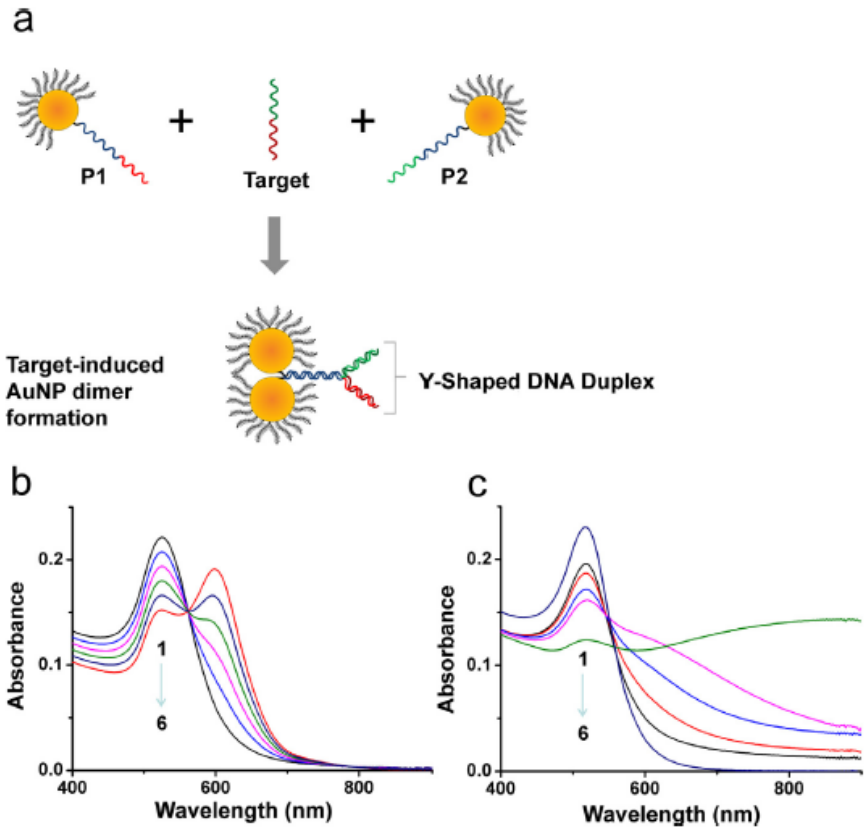

Figure 1.21. a) Schematic illustration of the oriented colorimetric biosensor. B) and c) represent typical extinction spectra of oriented (b) and non-oriented (c) sensors. The target concentrations for the spectra from 1 to 6 are 0, 1 pM, 10 pM, 100 pM, 1 nM and 10 nM for b), and 0, 10 nM, 30 nM, 100 nM, 300 nM and 1000 nM for c). Adapted from [113].

A 2D assay based on the aggregation of oligonucleotide-modified AuNP probes attached to the surface was reported by Charrier and coworkers (**Figure 1.22**)[114]. Gold nanoparticles (13 nm) were adsorbed on a fluid lipid bilayer supported on a substrate. The target ssDNA (22 bases) crosslinked the NPs, resulting in the formation of aggregates in the plane of the substrate. Subsequent desorption of non-crosslinked nanoparticles by dextran sulfate allowed to maintain the aggregates attached to the lipid bilayers. The detection limit for SNP discrimination was improved, reaching a concentration value of 47.6 nM.

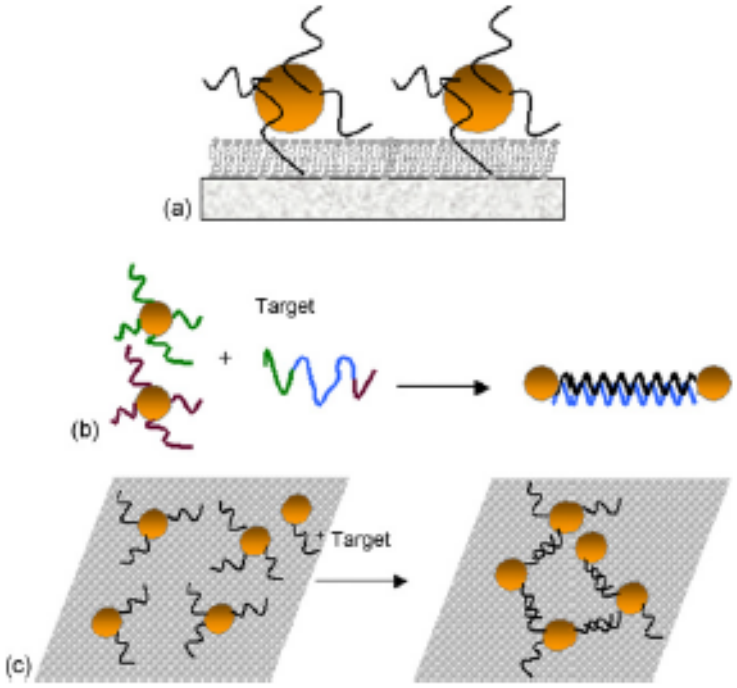

Figure 1.22. Schematic representation of a 2D assay. a) The system comprises three layers: the solid substrate, the lipid layer and the oligonucleotide-modified AuNPs – signal transducer. b) Crosslinking of single-stranded DNA through target DNA leads to the selective aggregation of nanoparticles. c) A top view of the system before and after hybridization. Adapted from [114].

A simple colorimetric method based on the enzyme-free toehold-mediated strand displacement reaction was proposed by Duan et al.[115]. In this method, AuNPs acted as signal generators for the real-time detection of the product of the strand displacement cascade of 34 bases of length. This assay could also be applied in complex mixtures, fetal bovine serum, and to detect single base mismatches achieving a limit of detection of 1 nM (**Figure 1.23**).

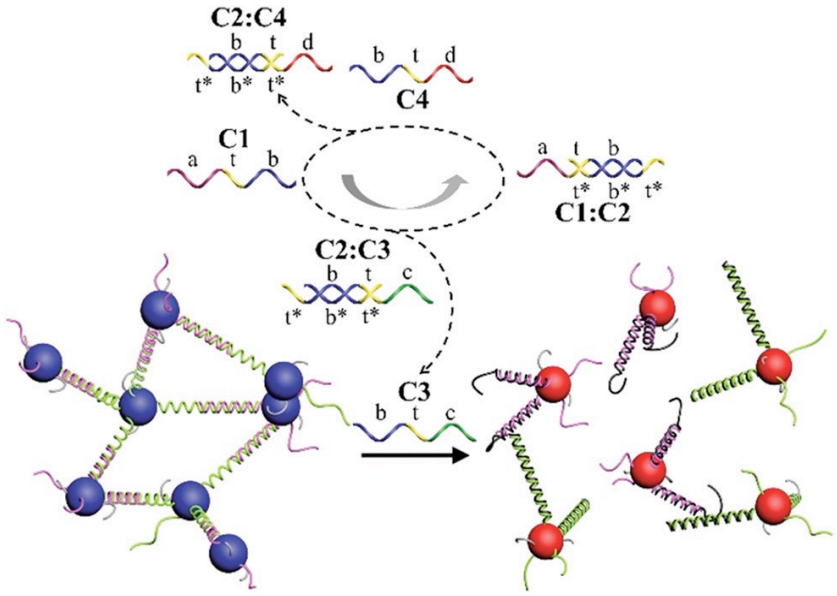

Figure 1.23. Colorimetric method for monitoring the enzyme-free strand displacement cascade. The product of the catalytic strand displacement cascade, the C3 strand, is consumed by the disassembly of the AuNP aggregates. Adapted from [115].

Locked Nucleic Acids (LNA) can be also employed for the functionalization of AuNPs. With this approach, these conjugates display remarkable binding affinity and selectivity towards 22 bases DNA target[116]. The use of LNA/DNA chimeras by Graham´s group ensured the enhanced stability of duplexes formed using AuNP conjugates and offered discrimination between mismatch and complementary target DNA. Despite the relatively good selectivity between the match and mismatch, the limit of detection was rather low, 100 nM.

The last method in colorimetric assays depicted in Figure 1.17 is related with a non crosslinking method. A non crosslinking assay was proposed for SNP detection based on the aggregation of AuNPs (13 nm), through the hybridization of 15 bases target DNA[117]. The single-base mutation was located on the 5' terminus, ensuring the stability of the particles at high salt concentration. On the contrary, the perfect match sequence (no mutation at 5' terminus) formed a double strand on the particle surface, leading to gradual aggregation at high salt concentration (**Figure 1.24**). Maeda and coworkers claimed that double strands on the particles' surface affect the electrostatic repulsion between the particles, due to the charge screening. Overall, this method allowed the authors to achieve the sensitivity of 500 nM for the discrimination of a single base mutation. The desing of this assay is very simple, easy and it allows to discriminate between two DNA sequences with a difference of only one base; but the main drawback is the low sensitivity.

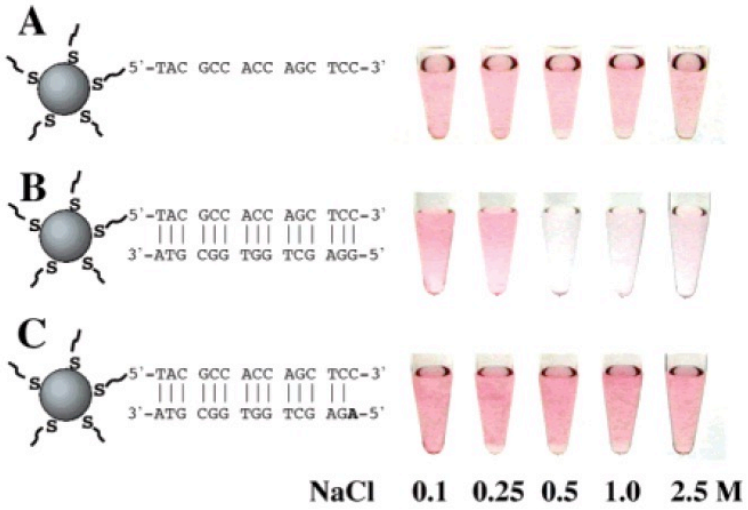

Figure 1.24. Aggregation behaviors of DNA-AuNPs at various NaCl concentrations, at room temperature: (A) without a target DNA, (B) with the complementary target, and (C) with a target containing a single base mismatch at its 5' terminus. The final concentrations of the particle, the probe DNA, and the targets were 2.3, 500, and 500 nM, respectively. Adapted from [117].

Au-nanoprobes were used for the specific identification of SNPs within the beta subunit of the RNA polymerase (*rpo*B locus), responsible for resistance to rifampicin in over 95% of rifampicin-resistant *M. tuberculosis* strains (**Figure 1.25**). This methodology developed by the group of Baptiste and coworkers[118] was applied to pathogen identification and SNP discrimination based on the differential non-crosslinking aggregation of Au-nanoprobes with a limit of detection of 117 nM. As the first step, a PCR amplification of a fragment of *rpo*B gene was performed, followed by the hybridization process. In the presence of the respective complementary target, the Au-nanoprobes are protected against the salt-induced aggregation and the solution remains stable; whereas the presence of noncomplementary target does not protect the Au-nanoprobes from the aggregation and the solution turns blue.

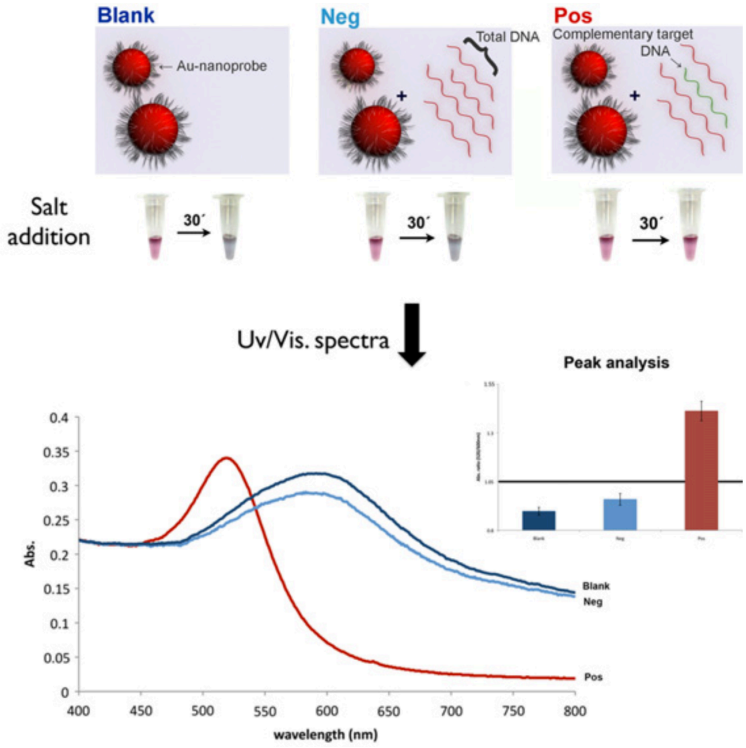

Figure 1.25. A strategy for detection of MTBC (*Mycobacterium tuberculosis* complex) members and mutations associated with RIF resistance. Schematic representation of the detection with Au-nanoprobes. The colorimetric assay consists of visual comparison of test solutions before and after salt induced Au-nanoprobe aggregation: Au-nanoprobe alone (blank), Au-nanoprobe in the presence of a complementary DNA sequence (POS), and Au-nanoprobe in the presence of a non-complementary DNA sequence (NEG). Adapted from [118].

A colorimetric method for the detection of mutations in the tyrosine kinase receptor c-Kit was reported by Lee and coworkers[119]. To detect a point mutation in codon 559 and in-frame deletion in codon 557/558 of c-Kit, the authors designed a target with different lengths (12-, 21-, and 42-mer) derived from the wild-type and the mutant-type c-Kit sequences. AuNPs were then modified with the PNA probes that were perfectly complementary to the wild-type target sequence. This made the PNA modified AuNPs neutrally charged, leading to destabilization and aggregation of AuNPs. The addition of the target to the PNA-modified AuNPs induced the hybridization between the PNA probes on AuNPs and the target, which renders the AuNPs negatively charged because of the phosphate backbone in the target DNA sequences (**Figure 1.26**). The diameter of the particles used in the assay was 18 nm and three targets with different lengths, 12, 21 and 42 bases were tested. The limit of detection achieved in the case of the 21 bases target was 100 fmol/µL.

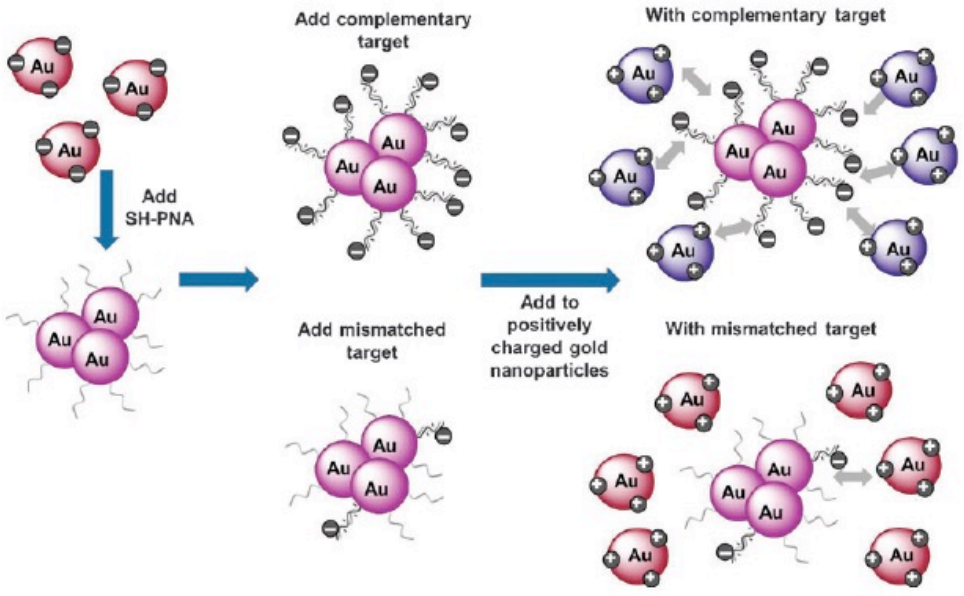

Figure 1.26. Scheme for the detection of wild type oligonucleotides with the PNA-modified AuNPs. Adapted from [119].

Taking into account the publications in the field, there are some problems that need to be solved and certain parameters to improve. For example, the sensitivity and selectivity, as well as the need for simple and easy-to-apply approaches. Also, in all the cases the diameter of the particles is approximately around 15 nm; so, if large particles are employed as transducers, the intensity of the plasmon will be higher and the sensitivity of the assay will be improved. On the other hand, in a real scenario the length of the target sequences that we want to detect is normally around 140 bases. But, in the most of the cases the length of the targets is between 20 and 30 bases, so far of a real application. Another important point is that all the articles reported different approaches to detect single stranded DNA, but in a real case, the DNA is double stranded. As final point to consider for the desing of an assay is the importance of the physiological media. This environment is rich in a huge variety of biomolecules such as proteins, membranes, phospholipids, endocytic vesicles, organelles which will inevitabily interact with the nanoparticle surface and the detection process will be affected.

1.5 References

(1) Ferlay, J.; Soerjomataram, I.; Dikshit, R.; Eser, S.; Mathers, C.; Rebelo, M.; Parkin, D. M.; Forman, D.; Bray, F. Cancer Incidence and Mortality Worldwide: Sources, Methods and Major Patterns in GLOBOCAN 2012. *Int. J. Cancer* **2015**, *136* (5), E359–E386.

(2) Ortmann, C. A.; Kent, D. G.; Nangalia, J.; Silber, Y.; Wedge, D. C.; Grinfeld, J.; Baxter, E. J.; Massie, C. E.; Papaemmanuil, E.; Menon, S.; Godfrey, A. L.; Dimitropoulou, D.; Guglielmelli, P.; Bellosillo, B.; Besses, C.; Döhner, K.; Harrison, C. N.; Vassiliou, G. S.; Vannucchi, A.; Campbell, P. J.; Green, A. R. Effect of Mutation Order on Myeloproliferative Neoplasms. *N. Engl. J. Med.* **2015**, *372* (7), 601–612.

(3) Sawyers, C. L. The Cancer Biomarker Problem. *Nature* **2008**, *452* (7187), 548–552.

(4) Crowley, E.; Di Nicolantonio, F.; Loupakis, F.; Bardelli, A. Liquid Biopsy: Monitoring Cancer-Genetics in the Blood. *Nat. Rev. Clin. Oncol.* **2013**, *10* (8), 472–484.

(5) Bedard, P. L.; Hansen, A. R.; Ratain, M. J.; Siu, L. L. Tumour Heterogeneity in the Clinic. *Nature* **2013**, *501* (7467), 355–364.

(6) Kim, E. S.; Hirsh, V.; Mok, T.; Socinski, M. A.; Gervais, R.; Wu, Y.-L.; Li, L.-Y.; Watkins, C. L.; Sellers, M. V.; Lowe, E. S.; Sun, Y.; Liao, M.-L.; Østerlind, K.; Reck, M.; Armour, A. A.; Shepherd, F. A.; Lippman, S. M.; Douillard, J.-Y. Gefitinib versus Docetaxel in Previously Treated Non-Small-Cell Lung Cancer (INTEREST): A Randomised Phase III Trial. *The Lancet* **2008**, *372* (9652), 1809–1818.

(7) Mandel, P.; Metais, P. Les Acides Nucleiques Du Plasma Sanguin Chez L'homme. *C. R. Seances Soc. Biol. Fil.* **1948**, *142* (3–4), 241–243.

(8) Alix-Panabières, C.; Pantel, K. Challenges in Circulating Tumour Cell Research. *Nat. Rev. Cancer* **2014**, *14* (9), 623–631.

(9) Taylor, D. D.; Gercel-Taylor, C. Exosomes/Microvesicles: Mediators of Cancer-Associated Immunosuppressive Microenvironments. *Semin. Immunopathol.* **2011**, *33* (5), 441–454.

(10) Kosaka, N.; Iguchi, H.; Ochiya, T. Circulating microRNA in Body Fluid: A New Potential Biomarker for Cancer Diagnosis and Prognosis. *Cancer Sci.* **2010**, *101* (10), 2087–2092.

(11) Luna Coronell, J. A.; Syed, P.; Sergelen, K.; Gyurján, I.; Weinhäusel, A. The Current Status of Cancer Biomarker Research Using Tumour-Associated Antigens for

Minimal Invasive and Early Cancer Diagnostics. *J. Proteomics* **2012**, *76 Spec No.*, 102–115.

(12) Bellassai, N.; Spoto, G. Biosensors for Liquid Biopsy: Circulating Nucleic Acids to Diagnose and Treat Cancer. *Anal. Bioanal. Chem.* **2016**, *408* (26), 7255–7264.

(13) Diaz, L. A.; Bardelli, A. Liquid Biopsies: Genotyping Circulating Tumor DNA. *J. Clin. Oncol. Off. J. Am. Soc. Clin. Oncol.* **2014**, *32* (6), 579–586.

(14) Aarthy, R.; Mani, S.; Velusami, S.; Sundarsingh, S.; Rajkumar, T. Role of Circulating Cell-Free DNA in Cancers. *Mol. Diagn. Ther.* **2015**, *19* (6), 339–350.

(15) Chaudhuri, A. A.; Binkley, M. S.; Osmundson, E. C.; Alizadeh, A. A.; Diehn, M. Predicting Radiotherapy Responses and Treatment Outcomes Through Analysis of Circulating Tumor DNA. *Semin. Radiat. Oncol.* **2015**, *25* (4), 305–312.

(16) Ignatiadis, M.; Lee, M.; Jeffrey, S. S. Circulating Tumor Cells and Circulating Tumor DNA: Challenges and Opportunities on the Path to Clinical Utility. *Clin. Cancer Res. Off. J. Am. Assoc. Cancer Res.* **2015**, *21* (21), 4786–4800.

(17) Polivka, J.; Pesta, M.; Janku, F. Testing for Oncogenic Molecular Aberrations in Cell-Free DNA-Based Liquid Biopsies in the Clinic: Are We There Yet? *Expert Rev. Mol. Diagn.* **2015**, *15* (12), 1631–1644.

(18) Diehl, F.; Schmidt, K.; Choti, M. A.; Romans, K.; Goodman, S.; Li, M.; Thornton, K.; Agrawal, N.; Sokoll, L.; Szabo, S. A.; Kinzler, K. W.; Vogelstein, B.; Diaz, L. A. Circulating Mutant DNA to Assess Tumor Dynamics. *Nat. Med.* **2008**, *14* (9), 985–990.

(19) Diehl, F.; Li, M.; Dressman, D.; He, Y.; Shen, D.; Szabo, S.; Diaz, L. A.; Goodman, S. N.; David, K. A.; Juhl, H.; Kinzler, K. W.; Vogelstein, B. Detection and Quantification of Mutations in the Plasma of Patients with Colorectal Tumors. *Proc. Natl. Acad. Sci. U. S. A.* **2005**, *102* (45), 16368–16373.

(20) Holdhoff, M.; Schmidt, K.; Donehower, R.; Diaz, L. A. Analysis of Circulating Tumor DNA to Confirm Somatic KRAS Mutations. *J. Natl. Cancer Inst.* **2009**, *101* (18), 1284–1285.

(21) Newman, A. M.; Bratman, S. V.; To, J.; Wynne, J. F.; Eclov, N. C. W.; Modlin, L. A.; Liu, C. L.; Neal, J. W.; Wakelee, H. A.; Merritt, R. E.; Shrager, J. B.; Loo, B. W.; Alizadeh, A. A.; Diehn, M. An Ultrasensitive Method for Quantitating Circulating Tumor DNA with Broad Patient Coverage. *Nat. Med.* **2014**, *20* (5), 548–554.

(22) Fan, X.; White, I. M.; Shopova, S. I.; Zhu, H.; Suter, J. D.; Sun, Y. Sensitive Optical Biosensors for Unlabeled Targets: A Review. *Anal. Chim. Acta* **2008**, *620* (1–2), 8–26.

(23) Jahr, S.; Hentze, H.; Englisch, S.; Hardt, D.; Fackelmayer, F. O.; Hesch, R. D.; Knippers, R. DNA Fragments in the Blood Plasma of Cancer Patients: Quantitations and Evidence for Their Origin from Apoptotic and Necrotic Cells. *Cancer Res.* **2001**, *61* (4), 1659–1665.

(24) Mouliere, F.; Robert, B.; Arnau Peyrotte, E.; Del Rio, M.; Ychou, M.; Molina, F.; Gongora, C.; Thierry, A. R. High Fragmentation Characterizes Tumour-Derived Circulating DNA. *PloS One* **2011**, *6* (9), e23418.

(25) Siravegna, G.; Bardelli, A. Blood Circulating Tumor DNA for Non-Invasive Genotyping of Colon Cancer Patients. *Mol. Oncol.* **2016**, *10* (3), 475–480.

(26) Spindler, K. L. G.; Pallisgaard, N.; Andersen, R. F.; Brandslund, I.; Jakobsen, A. Circulating Free DNA as Biomarker and Source for Mutation Detection in Metastatic Colorectal Cancer. *PLoS ONE* **2015**, *10* (4).

(27) Szpechcinski, A.; Chorostowska-Wynimko, J.; Struniawski, R.; Kupis, W.; Rudzinski, P.; Langfort, R.; Puscinska, E.; Bielen, P.; Sliwinski, P.; Orlowski, T. Cell-Free DNA Levels in Plasma of Patients with Non-Small-Cell Lung Cancer and Inflammatory Lung Disease. *Br. J. Cancer* **2015**, *113* (3), 476–483.

(28) Bettegowda, C.; Sausen, M.; Leary, R. J.; Kinde, I.; Wang, Y.; Agrawal, N.; Bartlett, B. R.; Wang, H.; Luber, B.; Alani, R. M.; Antonarakis, E. S.; Azad, N. S.; Bardelli, A.; Brem, H.; Cameron, J. L.; Lee, C. C.; Fecher, L. A.; Gallia, G. L.; Gibbs, P.; Le, D.; Giuntoli, R. L.; Goggins, M.; Hogarty, M. D.; Holdhoff, M.; Hong, S.-M.; Jiao, Y.; Juhl, H. H.; Kim, J. J.; Siravegna, G.; Laheru, D. A.; Lauricella, C.; Lim, M.; Lipson, E. J.; Marie, S. K. N.; Netto, G. J.; Oliner, K. S.; Olivi, A.; Olsson, L.; Riggins, G. J.; Sartore-Bianchi, A.; Schmidt, K.; Shih, Ie-M.; Oba-Shinjo, S. M.; Siena, S.; Theodorescu, D.; Tie, J.; Harkins, T. T.; Veronese, S.; Wang, T.-L.; Weingart, J. D.; Wolfgang, C. L.; Wood, L. D.; Xing, D.; Hruban, R. H.; Wu, J.; Allen, P. J.; Schmidt, C. M.; Choti, M. A.; Velculescu, V. E.; Kinzler, K. W.; Vogelstein, B.; Papadopoulos, N.; Diaz, L. A. Detection of Circulating Tumor DNA in Early- and Late-Stage Human Malignancies. *Sci. Transl. Med.* **2014**, *6* (224), 224ra24-224ra24.

(29) Collins, F. S.; Brooks, L. D.; Chakravarti, A. A DNA Polymorphism Discovery Resource for Research on Human Genetic Variation. *Genome Res.* **1998**, *8* (12), 1229–1231.

(30) Sachidanandam, R.; Weissman, D.; Schmidt, S. C.; Kakol, J. M.; Stein, L. D.; Marth, G.; Sherry, S.; Mullikin, J. C.; Mortimore, B. J.; Willey, D. L.; Hunt, S. E.; Cole, C. G.; Coggill, P. C.; Rice, C. M.; Ning, Z.; Rogers, J.; Bentley, D. R.; Kwok, P.-Y.; Mardis, E. R.; Yeh, R. T.; Schultz, B.; Cook, L.; Davenport, R.; Dante, M.; Fulton, L.; Hillier, L.; Waterston, R. H.; McPherson, J. D.; Gilman, B.; Schaffner, S.; Etten, W. J. V.; Reich, D.;

Higgins, J.; Daly, M. J.; Blumenstiel, B.; Baldwin, J.; Stange-Thomann, N.; Zody, M. C.; Linton, L.; Lander, E. S.; Altshuler, D. A Map of Human Genome Sequence Variation Containing 1.42 Million Single Nucleotide Polymorphisms. *Nature* **2001**, *409* (6822), 928–933.

(31) Kim, S.; Misra, A. SNP Genotyping: Technologies and Biomedical Applications. *Annu. Rev. Biomed. Eng.* **2007**, *9* (1), 289–320.

(32) Lovly, C.; Horn, L.; Pao, W. Molecular Profiling of Lung Cancer - My Cancer Genome https://www.mycancergenome.org/content/disease/lung-cancer/ (accessed Dec 9, 2016).

(33) Mitsudomi, T.; Yatabe, Y. Epidermal Growth Factor Receptor in Relation to Tumor Development: EGFR Gene and Cancer. *FEBS J.* **2010**, *277* (2), 301–308.

(34) Robinson, D.; Van Allen, E. M.; Wu, Y.-M.; Schultz, N.; Lonigro, R. J.; Mosquera, J.-M.; Montgomery, B.; Taplin, M.-E.; Pritchard, C. C.; Attard, G.; Beltran, H.; Abida, W.; Bradley, R. K.; Vinson, J.; Cao, X.; Vats, P.; Kunju, L. P.; Hussain, M.; Feng, F. Y.; Tomlins, S. A.; Cooney, K. A.; Smith, D. C.; Brennan, C.; Siddiqui, J.; Mehra, R.; Chen, Y.; Rathkopf, D. E.; Morris, M. J.; Solomon, S. B.; Durack, J. C.; Reuter, V. E.; Gopalan, A.; Gao, J.; Loda, M.; Lis, R. T.; Bowden, M.; Balk, S. P.; Gaviola, G.; Sougnez, C.; Gupta, M.; Yu, E. Y.; Mostaghel, E. A.; Cheng, H. H.; Mulcahy, H.; True, L. D.; Plymate, S. R.; Dvinge, H.; Ferraldeschi, R.; Flohr, P.; Miranda, S.; Zafeiriou, Z.; Tunariu, N.; Mateo, J.; Perez-Lopez, R.; Demichelis, F.; Robinson, B. D.; Schiffman, M.; Nanus, D. M.; Tagawa, S. T.; Sigaras, A.; Eng, K. W.; Elemento, O.; Sboner, A.; Heath, E. I.; Scher, H. I.; Pienta, K. J.; Kantoff, P.; de Bono, J. S.; Rubin, M. A.; Nelson, P. S.; Garraway, L. A.; Sawyers, C. L.; Chinnaiyan, A. M. Integrative Clinical Genomics of Advanced Prostate Cancer. *Cell* **2015**, *161* (5), 1215–1228.

(35) Grasso, C. S.; Wu, Y.-M.; Robinson, D. R.; Cao, X.; Dhanasekaran, S. M.; Khan, A. P.; Quist, M. J.; Jing, X.; Lonigro, R. J.; Brenner, J. C.; Asangani, I. A.; Ateeq, B.; Chun, S. Y.; Siddiqui, J.; Sam, L.; Anstett, M.; Mehra, R.; Prensner, J. R.; Palanisamy, N.; Ryslik, G. A.; Vandin, F.; Raphael, B. J.; Kunju, L. P.; Rhodes, D. R.; Pienta, K. J.; Chinnaiyan, A. M.; Tomlins, S. A. The Mutational Landscape of Lethal Castration-Resistant Prostate Cancer. *Nature* **2012**, *487* (7406), 239–243.

(36) O'Brien, C.; Wallin, J. J.; Sampath, D.; GuhaThakurta, D.; Savage, H.; Punnoose, E. A.; Guan, J.; Berry, L.; Prior, W. W.; Amler, L. C.; Belvin, M.; Friedman, L. S.; Lackner, M. R. Predictive Biomarkers of Sensitivity to the Phosphatidylinositol 3' Kinase Inhibitor GDC-0941 in Breast Cancer Preclinical Models. *Clin. Cancer Res. Off. J. Am. Assoc. Cancer Res.* **2010**, *16* (14), 3670–3683.

(37) Bose, R.; Kavuri, S. M.; Searleman, A. C.; Shen, W.; Shen, D.; Koboldt, D. C.;

Monsey, J.; Goel, N.; Aronson, A. B.; Li, S.; Ma, C. X.; Ding, L.; Mardis, E. R.; Ellis, M. J. Activating HER2 Mutations in HER2 Gene Amplification Negative Breast Cancer. *Cancer Discov.* **2013**, *3* (2), 224–237.

(38) Stemke-Hale, K.; Gonzalez-Angulo, A. M.; Lluch, A.; Neve, R. M.; Kuo, W.-L.; Davies, M.; Carey, M.; Hu, Z.; Guan, Y.; Sahin, A.; Symmans, W. F.; Pusztai, L.; Nolden, L. K.; Horlings, H.; Berns, K.; Hung, M.-C.; van de Vijver, M. J.; Valero, V.; Gray, J. W.; Bernards, R.; Mills, G. B.; Hennessy, B. T. An Integrative Genomic and Proteomic Analysis of PIK3CA, PTEN, and AKT Mutations in Breast Cancer. *Cancer Res.* **2008**, *68* (15), 6084–6091.

(39) Riely, G. J.; Kris, M. G.; Rosenbaum, D.; Marks, J.; Li, A.; Chitale, D. A.; Nafa, K.; Riedel, E. R.; Hsu, M.; Pao, W.; Miller, V. A.; Ladanyi, M. Frequency and Distinctive Spectrum of KRAS Mutations in Never Smokers with Lung Adenocarcinoma. *Clin. Cancer Res. Off. J. Am. Assoc. Cancer Res.* **2008**, *14* (18), 5731–5734.

(40) di Martino, E.; Tomlinson, D. C.; Knowles, M. A. A Decade of FGF Receptor Research in Bladder Cancer: Past, Present, and Future Challenges. *Adv. Urol.* **2012**, *2012*, 429213.

(41) van Oers, J. M. M.; Zwarthoff, E. C.; Rehman, I.; Azzouzi, A.-R.; Cussenot, O.; Meuth, M.; Hamdy, F. C.; Catto, J. W. F. FGFR3 Mutations Indicate Better Survival in Invasive Upper Urinary Tract and Bladder Tumours. *Eur. Urol.* **2009**, *55* (3), 650–657.

(42) Kurman, R. J.; Shih, I.-M. Molecular Pathogenesis and Extraovarian Origin of Epithelial Ovarian Cancer--Shifting the Paradigm. *Hum. Pathol.* **2011**, *42* (7), 918–931.

(43) Campbell, I. G.; Russell, S. E.; Phillips, W. A. PIK3CA Mutations in Ovarian Cancer. *Clin. Cancer Res. Off. J. Am. Assoc. Cancer Res.* **2005**, *11* (19 Pt 1), 7042; author reply 7042-7043.

(44) Ricarte-Filho, J. C.; Ryder, M.; Chitale, D. A.; Rivera, M.; Heguy, A.; Ladanyi, M.; Janakiraman, M.; Solit, D.; Knauf, J. A.; Tuttle, R. M.; Ghossein, R. A.; Fagin, J. A. Mutational Profile of Advanced Primary and Metastatic Radioactive Iodine-Refractory Thyroid Cancers Reveals Distinct Pathogenetic Roles for BRAF, PIK3CA, and AKT1. *Cancer Res.* **2009**, *69* (11), 4885–4893.

(45) De Bosscher, K.; Hill, C. S.; Nicolás, F. J. Molecular and Functional Consequences of Smad4 C-Terminal Missense Mutations in Colorectal Tumour Cells. *Biochem. J.* **2004**, *379* (Pt 1), 209–216.

(46) Syvänen, A.-C. Accessing Genetic Variation: Genotyping Single Nucleotide Polymorphisms. *Nat. Rev. Genet.* **2001**, *2* (12), 930–942.

(47) Tahira, T.; Kukita, Y.; Higasa, K.; Okazaki, Y.; Yoshinaga, A.; Hayashi, K. Estimation of SNP Allele Frequencies by SSCP Analysis of Pooled DNA. *Methods Mol. Biol. Clifton NJ* **2009**, *578*, 193–207.

(48) Millis, M. P. Medium-Throughput SNP Genotyping Using Mass Spectrometry: Multiplex SNP Genotyping Using the iPLEX® Gold Assay. *Methods Mol. Biol. Clifton NJ* **2011**, *700*, 61–76.

(49) Beaudet, L.; Bédard, J.; Breton, B.; Mercuri, R. J.; Budarf, M. L. Homogeneous Assays for Single-Nucleotide Polymorphism Typing Using AlphaScreen. *Genome Res.* **2001**, *11* (4), 600–608.

(50) Barreiro, L.; Henriques, R.; Mhlanga, M. High-Throughput SNP Genotyping: Combining Tag SNPs and Molecular Beacons. In *Single Nucleotide Polymorphisms*; Komar, A. A., Ed.; Methods in Molecular Biology™; Humana Press, 2009; pp 255–276.

(51) Deulvot, C.; Charrel, H.; Marty, A.; Jacquin, F.; Donnadieu, C.; Lejeune-Hénaut, I.; Burstin, J.; Aubert, G. Highly-Multiplexed SNP Genotyping for Genetic Mapping and Germplasm Diversity Studies in Pea. *BMC Genomics* **2010**, *11*, 468.

(52) Ding, C.; Jin, S. High-Throughput Methods for SNP Genotyping. In *Single Nucleotide Polymorphisms*; Komar, A. A., Ed.; Methods in Molecular Biology™; Humana Press, 2009; pp 245–254.

(53) International Union; of Pure and Applied Chemistry. *IUPAC Compendium of Chemical Terminology*, 2nd Edition (1997).; Research Triangle Park, 1992.

(54) Clark, L. C.; Lyons, C. Electrode Systems for Continuous Monitoring in Cardiovascular Surgery. *Ann. N. Y. Acad. Sci.* **1962**, *102* (1), 29–45.

(55) Vigneshvar, S.; Sudhakumari, C. C.; Senthilkumaran, B.; Prakash, H. Recent Advances in Biosensor Technology for Potential Applications – An Overview. *Process Ind. Biotechnol.* **2016**, 11.

(56) Zhu, L.; Yang, R.; Zhai, J.; Tian, C. Bienzymatic Glucose Biosensor Based on Co-Immobilization of Peroxidase and Glucose Oxidase on a Carbon Nanotubes Electrode. *Biosens. Bioelectron.* **2007**, *23* (4), 528–535.

(57) Hu, T.; Zhang, X.-E.; Zhang, Z.-P. Disposable Screen-Printed Enzyme Sensor for Simultaneous Determination of Starch and Glucose. *Biotechnol. Tech.* **1999**, *13* (6), 359–362.

(58) Cui, Y.; Barford, J. P.; Renneberg, R. Amperometric Trienzyme ATP Biosensors Based on the Coimmobilization of Salicylate Hydroxylase, Glucose-6-Phosphate Dehydrogenase, and Hexokinase. *Sens. Actuators B Chem.* **2008**, *132* (1), 1–4.

(59) Kwan, R. C. H.; Hon, P. Y. T.; Mak, K. K. W.; Renneberg, R. Amperometric Determination of Lactate with Novel Trienzyme/Poly(carbamoyl) Sulfonate Hydrogel-Based Sensor. *Biosens. Bioelectron.* **2004**, *19* (12), 1745–1752.

(60) Morgan, C. L.; Newman, D. J.; Price, C. P. Immunosensors: Technology and Opportunities in Laboratory Medicine. *Clin. Chem.* **1996**, *42* (2), 193–209.

(61) Yang, M.; McGovern, M. E.; Thompson, M. Genosensor Technology and the Detention of Interfacial Nucleic Acid Chemistry. *Anal. Chim. Acta* **1997**, *346* (3), 259–275.

(62) Kricka, L. J. Microchips, Microarrays, Biochips and Nanochips: Personal Laboratories for the 21st Century. *Clin. Chim. Acta* **2001**, *307* (1–2), 219–223.

(63) Wang, J. From DNA Biosensors to Gene Chips. *Nucleic Acids Res.* **2000**, *28* (16), 3011–3016.

(64) Willner, I.; Shlyahovsky, B.; Zayats, M.; Willner, B. DNAzymes for Sensing, Nanobiotechnology and Logic Gate Applications. *Chem. Soc. Rev.* **2008**, *37* (6), 1153–1165.

(65) Kosman, J.; Juskowiak, B. Peroxidase-Mimicking DNAzymes for Biosensing Applications: A Review. *Anal. Chim. Acta* **2011**, *707* (1–2), 7–17.

(66) Su, L.; Jia, W.; Hou, C.; Lei, Y. Microbial Biosensors: A Review. *Biosens. Bioelectron.* **2011**, *26* (5), 1788–1799.

(67) Lodeiro, C.; Luis Capelo, J.; Carlos Mejuto, J.; Oliveira, E.; M. Santos, H.; Pedras, B.; Nuñez, C. Light and Colour as Analytical Detection Tools: A Journey into the Periodic Table Using Polyamines to Bio-Inspired Systems as Chemosensors. *Chem. Soc. Rev.* **2010**, *39* (8), 2948–2976.

(68) Gopinath, S. C. B. Biosensing Applications of Surface Plasmon Resonance-Based Biacore Technology. *Sens. Actuators B Chem.* **2010**, *150* (2), 722–733.

(69) David, C.; Guillot, N.; Shen, H.; Toury, T.; Chapelle, M. L. de la. SERS Detection of Biomolecules Using Lithographed Nanoparticles towards a Reproducible SERS Biosensor. *Nanotechnology* **2010**, *21* (47), 475501.

(70) Nützenadel, C.; Züttel, A.; Chartouni, D.; Schmid, G.; Schlapbach, L. Critical Size and Surface Effect of the Hydrogen Interaction of Palladium Clusters. *Eur. Phys. J. D* **2000**, *8* (2), 245–250.

(71) The Lycurgus Cup http://www.britishmuseum.org/research/collection_online/collection_object_details.

aspx?objectId=61219&partId=1&searchText=lycurgus+cup&page=1 (accessed Apr 7, 2017).

(72) Faraday, M. The Bakerian Lecture: Experimental Relations of Gold (and Other Metals) to Light. *Philos. Trans. R. Soc. Lond.* **1857**, *147*, 145–181.

(73) Mie, G. Beiträge Zur Optik Trüber Medien, Speziell Kolloidaler Metallösungen. *Ann. Phys.* **1908**, *330* (3), 377–445.

(74) Horvath, H. Gustav Mie and the Scattering and Absorption of Light by Particles: Historic Developments and Basics. *J. Quant. Spectrosc. Radiat. Transf.* **2009**, *110* (11), 787–799.

(75) Burda, C.; Chen, X.; Narayanan, R.; El-Sayed, M. A. Chemistry and Properties of Nanocrystals of Different Shapes. *Chem. Rev.* **2005**, *105* (4), 1025–1102.

(76) Wiley, B.; Sun, Y.; Xia, Y. Synthesis of Silver Nanostructures with Controlled Shapes and Properties. *Acc. Chem. Res.* **2007**, *40* (10), 1067–1076.

(77) Mock, J. J.; Hill, R. T.; Degiron, A.; Zauscher, S.; Chilkoti, A.; Smith, D. R. Distance-Dependent Plasmon Resonant Coupling between a Gold Nanoparticle and Gold Film. *Nano Lett.* **2008**, *8* (8), 2245–2252.

(78) Willets, K. A.; Duyne, R. P. V. Localized Surface Plasmon Resonance Spectroscopy and Sensing. *Annu. Rev. Phys. Chem.* **2007**, *58* (1), 267–297.

(79) Li, Y.; Zhao, K.; Sobhani, H.; Bao, K.; Nordlander, P. Geometric Dependence of the Line Width of Localized Surface Plasmon Resonances. *J. Phys. Chem. Lett.* **2013**, *4* (8), 1352–1357.

(80) Gunnarsson, L.; Rindzevicius, T.; Prikulis, J.; Kasemo, B.; Käll, M.; Zou, S.; Schatz, G. C. Confined Plasmons in Nanofabricated Single Silver Particle Pairs: Experimental Observations of Strong Interparticle Interactions. *J. Phys. Chem. B* **2005**, *109* (3), 1079–1087.

(81) Myroshnychenko, V.; Rodríguez-Fernández, J.; Pastoriza-Santos, I.; Funston, A. M.; Novo, C.; Mulvaney, P.; Liz-Marzán, L. M.; Abajo, F. J. G. de. Modelling the Optical Response of Gold Nanoparticles. *Chem. Soc. Rev.* **2008**, *37* (9), 1792–1805.

(82) Sepúlveda, B.; Angelomé, P. C.; Lechuga, L. M.; Liz-Marzán, L. M. LSPR-Based Nanobiosensors. *Nano Today* **2009**, *4* (3), 244–251.

(83) Turkevich, J.; Stevenson, P. C.; Hillier, J. A Study of the Nucleation and Growth Processes in the Synthesis of Colloidal Gold. *Discuss. Faraday Soc.* **1951**, *11* (0), 55–75.

(84) Frens, G. Controlled Nucleation for the Regulation of the Particle Size in

Monodisperse Gold Suspensions. *Nature* **1973**, *241* (105), 20–22.

(85) Giersig, M.; Mulvaney, P. Preparation of Ordered Colloid Monolayers by Electrophoretic Deposition. *Langmuir* **1993**, *9* (12), 3408–3413.

(86) Brust, M.; Walker, M.; Bethell, D.; Schiffrin, D. J.; Whyman, R. Synthesis of Thiol-Derivatised Gold Nanoparticles in a Two-Phase Liquid–Liquid System. *J. Chem. Soc. Chem. Commun.* **1994**, No. 7, 801–802.

(87) Grzelczak, M.; Liz-Marzán, L. M. The Relevance of Light in the Formation of Colloidal Metal Nanoparticles. *Chem Soc Rev* **2014**, *43* (7), 2089–2097.

(88) LaMer, V. K.; Dinegar, R. H. Theory, Production and Mechanism of Formation of Monodispersed Hydrosols. *J. Am. Chem. Soc.* **1950**, *72* (11), 4847–4854.

(89) Turkevich, J. Colloidal Gold. Part I. *Gold Bull.* **1985**, *18* (3), 86–91.

(90) Sapsford, K. E.; Algar, W. R.; Berti, L.; Gemmill, K. B.; Casey, B. J.; Oh, E.; Stewart, M. H.; Medintz, I. L. Functionalizing Nanoparticles with Biological Molecules: Developing Chemistries That Facilitate Nanotechnology. *Chem. Rev.* **2013**, *113* (3), 1904–2074.

(91) de Dios, A. S.; Díaz-García, M. E. Multifunctional Nanoparticles: Analytical Prospects. *Anal. Chim. Acta* **2010**, *666* (1–2), 1–22.

(92) Mirkin, C. A.; Letsinger, R. L.; Mucic, R. C.; Storhoff, J. J. A DNA-Based Method for Rationally Assembling Nanoparticles into Macroscopic Materials. *Nature* **1996**, *382* (6592), 607–609.

(93) Elghanian, R.; Storhoff, J. J.; Mucic, R. C.; Letsinger, R. L.; Mirkin, C. A. Selective Colorimetric Detection of Polynucleotides Based on the Distance-Dependent Optical Properties of Gold Nanoparticles. *Science* **1997**, *277* (5329), 1078–1081.

(94) Lytton-Jean, A. K. R.; Mirkin, C. A. A Thermodynamic Investigation into the Binding Properties of DNA Functionalized Gold Nanoparticle Probes and Molecular Fluorophore Probes. *J. Am. Chem. Soc.* **2005**, *127* (37), 12754–12755.

(95) Jin, R.; Wu, G.; Li, Z.; Mirkin, C. A.; Schatz, G. C. What Controls the Melting Properties of DNA-Linked Gold Nanoparticle Assemblies? *J. Am. Chem. Soc.* **2003**, *125* (6), 1643–1654.

(96) Sandström, P.; Boncheva, M.; Åkerman, B. Nonspecific and Thiol-Specific Binding of DNA to Gold Nanoparticles. *Langmuir* **2003**, *19* (18), 7537–7543.

(97) Cárdenas, M.; Barauskas, J.; Schillén, K.; Brennan, J. L.; Brust, M.; Nylander, T.

Thiol-Specific and Nonspecific Interactions between DNA and Gold Nanoparticles. *Langmuir* **2006**, *22* (7), 3294–3299.

(98) Storhoff, J. J.; Elghanian, R.; Mirkin, C. A.; Letsinger, R. L. Sequence-Dependent Stability of DNA-Modified Gold Nanoparticles. *Langmuir* **2002**, *18* (17), 6666–6670.

(99) Cutler, J. I.; Auyeung, E.; Mirkin, C. A. Spherical Nucleic Acids. *J. Am. Chem. Soc.* **2012**, *134* (3), 1376–1391.

(100) Li, H.; Rothberg, L. Colorimetric Detection of DNA Sequences Based on Electrostatic Interactions with Unmodified Gold Nanoparticles. *Proc. Natl. Acad. Sci. U. S. A.* **2004**, *101* (39), 14036–14039.

(101) Storhoff, J. J.; Lazarides, A. A.; Mucic, R. C.; Mirkin, C. A.; Letsinger, R. L.; Schatz, G. C. What Controls the Optical Properties of DNA-Linked Gold Nanoparticle Assemblies? *J. Am. Chem. Soc.* **2000**, *122* (19), 4640–4650.

(102) Conde, J.; de la Fuente, J. M.; Baptista, P. V. RNA Quantification Using Gold Nanoprobes - Application to Cancer Diagnostics. *J. Nanobiotechnology* **2010**, *8*, 5.

(103) Baptista, P.; Pereira, E.; Eaton, P.; Doria, G.; Miranda, A.; Gomes, I.; Quaresma, P.; Franco, R. Gold Nanoparticles for the Development of Clinical Diagnosis Methods. *Anal. Bioanal. Chem.* **2008**, *391* (3), 943–950.

(104) Larguinho, M.; Baptista, P. V. Gold and Silver Nanoparticles for Clinical Diagnostics — From Genomics to Proteomics. *J. Proteomics* **2012**, *75* (10), 2811–2823.

(105) Storhoff, J. J.; Elghanian, R.; Mucic, R. C.; Mirkin, C. A.; Letsinger, R. L. One-Pot Colorimetric Differentiation of Polynucleotides with Single Base Imperfections Using Gold Nanoparticle Probes. *J. Am. Chem. Soc.* **1998**, *120* (9), 1959–1964.

(106) Xia, F.; Zuo, X.; Yang, R.; Xiao, Y.; Kang, D.; Vallée-Bélisle, A.; Gong, X.; Yuen, J. D.; Hsu, B. B. Y.; Heeger, A. J.; Plaxco, K. W. Colorimetric Detection of DNA, Small Molecules, Proteins, and Ions Using Unmodified Gold Nanoparticles and Conjugated Polyelectrolytes. *Proc. Natl. Acad. Sci.* **2010**, *107* (24), 10837–10841.

(107) Chakrabarti, R.; Klibanov, A. M. Nanocrystals Modified with Peptide Nucleic Acids (PNAs) for Selective Self-Assembly and DNA Detection. *J. Am. Chem. Soc.* **2003**, *125* (41), 12531–12540.

(108) Su, X.; Kanjanawarut, R. Control of Metal Nanoparticles Aggregation and Dispersion by PNA and PNA−DNA Complexes, and Its Application for Colorimetric DNA Detection. *ACS Nano* **2009**, *3* (9), 2751–2759.

(109) Kanjanawarut, R.; Su, X. Colorimetric Detection of DNA Using Unmodified

Metallic Nanoparticles and Peptide Nucleic Acid Probes. *Anal. Chem.* **2009**, *81* (15), 6122–6129.

(110) Zhu, X.; Liu, Y.; Yang, J.; Liang, Z.; Li, G. Gold Nanoparticle-Based Colorimetric Assay of Single-Nucleotide Polymorphism of Triplex DNA. *Biosens. Bioelectron.* **2010**, *25* (9), 2135–2139.

(111) Lee, H.; Kang, T.; Yoon, K.-A.; Lee, S. Y.; Joo, S.-W.; Lee, K. Colorimetric Detection of Mutations in Epidermal Growth Factor Receptor Using Gold Nanoparticle Aggregation. *Biosens. Bioelectron.* **2010**, *25* (7), 1669–1674.

(112) Zhou, W.; Ren, J.; Zhu, J.; Zhou, Z.; Dong, S. Accurate and Visual Discrimination of Single-Base Mismatch by Utilization of Binary DNA Probes in Gold Nanoparticles-Based Biosensing Strategy. *Talanta* **2016**, *161*, 528–534.

(113) Guo, L.; Xu, Y.; Ferhan, A. R.; Chen, G.; Kim, D.-H. Oriented Gold Nanoparticle Aggregation for Colorimetric Sensors with Surprisingly High Analytical Figures of Merit. *J. Am. Chem. Soc.* **2013**, *135* (33), 12338–12345.

(114) Charrier, A.; Candoni, N.; Liachenko, N.; Thibaudau, F. 2D Aggregation and Selective Desorption of Nanoparticle Probes: A New Method to Probe DNA Mismatches and Damages. *Biosens. Bioelectron.* **2007**, *22* (9–10), 1881–1886.

(115) Duan, R.; Wang, B.; Hong, F.; Zhang, T.; Jia, Y.; Huang, J.; Hakeem, A.; Liu, N.; Lou, X.; Xia, F. Real-Time Monitoring of Enzyme-Free Strand Displacement Cascades by Colorimetric Assays. *Nanoscale* **2015**, *7* (13), 5719–5725.

(116) McKenzie, F.; Faulds, K.; Graham, D. Sequence-Specific DNA Detection Using High-Affinity LNA-Functionalized Gold Nanoparticles. *Small* **2007**, *3* (11), 1866–1868.

(117) Sato, K.; Hosokawa, K.; Maeda, M. Rapid Aggregation of Gold Nanoparticles Induced by Non-Cross-Linking DNA Hybridization. *J. Am. Chem. Soc.* **2003**, *125* (27), 8102–8103.

(118) Veigas, B.; Machado, D.; Perdigão, J.; Portugal, I.; Couto, I.; Viveiros, M.; Baptista, P. V. Au-Nanoprobes for Detection of SNPs Associated with Antibiotic Resistance in Mycobacterium Tuberculosis. *Nanotechnology* **2010**, *21* (41), 415101.

(119) Lee, H.; Kim, A.; Ahn, I.-S.; Joo, S.-W.; Lee, S. Y.; Yoon, K.-A.; Lee, K. Colorimetric Detection Ofc-Kit Mutations Using Electrostatic Attraction Induced Aggregation of Peptide Nucleic Acid Modified Gold Nanoparticles. *Chem. Commun.* **2011**, *47* (41), 11477–11479.

Chapter 2. Sensitivity Limit of Nanoparticle Biosensors in the Discrimination of Single Nucleotide Polymorphism

Abstract

Selective aggregation of nanoparticles offers a rapid determination of cancer biomarkers, detectable by the naked eye. The number of available target DNA molecules per particle is the limiting factor of sensitivity of such colloidal sensors. Although the particle size is an important experimental parameter of in the design of the assay towards the modulation of the target-to-particle ratio at constant metal concentration, the NPs size is often omitted due to the issues with colloidal stability of large particles functionalized with DNA. In this chapter, the gold nanoparticles with increasing diameter from 13, 46, to 63 nm are used as colloidal signal transducer to find the optimal ratio between the analyte and nanoparticls in the discrimination of SNP. It has been found that 5-fold increase in particle size, at constant gold concentration, leads to an improvement in the limit of detection by 3 orders of magnitude, which is 5, 0.1, and 0.05 nM for 13, 46, and 63 nm, respectively. Interestingly, regardless of particles diameter a target-to-particle ratio equal to 4 sets the limit of detection and sensitivity of presented colloidal assay.

2.1 Introduction

Back in 1997, Mirkin's group has demonstrated the feasibility of using plasmonic nanoparticles for single-nucleotide detection[1,2]. A sandwich approach was stablished in which gold nanoparticles capped with different DNA strands underwent aggregation in the presence of a mutually complementary DNA sequence. Interestingly, by introducing a single-base mutation into the analyte sequence, the aggregation was less pronounced. Since then, progress in the field has allowed an increasing complexity in colorimetric assays, thus improving their performance in parameters such as sensitivity, selectivity, and detection time[3–5]. In most of these studies, 13 nm gold nanoparticle signal transducers were used, primarily due to the simplicity of the Turkevich synthesis method[6]. Although these nanoparticles are useful for conceptual definition of the assay, their extinction coefficient is low compared to particles with larger diameter ($\sigma_{ext} \propto D^6$)[7], rendering limited capacity of transducing a chemical event into an optical signal. The central hypothesis of this chapter relates to the fact that the physical limitation of any colloidal (bio)sensor relates to the ratio of target molecules (here DNA) to nanoparticles. Therefore, with increasing the nanoparticles diameter at constant metal concentration, the number of nanoparticles decreases, lowering thus the amount of molecules required to aggregate and therefore transduce the signal. In addition, the lower curvature of larger particles would facilitate multiple binding events by DNA to connect NP probes[8]. Figure 1 describes the composition of the colloidal assay used in this chapter for the discrimination of SNP.

The effect of particle size on the discrimination of single nucleotide polymorphism was evaluated in the case of BRCA1 gene. This gene is one of the most studied one in the context of the single base mutation. To ensure relatively facile discrimination of the mutation, the match and the mismatch sequences were parametrized according to the nearest-neighbor model[9], which dictates the following structural requirements: 1) central position of the mutation in the sequence; 2) relatively short sequences (19 bases); 3) low CG content (26% for mismatch and 31% of match); 4) mismatch type affecting the C–G base pair instead of A–T (see **Figure 2.1**).

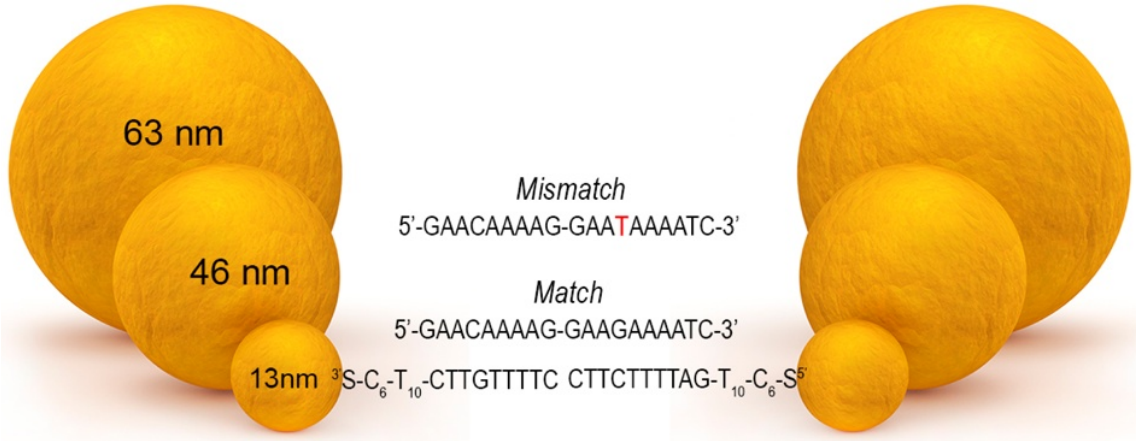

Figure 2.1. Scheme displaying the sequences of thiolated oligonucleotides and target DNA (match and mismatch), together with particles of different sizes.

2.2 Experimental Part

2.2.1 Chemicals

Hydrogen tetrachloroaurate (III) hydrate ($HAuCl_4 \cdot 3H_2O$) was purchased from Alfa Aesar. Sodium dodecyl sulfate (SDS) (98%), sodium chloride (NaCl) (99.5%), sodium citrate tribasic dihydrate (98%), and phosphate buffer (PB) 1 M, pH 7.4, were purchased from Sigma-Aldrich. To quantify the concentration of DNA loaded on NPs, the Quant-iT Oli Green ssDNA Kit was purchased from Thermo Fisher Scientific. Phosphate buffered saline (PBS) 0.01 M, pH 7.4, containing 0.138 M NaCl and 2.7 mM KCl (Sigma- Aldrich) was used to mimic physiological conditions. DNA-targets (match and mismatch) and thiolated-oligonucleotides (**Figure 2.1**) were purchased from Biomers (Germany).

2.2.2 Instrumentation

UV−vis spectra were measured at room temperature on an Agilent 8453 UV−vis spectrophotometer, using UV Micro cuvettes with 1.0 cm optical path length. Transmission electron microscopy (TEM) was measured in a JEOL JEM-1400 PLUS, operating at 120 kV, equipped with a GATAN US1000 CCD camera (2k×2k). Fluorescence measurements were performed in a MicroPlate Reader with an

excitation wavelength of 485 nm, an emission wavelength of 535 nm, number of reads: 10 and 40 µs of integration time.

2.2.3 Synthesis of Gold Nanoparticles

13 nm AuNPs. 13 nm AuNPs were prepared according to the standard Turkevich method[6]. In brief, a solution of $HAuCl_4$ (500 mL, 0.5 mM) was heated up to boiling in an 1 L Erlenmeyer flask, followed by the addition of trisodium citrate solution (25 mL, 1% w/v) under vigorous stirring. After 15 min of boiling, the solution was set aside to cool down to room temperature and stored at 4 °C for further use. The final concentration of metallic gold was 0.5 mM.

46 and 63 nm AuNPs. 46 and 63 nm AuNPs were synthesized following an Au-assisted seeded growth method[10]. Synthesis of Au seeds: a solution of trisodium citrate (150 mL, 2.2 mM) was heated for 15 min under vigorous stirring until boiling, followed by injection of a solution of HAuCl4 (1 mL, 25 mM). The color of the solution changed from yellow to bluish gray and then to light pink in 10 min. *Seeded Growth:* The seeded growth process comprised cyclic addition of metal precursor and extraction of particles product. In a typical process, the seed solution was cooled down to 90 °C and then HAuCl4 solution (1 mL, 25 mM) was added, followed by a second addition after 30 min. After a further 30 min period, part of the growth solution (55 mL) was extracted and to the remaining solution (98 mL) water (53 mL) and sodium citrate (2 mL, 60 mM) were added. This addition/extraction process was repeated 3 times to obtain gold nanoparticles with 46 nm diameter (55 mL). Subsequent repetitions of the process yielded 63 nm AuNPs (55 mL). The final concentration of metallic gold was 0.8 mM in both samples.

2.2.4 Functionalization of AuNPs

AuNPs were functionalized with thiolated oligonucleotides (1Triplex and 2Triplex) according to the method reported by Hurst et al[11]. Briefly, to the AuNPs colloid (1.11 mL) containing SDS (0.1%) and PBS (0.01 M) was added a solution of oligonucleotides to reach a final concentration of 1 OD/mL. An excess of oligonucleotides was used in all the samples, estimated as 2, 3, and 4 oligonucleotides

per nm^2 of gold surface, for 13, 43, and 63 nm AuNPs, respectively. The mixture of oligonucleotides and AuNPs was incubated at room temperature for 20 min. To improve oligonucleotide binding onto the gold surface a salt aging process was implemented. A solution containing NaCl (2 M), SDS (0.01%), and PBS (0.01 M) was added sequentially to the mixture containing AuNPs and oligonucleotides in the following aliquots: 5, 5, 15, 25, and 50 µL, ultimately reaching a final NaCl concentration of 0.2 M. After each addition the mixture was sonicated for 10 s followed by a 20 min incubation period. The final solution was incubated for 12 h. To remove excess oligonucleotides, the solutions were centrifuged three times (13 nm at 13000 rpm for 20 min; 46 nm at 8500 rpm for 15 min; 63 nm at 8500 rpm for 10 min), each time redispersed in SDS (1 mL, 0.01%). The final concentration of nanoparticles was 0.4 mM in terms of metallic gold for all the samples.

2.2.5 Quantification of Oligonucleotides Loaded on Gold Nanoparticles

The assay procedure is designed for use with standard microplate reader in a total volume of 200 µL. First, commercially-available oligonucleotide standard (100 µg/mL) was diluted 50-fold in TE buffer (10 mM Tris-HCl, 1 mM EDTA, pH 7.5) to give working solution (2 µg/mL). The working solution was diluted 20-fold to yield a 100 ng/mL oligonucleotide stock solution. For the standard curve, both oligonucleotide stock solutions (2 µg/mL and 100 ng/mL) were diluted into the 96-well microplate as shown in **Table 2.1**, followed by mixing and incubation for 5 minutes at room temperature, protected from light. After incubation, measure the fluorescence in the microplate reader with standard fluorescenin wavelengths (excitation 485 nm and emission 535 nm).

Volume of TE buffer	Volume of 2 µg/mL oligomer stock	Volume of diluted Quant-iT OliGreen reagent	Final oligomer concentration in Quant-iT OliGreen Assay
90 µL	10 µL	100 µL	100 ng/mL
95 µL	5 µL	100 µL	50 ng/mL
99 µL	1 µL	100 µL	10 ng/mL

Volume of TE buffer	Volume of 100 ng/mL oligomer stock	Volume of diluted Quant-iT OliGreen reagent	Final oligomer concentration in Quant-iT OliGreen Assay
90 µL	10 µL	100 µL	5 ng/mL
99 µL	1 µL	100 µL	0.5 ng/mL

Table 2.1. Protocol for preparing a low-range standard curve.

For the sample analysis, the DNA was chemically displaced from the nanoparticle surface using DTT. The displacement was achieved by adding equal volumes of oligonucleotide-functionalized gold nanoparticles (200 µL) and 1.0 M DTT in 0.18 M PB, pH 8.0 (200 µL). The oligonucleotides were released into solution during 3h incubation, and the gold precipitate was removed by centrifugation (6500 rpm, 5 min). To determine oligonucleotide concentration, supernatant (25 µL) was placed in a 96-well plate containing 75 µL of 1x TE buffer and 100 µL of Quant-iT OliGreen reagent. The fluorescence was measured and compared to the standard curve. The number of oligonucleotides per particle for each aliquot was calculated by dividing the concentration of oligonucleotides by the concentration of nanoparticles.

2.2.6 Hybridization of AuNP-DNA Probes and Detection of ssDNA Targets

Equal volumes (62.5 µL) of two batches containing Au@DNA (Au@1Triplex and Au@2Triplex) were combined into the UV mikro cuvette, followed by the addition of PBS (×1, 325 µL). To this solution was added 50 µL of a mixture containing PB (0.01 M) and NaCl (2 M) to reach the final volume of 0.5 mL. Finally, an aliquot of target ssDNA (either match or mismatch of the desired concentration) was added to the solution. Immediately after the addition of target ssDNA, UV−vis spectra were recorded during

30 at 0.5 min intervals. Since the stock solutions containing Au@DNA ([Au^0] = 0.4 mM) were stored in 0.01% SDS, the final concentration of the surfactant was 0.001% while the final concentration of metallic gold was 0.1 mM. The pH of the mixture was 7.4.

2.2.7 Hybridization of AuNP-DNA Probes and Detection of ssDNA Targets in Binary Mixtures

Equal volumes (62.5 µL) of two batches of NPs (Au@1Triplex and Au@2Triplex) were combined into a eppendorf, followed by the addition of PBS (x1, 325 µL). To this solution was added 50 µL of a mixture containing PB (0.01 M) and NaCl (2 M) to reach the final volume of 05mL. Finally, an aliquot of 23bases target ssDNA (match and mismatch in different molar ratios) in a total concentration of 5 nM was added to the solution. UV-Vis spectra were recorded each hour to study the aggregation process.

2.2.8 Dynamic Light Scattering Measurements

The conditions for the DLS experiments were: 6 measurements with 5 runs of 5 sec each one. The study was carried out at 25ºC with an equilibration time of the sample of 30s.

2.3 Results and Discussion

It is well-known that gold nanoparticles stabilized with sodium citrate can be readily functionalized with other thiolated ligands. Initially AuNPs were synthesised with an average diameter of 13.3 ± 1.2 nm, using the Turkevich method. These nanoparticles were used as seeds to grow larger AuNPs (45.9 ± 5.8 and 62.4 ± 6.5 nm in diameter), as described by Bastuś et al.[10] (for simplicity, we label the corresponding AuNPs as 13, 46, and 63 nm). Detailed TEM analysis revealed that all AuNPs displayed relatively low polydispersity values of 9%, 13%, and 11%, for 13, 46, and 63 nm, respectively (**Figure 2.2**).

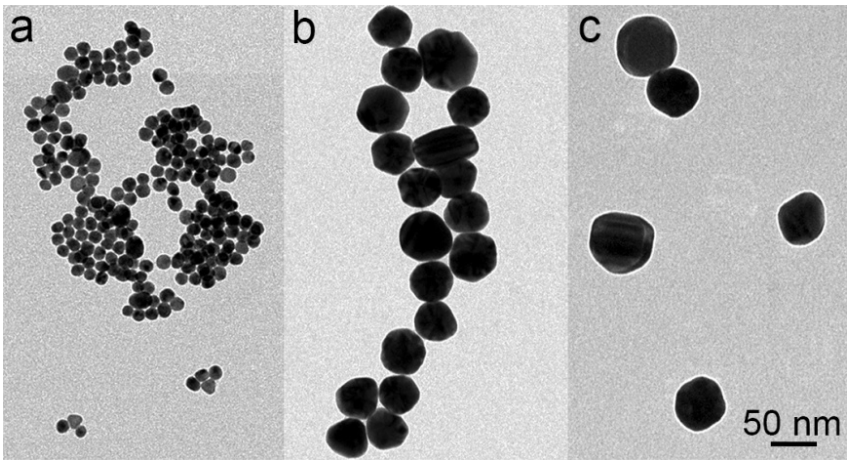

Figure 2.2. Gold nanoparticles used in this study. TEM images of initial AuNPs with different diameters: a) 13 nm, b) 46 nm, and c) 63 nm.

The replacement of citrate by the corresponding ssDNA was carried out as described by Mirkin's group[11], by mixing AuNPs of different sizes with excess of thiol-terminated oligonucleotides (1 OD/mL). To maximize surface coverage of the particles with oligonucleotides, the salting-out process was applied at higher NaCl concentration (0.2 M).

The maxima of the localized surface plasmon resonance (LSPR) bands of AuNP colloids were 519, 535, and 538 nm, for 13, 46, and 63 nm AuNPs, respectively. The presence of ssDNA on the particles surface caused a slight LSPR redshift of 2–5 nm, regardless of the particle size (**Figure 2.3**a), that was due to the increase in local refractive index. The presence of ssDNA on the particle surface was confirmed by DLS

measurements before and after functionalization. As expected, the hydrodynamic diameters increased by ≈10 nm (**Figure 2.3**b). In the case of 46 nm AuNPs, however, the increase of the recorded hydrodynamic diameter was less pronounced, likely due to a higher polydispersity (13%) of the sample.

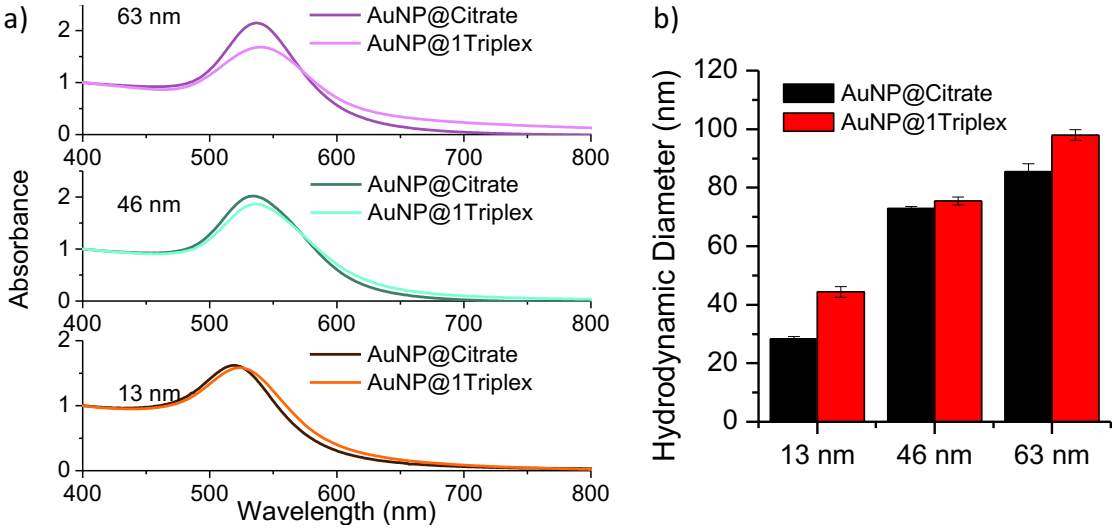

Figure 2.3. a) UV–vis spectra of AuNPs stabilized with citrate and DNA (1Triplex). b) Average hydrodynamic diameters of initial, citrate- stabilized AuNPs (black bars), and AuNP-1Triplex (red bars).

Once the nanoparticles were functionalized with DNA strands, a quantification of the oligonucleotides was carried out with the Quant-iT OliGreen ssDNA kit. First, a calibration curve was established in a concentration range between 0.5 and 100 ng/mL (**Figure 2.4**). Then DNA strands were displaced from AuNPs surface by using DTT (see experimental part) and the resulting supernatant was subjected for quantative determination of the DNA, using calibration curve as a reference. It has been found that with the increase of nanoparticle diameter the number of DNA ligands increased in the following order: 80, 450 and 850 DNA per 13 nm, 46 nm, 63 nm AuNP, respectively. The results reported in ref[11] are in agree with the data obtained from the fluorescence measurements.

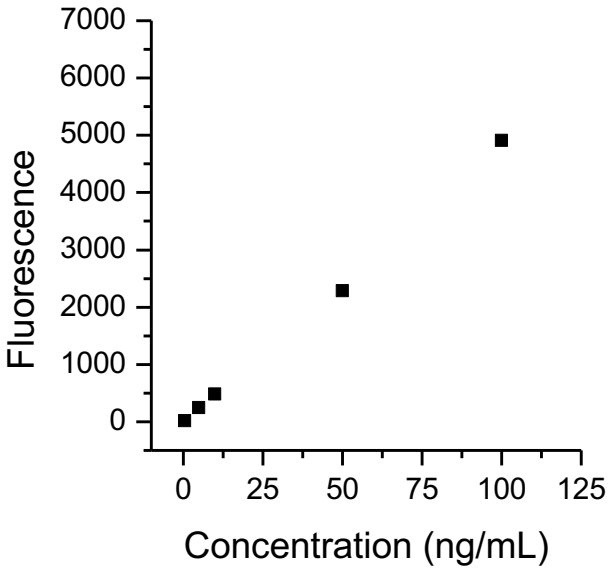

Figure 2.4. Linear quantification of a synthetic 24 bases from 0.5 to 500 ng/mL using the Quant-iT OliGreen ssDNA reagent. Samples were excited at 485 nm. The fluorescence emission intensity was measured at 535 nm and plotted as a function of oligonucleotide concentration.

To discriminate the mutation, a sandwich assay was performed involving the addition of a target sequence (either match or mismatch) to the mixture of probe nanoparticles, AuNP- 1Triplex and AuNP-2Triplex. The bridging of both probes on the surface of nanoparticles by the complementary target was expected to promote aggregation of the nanoparticles, in turn affecting the optical properties of the colloid[12,13]. In particular, the LSPR bands are expected to redshift and broaden, as a result of aggregation and plasmon coupling (**Figure 2.5**a,b). The aggregation of the particles was monitored over time by UV−Vis spectroscopy, using the unitless magnitude R = Abs_{620}/Abs_{max}, as a measure of the degree of aggregation[14]. Before target addition, the R value was ≈ 0.2. Once the target was added to the probes solution, R increased to reach a maximum value of ≈ 1.2 (best scenario). In addition, upon aggregation, the characteristic absorption band for oligonucleotides, located at 260 nm, was found to gradually decrease (**Figure 2.5**c), due to delocalization of the excitonic states in denatured DNA[15], wich is an additional sign of hybridization events.

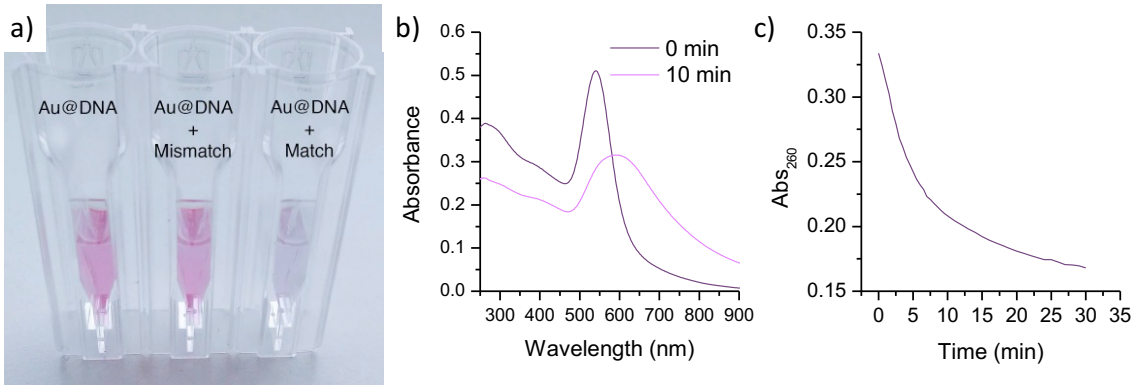

Figure 2.5. a) Digital images of the solution containing gold nanoparticles (63 nm) in the absence of target molecules (left), in the presence of the mismatch sequence (middle) and in the presence of the match sequence (right). In all cases, target concentration was 5 nM. b) UV-Vis spectra of the assay mixture containing 63 nm AuNPs and match sequence in a concentration of 5 nM at 0 and 10 minutes after the hybridization started. c) time-dependent changes of absorbance at 260 nm as a sign of DNA hybridization.

To properly evaluate the sensitivity of the assay for different particle sizes, the concentration [Au^0] = 0.1 mM was kept constant in all experiments. Therefore, changes in particle diameter affect to the number of particles (expressed in molar concentration) for each assay. The concentration of particles was 1.5, 0.033, and 0.013 nM for 13, 46, and 63 nm, respectively. Note that adjusting the assays to a constant number of particles (as opposite to Au^0 concentration) was not practical due to the dramatic difference in extinction cross section for different particle sizes (**Figure 2.6**a). For example, bringing the concentration of 13 nm AuNPs down to 0.013 nM made it impossible to record a meaningful UV−vis spectrum (**Figure 2.6**b). In addition, the difference in absorbance affected the value of R, which hindered a comparative analysis (**Figure 2.6**c).

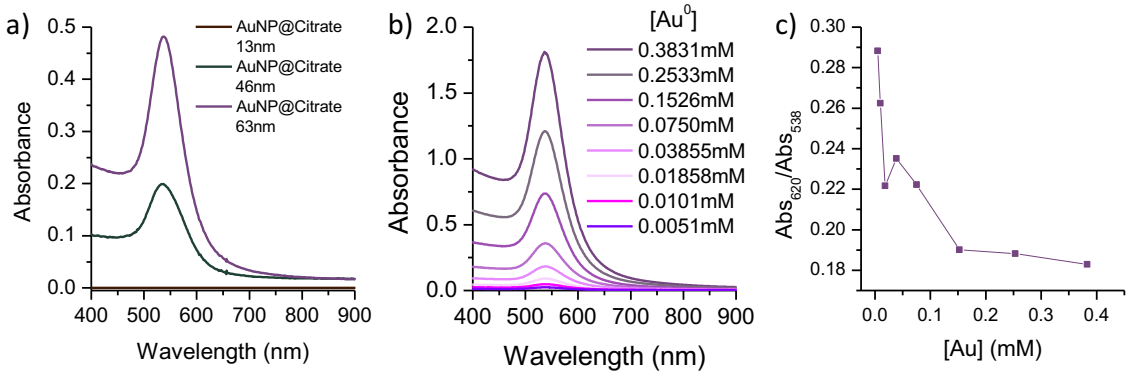

Figure 2.6. a) UV-Vis spectra of the colloids containing AuNP of different sizes, but with constant number of NPs (0.013 nM). The spectral features of the smallest nanoparticles are barely visible. b) UV-Vis spectra of the solutions containing different concentrations of gold nanoparticles. b) Variation of R (Abs_{620}/Abs_{538}) for various particle concentrations obtained from a.

An important experimental parameter was the concentration of NaCl used in an assay. It is commonly known that an extra amount of NaCl is required to favour particles aggregation through the icrease of ionic strength. In the absence of NaCl the particles remain colloidally stable even in the large excess of DNA. Opositely, at large mount of NaCl the ionic strength can abruptly cause particles aggregation regardless the presence of match or mismatch sequences, therefore affecting the selectivity of the assay. It was mandatory to find an optimal concentration of NaCl to reach best sensitivity and selectivity of the assay. Four different concentrations of NaCl (0, 0.2, 0.33 and 0.4 M) were used in colloidal assay using match and mismatch sequences (**Figure 2.7**). The raw spestra obtained in Figure 7 were further analysed by ploting aggregation rate values (R) vs. time (**Figure 2.8**). It has been found that the 0.33 M of NaCl was the most optimal salt concentration at which the highiest selectivity toward single base mutation was achieved.

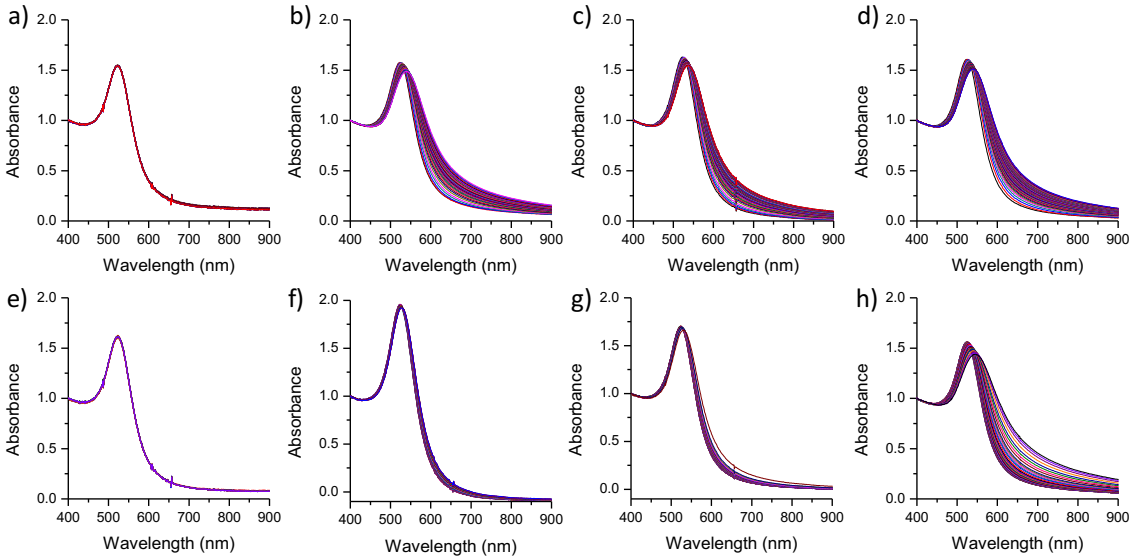

Figure 2.7. Effect of NaCl concentration on the aggregation of the particles. a-d) Aggregation of 13 nm AuNPs (1.5 nM) in the presence of match sequence (50 nM) with NaCl concentration increasing in following order 0, 0.2, 0.33 and 0.4 M. e-h) The same experimental conditions as in a-d but using mismatch sequence instead of match.

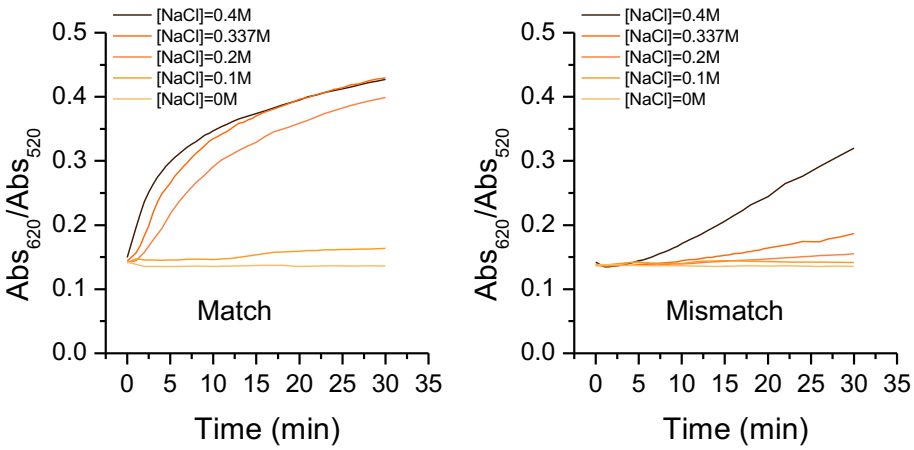

Figure 2.8. Effect of NaCl concentration on the specificity and hybridization rate of the assay towards single base mutation. Left) Aggregation of particles in the presence of match sequence obtained from Figure 2.7a-d. Right) Aggregation of particles in the presence of mismatch sequence obtained from Figure 2.7e-h. The greatest difference in particles aggregation for match and mismatch sequences was observed at 0.33 M of NaCl.

The aggregation degree was studied for the three nanoparticles diamenters and the different concentrations of match and mismatch sequences ranging from 0.05 to 50 nM. Figure 9 shows raw UV-Vis spectra of all solutions at given aggregation time, showing how the concentration of the target DNA molecules (match or mismatch) affects the colloidal stability of the nanoparticles.

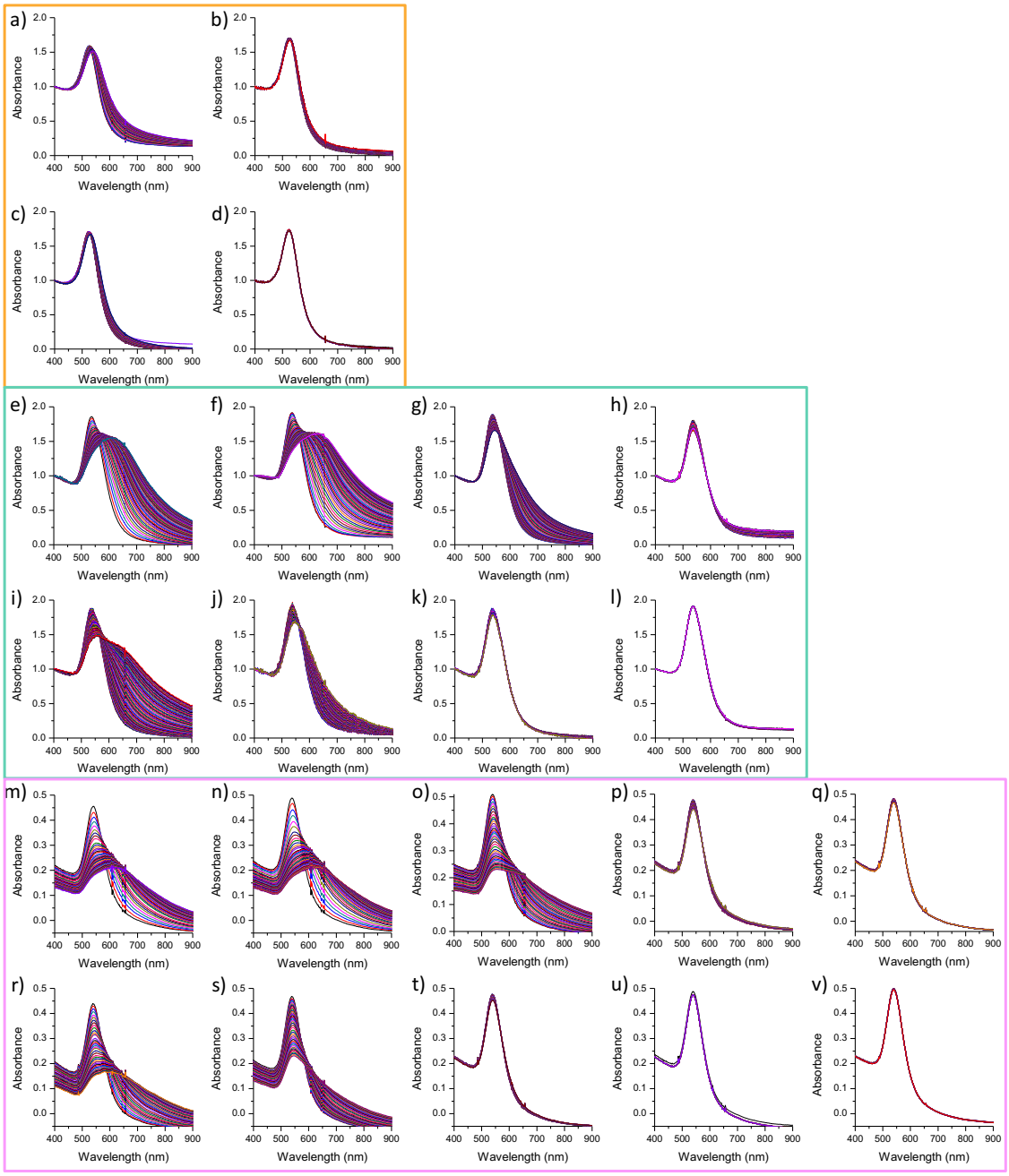

Figure 2.9. a-b) UV-Vis spectra for 13 nm AuNPs with match sequence in a concentration of 50 and 5 nM, respectively. c-d) UV-Vis spectra for 13 nm AuNPs with mismatch sequence in a concentration of 50 and 5 nM, respectively. e-h) UV-Vis spectra for 46 nm AuNPs with match sequence in a concentration of 50, 5, 0.5 and 0.25 nM, respectively. i-l) UV-Vis spectra for 46 nm AuNPs with mismatch sequence in a concentration of 50, 5, 0.5 and 0.25 nM, respectively. m-q) UV-Vis spectra for 63 nm AuNPs with match sequence in a concentration of 50, 5, 0.5, 0.1 and 0.05 nM, respectively. r-v) UV-Vis spectra for 63 nm AuNPs with mismatch sequence in a concentration of 50, 5, 0.5, 0.1 and 0.05 nM, respectively.

Further analysis of the data in Figure 2.9, allowed for the presentation of aggregation rate vs. time (**Figure 2.10**), clearly indicating the selectivity of the colloidal assay toward single base mutation (copare left and right columns). As expected, with increasing particle size, the sensitivity of the assay also increased. The smaller AuNPs (13 nm) aggregated in the presence of match sequence, within a concentration range between 50 and 5 nM. For the mismatch sequence, however, aggregation was only observed for concentrations above 50 nM (**Figure 2.10**a). The intermediate AuNPs (46 nm) aggregated in the presence of the match sequence at a broader concentration range between 50 and 0.25 nM. For the mismatch sequence, aggregation was detected for target concentrations above 5 nM. Finally, the larger particles (63 nm) were sensitive to an even widerconcentration range (50-0.05 nM) of the match sequence, but only between 5 and 50 nM for the mismatch sequence.

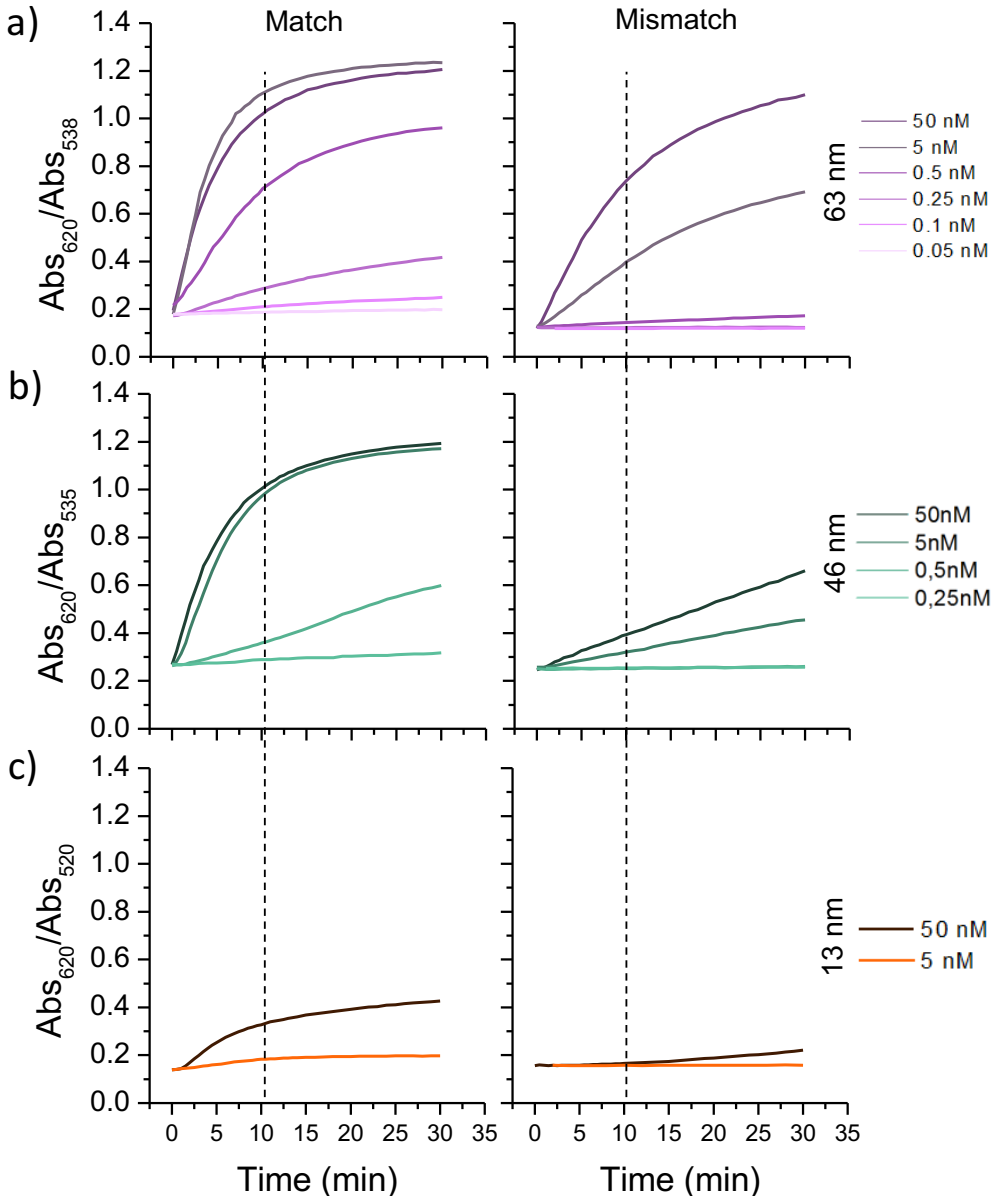

Figure 2.10. Sensitivity of the assay for AuNPs with different diameters. Comparison of the aggregation degree for match (left column) and mismatch (right column) sequences, with AuNPs of different sizes: (a) 63 nm, (b) 46 nm, (c) 13 nm. [Au^0] = 0.1 mM for all cases, while [AuNPs] varied as 1.5, 0.033, and 0.013 nM, for 13, 46, and 63 nm, respectively.

These results clearly suggest that the sensitivity of the assay depends on the available number of target molecules per particle. A careful comparison of the concentrations of target and particles revealed that it was necessary to add ≈4 molecules of match sequence per particle to induce meaningful changes in the R value (**Table 2.2**). Interestingly, the concentration of the mismatch sequence that was required to induce aggregation was 20-40 times higher than the concentration of nanoparticles, showing that the single base mutation has a large impact on the aggregation process.

[ssDNA Target]	Number of target ssDNA per NPs		
	AuNP 13 nm	AuNP 46 nm	AuNP 63 nm
50 nM	34	1505	3867
5 nM	3.4	150.5	386.7
0.5 nM	n.a	15.05	38.67
0.25 nM	n.a	7.53	19.34
0.1 nM	n.a	3.01	7.73
0.05 nM	n.a	n.a	3.87

Table 2.2. Number of target sDNA per particle at different sizes.

To further evaluate the aggregation process, DLS technique was implemented to measured the time-dependent growth of the aggregates. A fixed concentration (5 nM) of match and mismatch sequences were used for aggregation, yielding the following target-to-particle ratios: ≈3 (13 nm), ≈150 (46 nm), and ≈380 (63 nm). A possible hypothesis is that the small nanoparticles should remain stable, since insufficient target was provided, while the bigger particles should aggregate. As shown in **Figure 2.11**a, b, when exposed to the match sequence, the aggregates containing NPs of 46 and 63 nm were 2.5-fold larger than those from the same particles after 1 h in the presence of the mismatch sequence. After 60 min of aggregation in the presence of the match sequence, the clusters were ca. 550 nm in diameter for both 46 and 63 nm AuNPs, corresponding to ≈150 and ≈320 particles per cluster, respectively. In the case of small NPs, no aggregation was observed when the mismatch sequence was used **(Figure 2.11**c). In the presence of the match sequence, the measured diameter

increased up to 20 nm, which is likely related to intercalation of target DNA with the complementary DNA attached to the particle surface. No further aggregation was observed upon extended incubation, probably due to an insufficient number of target molecules per particle (≈3).

TEM analysis of the aggregates (in the presence of the match sequence) was performed at 1, 10, and 15 min after target addition (**Figure 2.11**d-f). The number of particles per aggregate increased from 3–5 to 15–20 for 1 and 10 min, respectively. After 15 min, the diameter of the aggregates was nearly 1 µm, i.e., >100 AuNPs. Note that the diameter of the aggregates on TEM grids appears larger than in solution due to flattening upon drying.

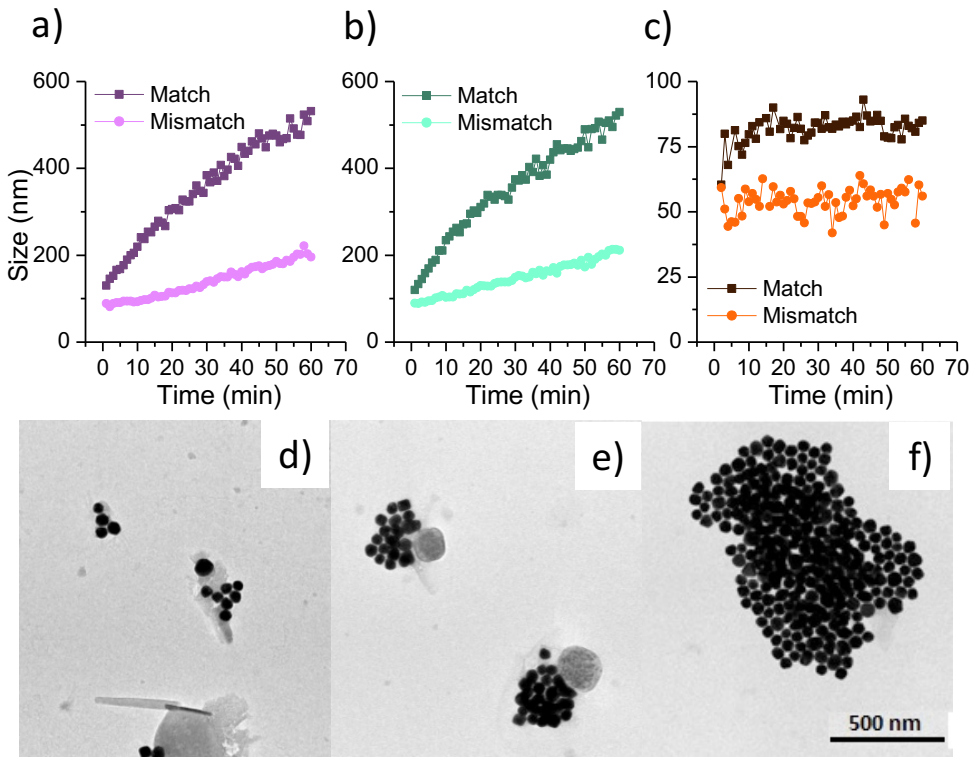

Figure 2.11. a–c) DLS measurements for the hybridization process using the match and mismatch sequences at 5 nM concentration for AuNPs of: a) 63 nm, b) 46 nm, and c) 13 nm. d–f) TEM images of aggregates formed upon hybridization with the match sequence at a concentration of 5 nM for AuNP of 63 nm at: d) 1 min, e) 10 min, and f) 15 min.

Several control experiments were additionally conducted. No aggregation was observed in the absence of the target ssDNA for 63 nm AuNPs (**Figure 2.12**a). A melting profile analysis confirmed the selective role of the match sequences in the particle aggregation. For the match sequence, a sharp transition in the profile was observed at 43 °C, whereas for the mismatch sequence no change in particle size was detected (**Figure 2.12**b). The heating process had no effect on the stability of the particles, as cyclic aggregation kinetics showed a similar degree of aggregation during three cycles of heating (**Figure 2.12**c, d).

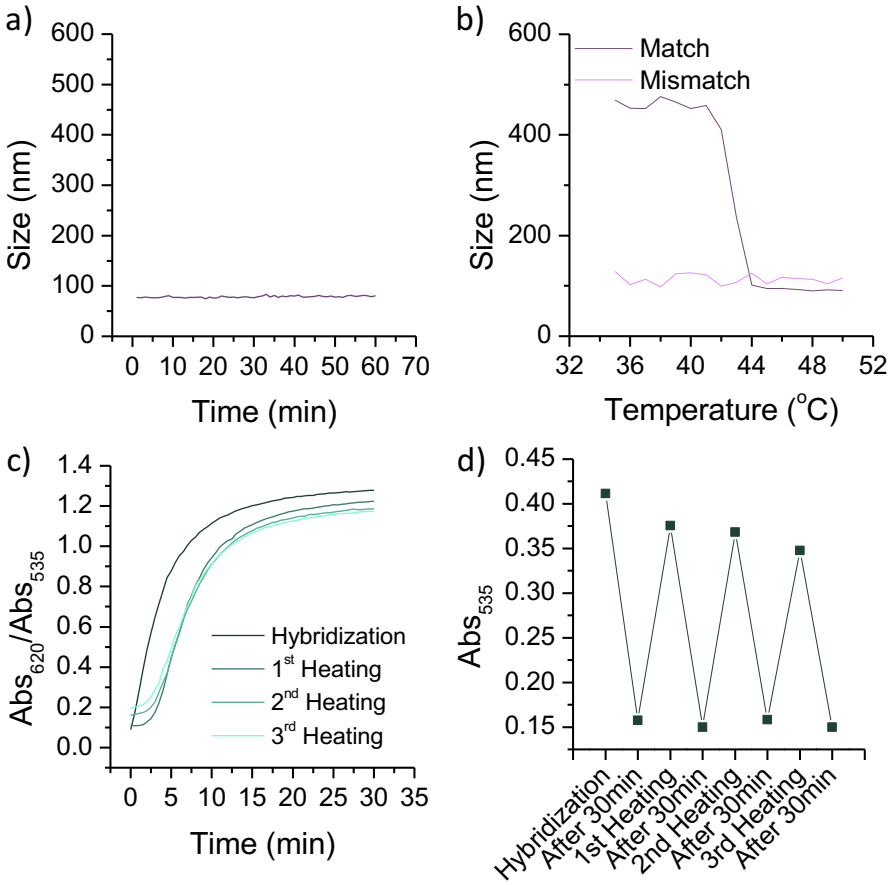

Figure 2.12. a) Time dependent DLS measurements of the control solution of 63 nm AuNPs assay in the absence of match target sequence showing stability of the particles over the experiment time-scale. b) Melting profile of the aggregates containing AuNPs of 63 nm, in the presence of match and mismatch sequences (5 nM). c) Aggregation degree for three hybridization cycles after several heating processes. d) Absorbance values recorded at 535 nm during the hybridization and heating processes.

The next step was to evaluate the effect of particle size on the selectivity of the assay. The R values for the match and mismatch after 10 min of aggregation were compared (see vertical dashed line in **Figure 2.10**). The values of R for selected particle sizes and target concentrations are shown in **Figure 2.13**a, demonstrating that the values of R converge for match and mismatch sequences when decreasing the concentration of the target. Further analysis of the selectivity allows differentiating the value of R_{match} from $R_{mismatch}$ after 10 min of aggregation (**Figure 2.13**b). A target concentration window can be identified for the bigger particles, at which they display the best sensing performance. For example, in the case of the 63 nm particles it is possible to differentiate between the match and mismatch down to 0.05 nM. However, when the concentration of the target was increased the difference becomes less pronounced. This behavior is due to a cooperative effect, meaning that the lower curvature of the larger particles facilitates aggregation through binding more than one DNA target molecule per particle. Note that at 50 nM target concentration, each 63 nm particle carries ≈4000 target molecules for either match or mismatch DNA. Therefore, the differentiation between match and mismatch is less pronounced if multiple binding events take place[16]. In the case of the particles with a diameter of 46 nm, the selectivity between the match and mismatch at higher concentration (50 nM) is better than that for 63 nm particles (**Figure 2.13**b). The higher curvature in 46 nm particles minimizes the cooperative effect and favors the specificity of the system at higher target concentrations. However, at lower target concentrations (<1 nM) the system becomes less specific due to the smaller number of available DNA target molecules per particle. Accordingly, for the small (13 nm) particles the specificity increases with increasing target concentration, but with no selectivity below 5 nM.

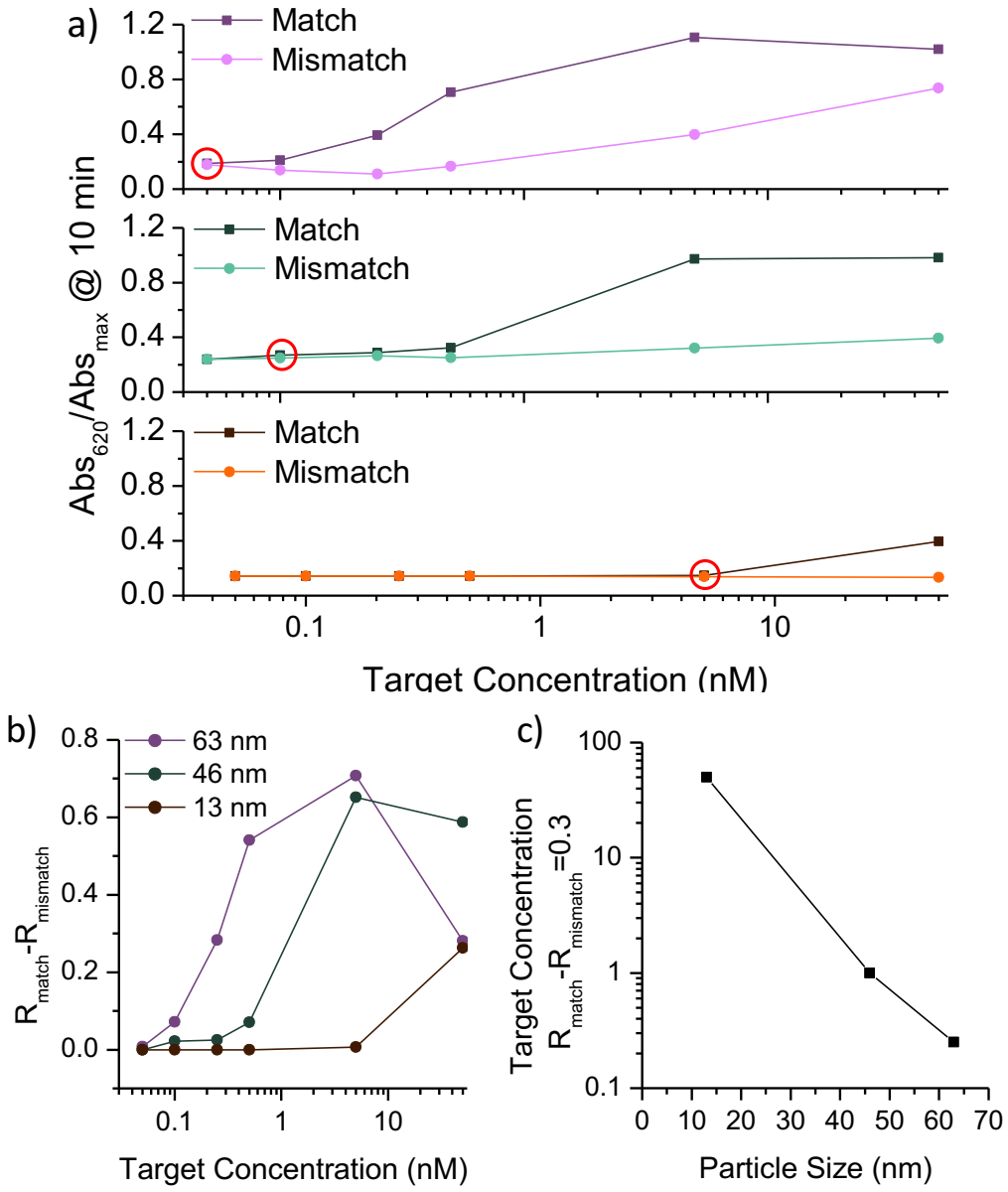

Figure 2.13. Selectivity between match and mismatch sequences for different concentrations of target, using AuNPs of different sizes. a) Differences in the aggregation degree (Abs_{620}/Abs_{max}) for the different particle sizes, at a target concentration range from 50 to 0.05 nM. The points circled in red represent the limit of selectivity (match/mismatch) and correspond to a target-to-particle ratio equal to 4. b) Difference between R values for match and mismatch versus target concentration, showing better specificity for larger particles. c) Target concentration at R_{match} - $R_{mismatch}$ = 0.3 versus particle size, showing a linear dependence in a logarithmic scale.

To further show how the particle dimension affects the performance of the assay, the selectivity of the assay was correlated with particle diameter at constant specificity. A plot of target concentration at R_{match} - $R_{mismatch}$ = 0.3 versus particle diameter shows a linear dependence in a semilog plot (**Figure 2.13**c). This relationship indicates that a 5-fold increase in particle size leads to an improvement of SNP differentiation by 3 orders of magnitude. In other words, by using particles with diameter of 150 nm, we should be able to differentiate SNP down to 10 fM. These results show that the design of the colloidal assay for biomolecule detection requires a precise knowledge of the concentration window for the target detection.

To further evaluate the importance of the ratio between number of target molecules and the number of gold nanoparticles, three different assays were performed in which the concentration of target DNA and nanoparticles were correspondingly decreased to maintain the tareget-to-particles ratio equal to 4 (**Figure 2.14**). For the 63 nm AuNPs in a concentration of 13 pM, a ratio of 4 is the minimum required to appreciate aggregation, which corresponds to 50 pM of match DNA (**Figure 2.14**a). With a further decrease of particle and target concentrations (keeping the target-to-particle ratio constant ≈4) the limit of detection could be improved. **Figure 2.14**b shows the time evolution of R using 10 pM of match and mismatch DNA with an AuNP concentration of 3 pM. A meaningful difference between match and mismatch is observed after 10 min of aggregation. Additionally, another experiment was carried out using a target-to-particle ratio of 0.8 (**Figure 2.14**c) to detect the same concentration of target, 10 pM, but with a higher concentration of NPs, 13 pM. With these conditions is not possible to see differences between the match and the mismatch aggregation. The results confirm that the limits in colorimetric assays are related to the minimum number of target molecules available to induce particle aggregation, clearly indicating that the target concentration should always be larger than that of nanoparticles. Finally, when decreasing the target concentration down to 5 pM while keeping the target-to-particle ratio equal to 4, a significant fluctuation of the R value was observed for both match and mismatch making impossible to distinguish between them (**Figure 2.14**d).

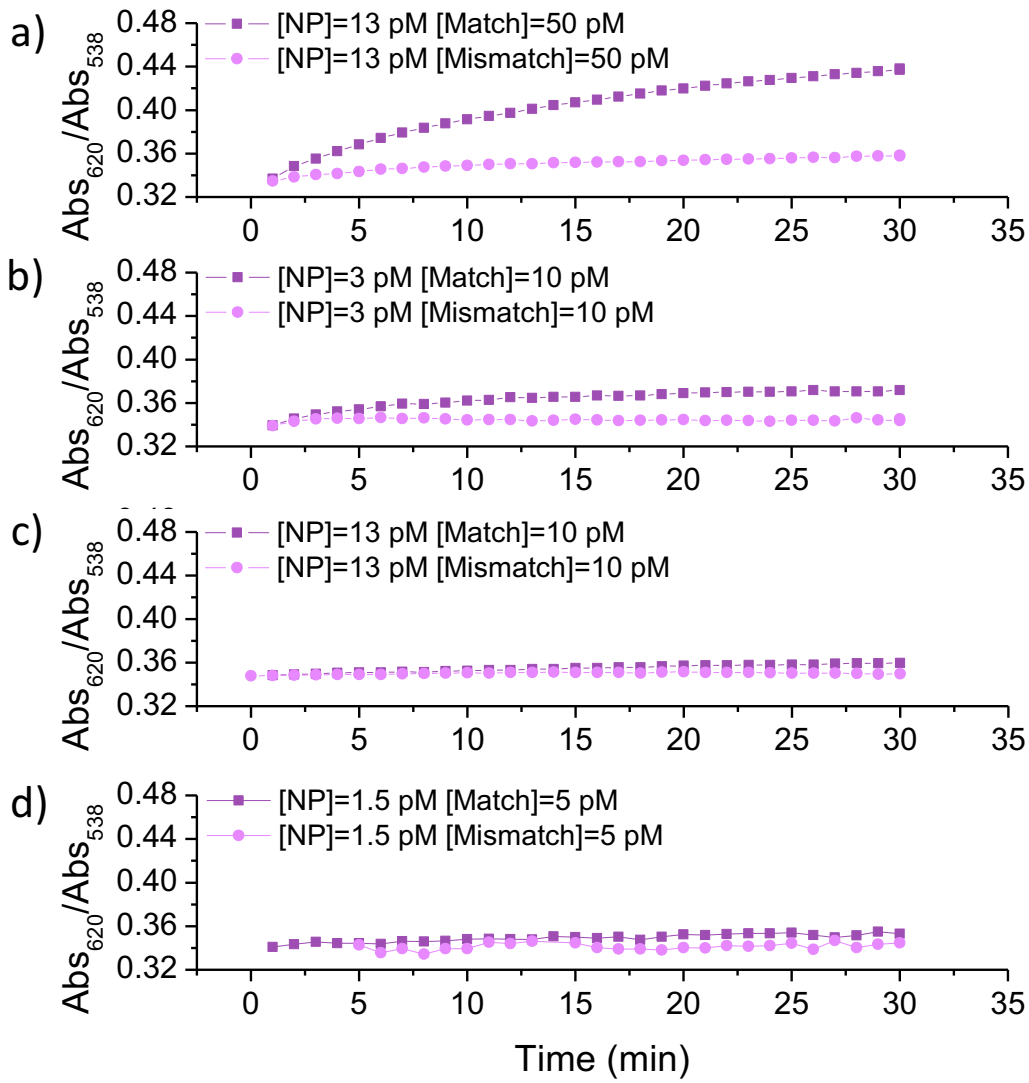

Figure 2.14. Comparation of the aggregation degree with different concentrations of target sequences and NPs a,b) target-to-particle ratio was 4. c) target-to-particle was 0.8, showing no differentiation. d) target-to-particle was 4, but at nanoparticle concentration below detection limit of the spectrophotometer.

An important parameter for clinical assays is the ability to detect a single base mutation (point mutation) in a mixture, containing both match and mismatch sequences in different concentrations. Different mixtures were investigated with different match/mismatch molar ratio, keeping constant the total concentration at 5 nM. The hybridization rate for 0:100, 30:70, 50:50, 70:30, 90:10 and 100:0 M:MM mixtures are shown in **Figure 2.15**.

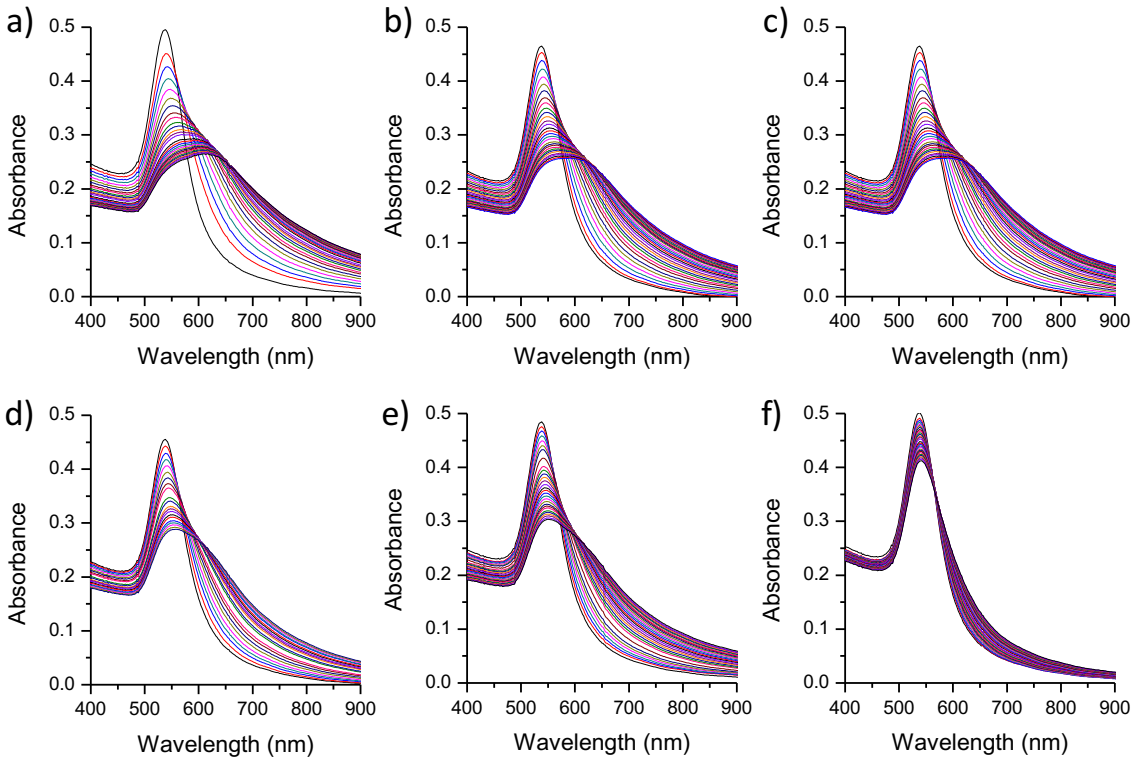

Figure 2.15. UV-Vis spectra for the binary mixtures comprising match and mismatch sequences in different ratios: a) 100:0, b) 90:10, c) 70:30, d) 50:50, e) 30:70 and f) 0:100.

The raw data shown in Figure 2.15 were analyzed by plotting the aggregation rate vs. time, showing that the extend of nanoparticles aggregation increases with decreasing the amount of mismatch sequences in the solution (**Figure 2.16a**). The 100% of match or mismatch sequences defines the upper and lower limits of the aggregation rate for given time. The intermediate portion between match and mismatch falls witin such limit, as expected. In addition, the tendency of increased aggregation rate with decreasing the amount of mismatch sequences was clearly reflected. This observation suggests that the mismatch target acts as interference in the hybridization process of the match target, behaving as a competitor. In addition, the linear relation between the aggregation rate and the concentration of mismatch (**Figure 2.16**b) can serve as a calibration curve form which one can deduce the relative molar ratios between the match and mismatch sequences.

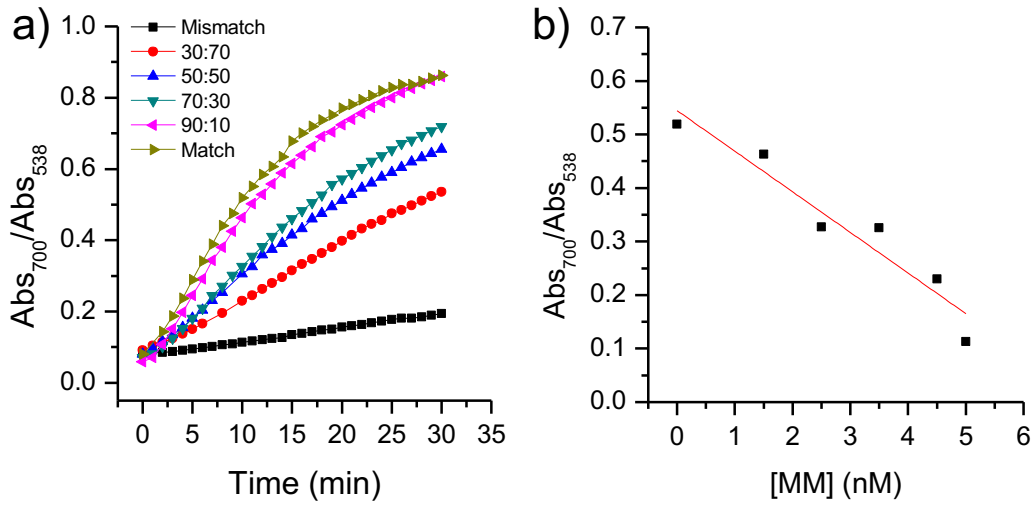

Figure 2.16. a) Kinetic analysis of binary system (match and mismatch) as a function of time for different molar ratios. b) Calibration curve for the aggregation degree at 10 minutes versus the concentration of mismatch sequence in the mixture.

2.4 Conclusions

In this chapter, it has been demonstrated that nanoparticle size is an important experimental factor defining sensitivity and selectivity of a colorimetric detection assay of the BRCA1 mutation. It was shown that at constant gold concentration and varying particle size, the best sensitivity was obtained when using larger particles of 63 nm. This trend was explained in terms of a higher target-to-particles ratio, as compared to smaller AuNPs. Using 63 nm particles it is possible to differentiate the match from the mismatch sequence at concentrations down to 10 pM. Particle size was also found to affect the selectivity of the assay. Larger particles were more selective at lower target concentrations, but less selective at larger target concentrations, which was due to the lower surface curvature, that increased the probability of multiple binding events. The results of the study show that colloidal biosensors based on AuNP aggregation have an intrinsic limitation, related to the number of target molecules per particle. Furthermore, it is possible to know the molar ratio between the match and the mismatch sequence in a binary solution taking into account only the value of the aggregation degree at 10 minutes.

2.5 References

(1) Elghanian, R.; Storhoff, J. J.; Mucic, R. C.; Letsinger, R. L.; Mirkin, C. A. Selective Colorimetric Detection of Polynucleotides Based on the Distance-Dependent Optical Properties of Gold Nanoparticles. *Science* **1997**, *277* (5329), 1078–1081.

(2) Storhoff, J. J.; Elghanian, R.; Mucic, R. C.; Mirkin, C. A.; Letsinger, R. L. One-Pot Colorimetric Differentiation of Polynucleotides with Single Base Imperfections Using Gold Nanoparticle Probes. *J. Am. Chem. Soc.* **1998**, *120* (9), 1959–1964.

(3) Quan, K.; Huang, J.; Yang, X.; Yang, Y.; Ying, L.; Wang, H.; Wang, K. An Enzyme-Free and Amplified Colorimetric Detection Strategy: Assembly of Gold Nanoparticles through Target-Catalytic Circuits. *Analyst* **2015**, *140* (4), 1004–1007.

(4) Ma, C.; Wang, W.; Mulchandani, A.; Shi, C. A Simple Colorimetric DNA Detection by Target-Induced Hybridization Chain Reaction for Isothermal Signal Amplification. *Anal. Biochem.* **2014**, *457*, 19–23.

(5) Wang, Q.; Li, R.-D.; Yin, B.-C.; Ye, B.-C. Colorimetric Detection of Sequence-Specific microRNA Based on Duplex-Specific Nuclease-Assisted Nanoparticle Amplification. *Analyst* **2015**, *140* (18), 6306–6312.

(6) Turkevich, J.; Stevenson, P. C.; Hillier, J. A Study of the Nucleation and Growth Processes in the Synthesis of Colloidal Gold. *Discuss. Faraday Soc.* **1951**, *11* (0), 55–75.

(7) Jain, P. K.; Lee, K. S.; El-Sayed, I. H.; El-Sayed, M. A. Calculated Absorption and Scattering Properties of Gold Nanoparticles of Different Size, Shape, and Composition: Applications in Biological Imaging and Biomedicine. *J. Phys. Chem. B* **2006**, *110* (14), 7238–7248.

(8) Hurst, S. J.; Hill, H. D.; Mirkin, C. A. "Three-Dimensional Hybridization" with Polyvalent DNA–Gold Nanoparticle Conjugates. *J. Am. Chem. Soc.* **2008**, *130* (36), 12192–12200.

(9) Naiser, T.; Ehler, O.; Kayser, J.; Mai, T.; Michel, W.; Ott, A. Impact of Point-Mutations on the Hybridization Affinity of Surface-Bound DNA/DNA and RNA/DNA Oligonucleotide-Duplexes: Comparison of Single Base Mismatches and Base Bulges. *BMC Biotechnol.* **2008**, *8*, 48.

(10) Bastús, N. G.; Comenge, J.; Puntes, V. Kinetically Controlled Seeded Growth Synthesis of Citrate-Stabilized Gold Nanoparticles of up to 200 Nm: Size Focusing versus Ostwald Ripening. *Langmuir* **2011**, *27* (17), 11098–11105.

(11) Hurst, S. J.; Lytton-Jean, A. K. R.; Mirkin, C. A. Maximizing DNA Loading on a Range of Gold Nanoparticle Sizes. *Anal. Chem.* **2006**, *78* (24), 8313–8318.

(12) Murphy, C. J.; Gole, A. M.; Stone, J. W.; Sisco, P. N.; Alkilany, A. M.; Goldsmith, E. C.; Baxter, S. C. Gold Nanoparticles in Biology: Beyond Toxicity to Cellular Imaging. *Acc. Chem. Res.* **2008**, *41* (12), 1721–1730.

(13) Ghosh, S. K.; Pal, T. Interparticle Coupling Effect on the Surface Plasmon Resonance of Gold Nanoparticles: From Theory to Applications. *Chem. Rev.* **2007**, *107* (11), 4797–4862.

(14) Liu, Y.; Liu, Y.; Mernaugh, R. L.; Zeng, X. Single Chain Fragment Variable Recombinant Antibody Functionalized Gold Nanoparticles for a Highly Sensitive Colorimetric Immunoassay. *Biosens. Bioelectron.* **2009**, *24* (9), 2853–2857.

(15) D'Abramo, M.; Castellazzi, C. L.; Orozco, M.; Amadei, A. On the Nature of DNA Hyperchromic Effect. *J. Phys. Chem. B* **2013**, *117* (29), 8697–8704.

(16) Reynolds, R. A.; Mirkin, C. A.; Letsinger, R. L. Homogeneous, Nanoparticle-Based Quantitative Colorimetric Detection of Oligonucleotides. *J. Am. Chem. Soc.* **2000**, *122* (15), 3795–3796.

Chapter 3. Nanoparticle-based Discrimination of Single Nucleotide Polymorphism in Long Single-Stranded DNA Sequence

Abstract

As discussed in Chapter 1, circulating DNA and specifically the detection cancer-associated mutations in liquid biopsies promises to revolutionize cancer detection. The main difficulty however is that the length of typical ctDNA fragments (~150 bases) can form secondary structures potentially obscuring the mutated fragment from detection. This chapter deals with an assay based on gold nanoparticles that discriminate single nucleotide polymorphism in clinically relevant ssDNA sequences (70–140 bases). The preincubation step was crucial to this process, allowing sequential bridging of Au@DNA, so that single base mutation can be discriminated, down to 100 pM concentration.

3.1 Introduction

Tumor cells release into the blood circulating tumor DNA (ctDNA) that contains the mutations of the original tumor[1]. These sequences can be either single- or double-stranded DNA, possessing cancer-related molecular characteristics, such as single nucleotide mutations[2,3], methylation changes[4,5] and cancer-derived viral sequences[6]. As demonstrated in Chapter 2, as well as other groups works, the detection of single nucleotide polymorphisms (SNP) in ssDNA sequences by selective aggregation of plasmonic nanoparticles provide the potential for rapid determination of cancer biomarkers[7–9]. Although the literature data shows that detection of sequences of up to 40 bases without any signal amplification is feasible[10,11], the average size of circulating DNA is ≈150 bases in length[12], and these longer fragments are more problematic as the increase of the sequence length affects the plasmon coupling (larger gaps between the particles), that decrease the limit of detection[13]. In addition, long DNA sequences form thermodynamically stable secondary structures that render the detection even more difficult[14]. Therefore, there is an obvious need for new solutions to detect long DNA sequences. In Chapter 2, It was shown that plasmonic assay comprising DNA-coated gold nanoparticles (AuNPs) could discriminate SNP in less than 10 min. Even though relatively large particles may lead to plasmon coupling upon aggregation, the assay was limited to the detection of rather short sequences (up to 23 bases). Therefore, to meet the main hypothesis of the presented thesis, large plasmonic particles (65 nm) functionalized with modified DNA[15] are used to detect single base mutation in clinically relevant sequences, that is, with 140 bases in length. **Figure 3.1** describes in comparative manner the detection strategies discussed in present Chapter. In standard assay, the addition of the target DNA to the mixture of two batches had no effect on the aggregation (**Figure 3.1**a). However, premixing the AuNPs (batch) with the target DNA was sufficient to induce aggregation upon the addition of batch 2 (**Figure 3.1**b), hence preincubation assay.

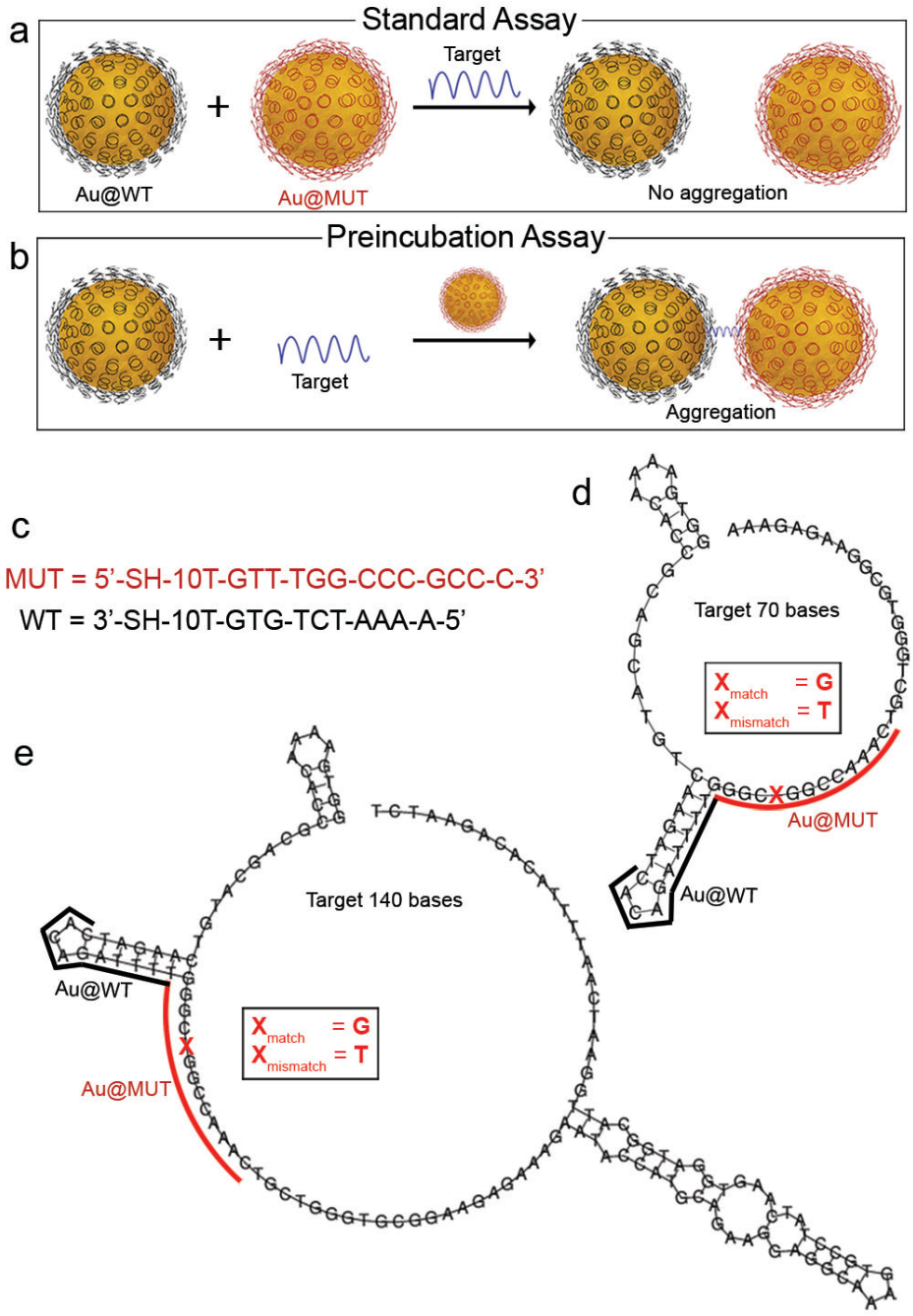

Figure3.1. General description of the detection strategy. a) Standard sandwich assay in which the addition of the long DNA target to the mixture of two different AuNP-DNA probes has no effect on the aggregation. b) Preincubation of one batch of AuNP-DNA probes with the target, followed by the addition of the second batch of probes, leads to sensitive detecrtion. c) Selected sequence of DNA stabilizing gold nanoparticles. d,e) Possible secondary structure (Dynalign) of the target sequences sed in this study showing the complementary sequences to those on the nanoparticles and position of the mutation.

3.2 Experimental Part

3.2.1 Chemicals

Hydrogen tetrachloroaurate (III) hydrate ($HAuCl_4 \cdot 3H_2O$) was purchased from Alfa Aesar. Sodium dodecyl sulfate (SDS) (98%), sodium chloride (NaCl) (99.5%), sodium citrate tribasic dihydrate (98%), and phosphate buffer (PB) 1 M, pH 7.4, were purchased from Sigma-Aldrich. Phosphate buffered saline (PBS) 0.01 M, pH 7.4, containing 0.138 M NaCl and 2.7 mM KCl (Sigma-Aldrich) was used to mimic physiological conditions. DNA-targets (match, mismatch and random) and thiolated-oligonucleotides (**Table 3.1**) were purchased from Biomers (Germany). To quantify the concentration of DNA loaded on NPs, the Quant-iT Oli Green ssDNA Kit was purchased from Thermo Fisher Scientific.

Name	Oligonucleotide Sequence
Probe DNA conjugated on NPs	
MUT	HS-5'-C6-TTT-TTT-TTT-TGT-TTG-GCC-CGC-CC-3'
WT	HS-3'-C6-TTT-TTT-TTT-TGT-GTC-TAA-AA-5'
Target DNA for hybridization	
Match 70mer	5'-GGT-GAA-AAC-ACC-GCA-GCA-TGT-CAA-GAT-CAC-AGA-TTT-TGG-GC***G***-GGC-CAA-ACT-GCT-GGG-TGC-GGA-AGA-GAA-A-3'
Mismatch 70mer	5'-GGT-GAA-AAC-ACC-GCA-GCA-TGT-CAA-GAT-CAC-AGA-TTT-TGG-GC***T***-GGC-CAA-ACT-GCT-GGG-TGC-GGA-AGA-GAA-A
Match 140mer	5'-GGT-GAA-AAC-ACC-GCA-GCA-TGT-CAA-GAT-CAC-AGA-TTT-TGG-GC***G***-GGC-CAA-ACT-GCT-GGG-TGC-GGA-AGA-GAA-AGA-ATA-CCA-TGC-AGA-AGG-AGG-CAA-AGT-GCC-TAT-CAA-GTG-GAT-GGC-ATT-GGA-ATC-AAT-TTT-ACA-CAG-AAT-CT-3'
Mismatch 140mer	5'-GGT-GAA-AAC-ACC-GCA-GCA-TGT-CAA-GAT-CAC-AGA-TTT-TGG-GC***T***-GGC-CAA-ACT-GCT-GGG-TGC-GGA-AGA-GAA-AGA-ATA-CCA-TGC-AGA-AGG-AGG-CAA-AGT-GCC-TAT-CAA-GTG-GAT-GGC-ATT-GGA-ATC-AAT-TTT-ACA-CAG-AAT-CT-3'
Random 70mer	5'-TTT-CTC-TTC-CGC-ACC-CAG-CAG-TTT-GGC-CCG-CCC-AAA-ATC-TGT-GAT-CTT-GAC-ATG-CTG-CGG-TG-TTT-CAC-C-3'

Table 3.1. DNA sequences of probes and targets used in the study.

3.2.2 Instrumentation

UV–Vis spectra were measured at room temperature on an Agilent 8453 UV–Vis spectrophotometer using UV Micro cuvettes with 1.0 cm optical path length. Transmission electron microscopy (TEM) was measured in a JEOL JEM-1400 PLUS, operating at 120 kV, equipped with a GATAN US1000 CCD camera (2k×2k). Dynamic light scattering (DLS) measurements were carried out in a Malvern NanoSizer.

3.2.3 Synthesis of Gold Nanoparticles

13, 46 and 63 nm AuNPs. 13 nm AuNPs were prepared according to the standard Turkevich method[16], while 46 and 63 nm AuNPs were prepared according to method reported by Puntes and co-workers[17]. Detailed description of the experimental procedure is described in Chapter 2.

3.2.4 Functionalization of AuNPs

AuNPs were functionalized with thiolated oligonucleotides (MUT and WT) according to the method reported by Hurst et al[15]. Briefly, to the AuNPs colloid (1.11 mL) containing SDS (0.1%) and PBS (0.01 M) was added a solution of oligonucleotides to reach a final concentration of 1 OD/mL. An excess of oligonucleotides was used in all the samples, estimated as 2, 3, and 4 oligonucleotides per nm^2 of gold surface, for 13, 43, and 63 nm AuNPs, respectively. The mixture of oligonucleotides and AuNPs was incubated at room temperature for 20 min. To improve oligonucleotide binding onto the gold surface, a salt aging process was carried out. A solution containing NaCl (2 M), SDS (0.01%), and PBS (0.01 M) was added sequentially to the mixture containing AuNPs and oligonucleotides in the following aliquots: 5, 5, 15, 25, and 50 µL, ultimately reaching a final NaCl concentration of 0.2 M. After each addition, the mixture was sonicated for 10 s followed by a 20 min incubation period. The final solution was incubated for 12 h. To remove excess oligonucleotides, the solutions were centrifuged three times at 8500 rpm for 10 min, each time redispersed in SDS (1 mL, 0.01%). The final concentration of nanoparticles was 0.4 mM in terms of metallic gold for all the samples.

3.2.5 Quantification of DNA Loaded on Gold Nanoparticles

To determine the number of oligonucleotides per particle, the concentration of NPs was determined by the combination of TEM and UV-Vis spectroscopy measurements[18]. To quantify the concentration of surface DNA, the oligonucleotide was detached from the NP and quatified by fluorescence assay (for details see **Chapter 2, Section 2.5.5**).The amount of DNA per NP was calculated dividing the concentration of oligonucleotides by the concentration of NPs.

3.2.6 Hybridization of AuNP-DNA Probes – Standard Assay

Equal volumes (62.5 µL) of two batches of NP (Au@WT and Au@MUT) were combined into a UV-Vis mikro cuvette, followed by the addition of PBS (x1, 325 µL). To this solution was added 50 µL of a mixture containing PB (0.01 M) and NaCl (2 M) to reach the final volume of 0.5 mL. Finally, an aliquot of 70base target ssDNA (either match or mismatch) in a concentration of 5 nM was added to the solution.

3.2.7 Hybridization of AuNP-DNA Probes – Preincubation Assay

To the solution containing Au@WT (62.5 µL) and PBS (x1, 325 µL) was added 50 µL of a mixture containing PB (0.01 M) and NaCl (2 M). Subsequently, an aliquot of target ssDNA (either match or mismatch of the desired concentration) was added to the solution and left on for incubation in a roller mixer. After 1 hour, AuNP@MUT (62.5 µL) were added and the incubation process continues for the next 3 hours. UV-Vis spectra were recorded each hour and DLS measurements were performed to study the aggregation process.

3.2.8 Dynamic Light Scattering Measurements

The conditions for the DLS experiments were: 6 measurements with 5 runs of 5 sec each one. The study was carried out at 25ºC with an equilibration time of the sample of 30s.

3.3 Results and Discussion

The goal of this Chapter is the detection of the most common point mutation in non-small cell lung cancer (NSCLC), the L858R mutation which occurs in the Epidermal Growth Factor Receptor (EGFR) gene[19]. Detection of this mutation is an FDA and EMA approved biomarker for the administration of TKI-therapy to NSCLC patients. **Figure 3.1**d,e show possible secondary structures of target sequences comprising 70 and 140 bases, with indication of the binding sites of Au@DNA and the location of a single-point mutation. As a signal transducer, AuNPs with 65 nm in diameter were used. These particles were stabilized by short sequences that were complementary to either a mutation-free region in the target DNA (WT) or to a region that contained a single-base mutation (MUT) (**Figure 3.1**c). Each AuNP was stabilized by ≈1500 WT or MUT strands grafted to the surface via thiol groups, as determined by a fluorescence kit. As first attempt, a standard sandwich approach was implemented but found no effect on Au@DNA aggregation, meaning that the solution containing both Au@MUT and Au@WT remained stable upon the addition of target sequence (5 nM), in the presence of PBS and NaCl, as confirmed by UV–Vis and DLS characterization (**Figure 3.2**).

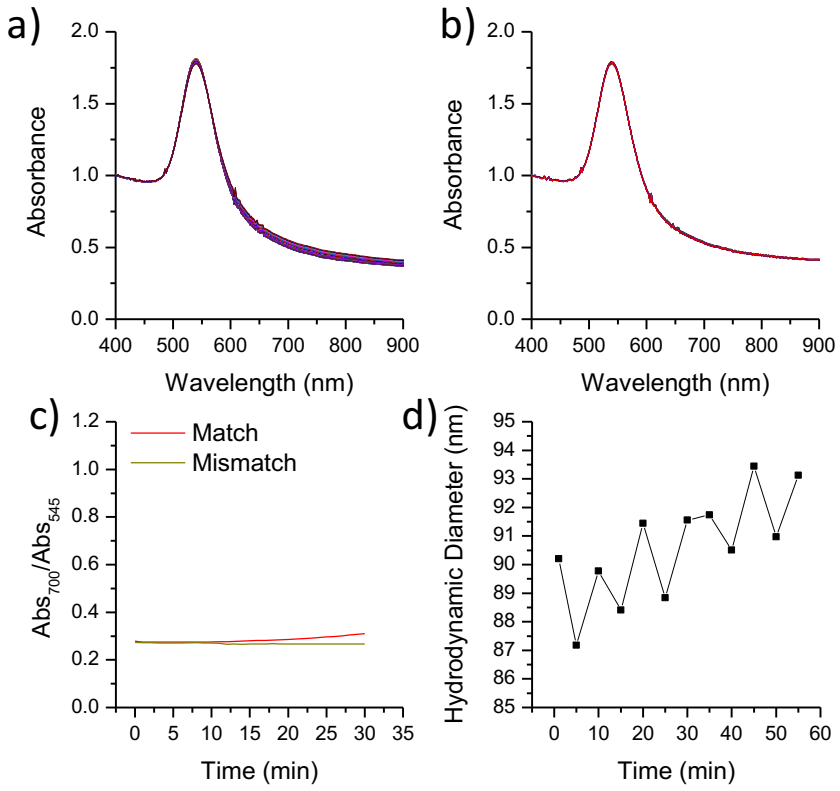

Figure 3.2. Detection of 70 bases target by standard assay, target (5nM) added to the solution containing both types of nanoparticles (Au@WT and Au@MUT). UV-Vis spectra in the presence of a) match and b) mismatch. c) Aggregation rate for the match and the mismatch. d) DLS measurements versus time.

However, aggregation is possible by tailoring the incubation process (**Figure 3.1**b). Au@WT was preincubated with a target DNA (70 bases), either match or mismatch, for 1 h under constant shaking. Subsequent addition of the second Au@MUT batch led to selective aggregation within 3 h. The concentration of target sequence was 5 nM, which translates into 380 copies of target DNA per NP. **Figure 3.3**a,b shows UV−Vis spectra at different times after addition of Au@MUT, that is, after addition of a second batch. The localized surface plasmon resonance (LSPR) band is broadened suggesting more pronounced aggregation of the AuNPs in the presence of the match sequence than in the presence of the mismatch. By monitoring the aggregation degree ($R = Abs_{700}/Abs_{538}$), a difference of 0.4 was observed between match and mismatch sequences, after 1 h of incubation, which increased up to 0.6 after 3 h (**Figure 3.3**c). These data support the hypothesis that the preincubation step

allows a colorimetric detection of the single-base mutation. DLS measurements (**Figure 3.3**d) confirmed the trends observed by UV−Vis spectroscopy. The average diameter of the initial mixture in 1xPBS increased from 81 to 262 nm after 3 h of incubation. For the mismatch sequence, a diameter increaseof 18 nm was observed after 3 h of incubation. In the case of the control (no target), the size remained constant. Next, the focuse was turn toward the performance of the assay for discrimination of a single base mutation in even longer target DNA of 140 bases (**Figure 3.3**e−h). The LSPR of the solution containing the match sequence decreased and broadened (**Figure 3.3**e). In the case of the mismatch sequence only a slight decrease of the plasmon band was observed (**Figure 3.3**f). Although the aggregation degree (**Figure 3.3**g) was similar (0.4) for match and mismatch sequences after 1 h of incubation, the difference was more pronounced at longer incubation times (3 h), clearly showing that specificity was lower for 140 bases long sequences as compared to the sequences containing 70 bases. The initial average diameter of the Au@DNA was 92 nm and increased to 158 nm after 3 h (**Figure 3.3**h). For the mismatch sequence, the final diameter after 3 h was 114 nm, whereas the particle size in the control experiment remained constant.

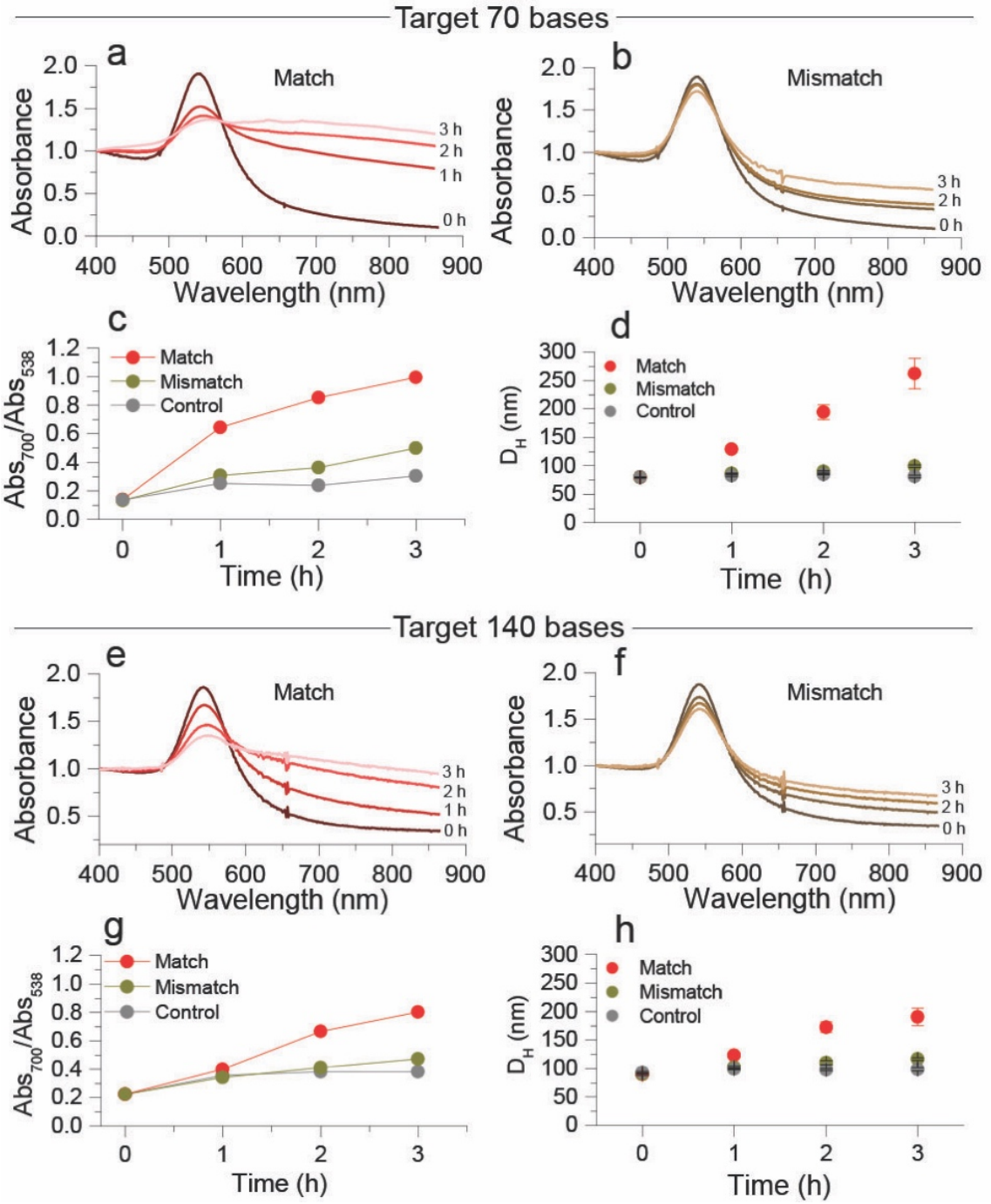

Figure 3.3. Selective discrimination of single base mutation in a target DNA of 70 (a-d) and 140 (e-h) bases. (a,b) UV-Vis spectra of AuNPs in the presence of match (a) and mismatch (b) containing 70 bases (c) Aggregation rate for match, mismatch and control (no target). (d) DLS monitoring of the aggregation process in the presence of target (70 bases, 5 nM). (e-h) Selective discrimination of single base mutation in a target of 140 bases. (e,f) UV-Vis spectra of AuNPs in the presence of match (e) and mismatch (f). (g) Aggregation rate for match, mismatch and control. (h) DLS characterisation of the aggregation process in the presence of target 140 bases, 5 nM.

To further study the importance of the preincubation step, the order of premixing was reversed. The target was first mixed with Au@MUT, and then Au@WT was added. Although selectivity toward SNP was indeed appreciated, the difference in aggregation degree was much lower as compared to the preincubation with Au@WT. For the target comprising 70 bases, the R was equal to 0.15, while for the target of 140 bases, we found R = 0.05 (**Figure 3.4**).

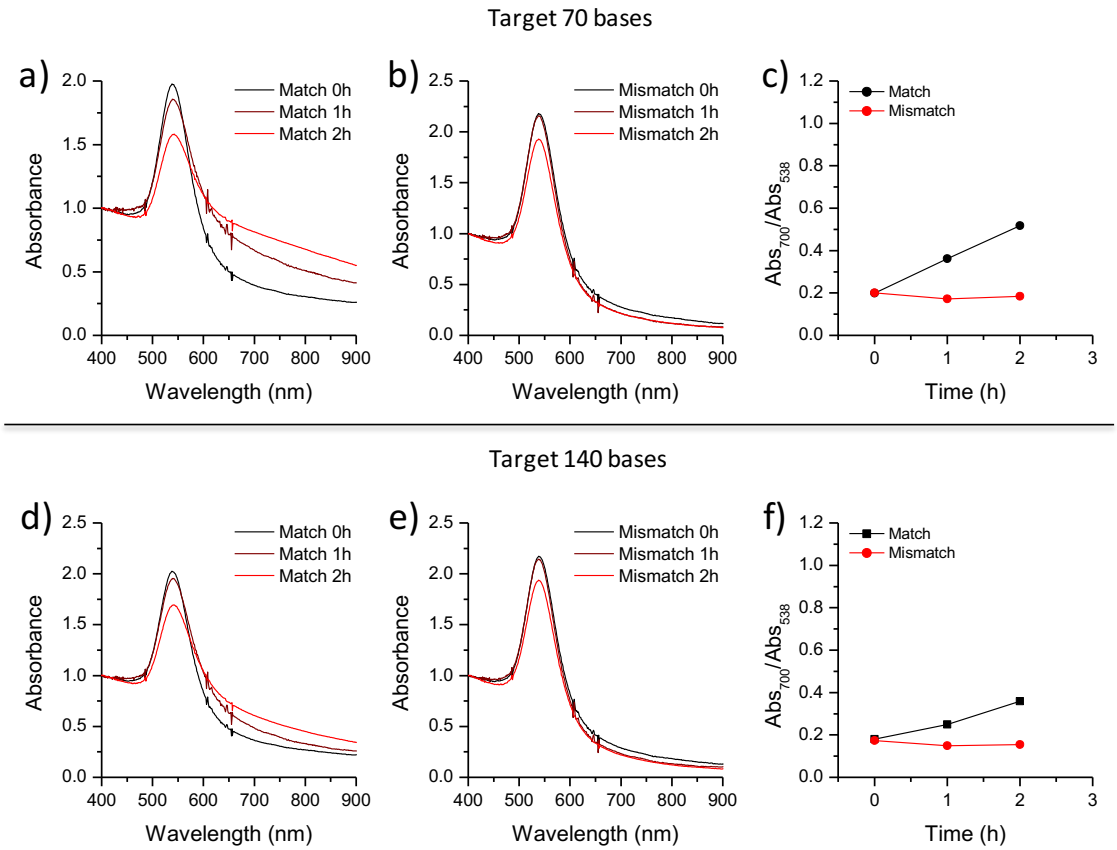

Figure 3.4. Selective discrimination of single base mutation in a target DNA of 70 (a-c) and 140 (d-f) bases through reversed pre-incubation assay: first Au@MUT, second Au@WT. (a,b) UV-Vis spectra of AuNPs in the presence of match (a) and mismatch (b) containing 70 bases. (c) Aggregation rate for match and mismatch. (d-e) UV-Vis spectra of AuNPs in the presence of match (d) and mismatch (e). (f) Aggregation rate for match and mismatch.

These observations indicate that the target exhibits better accessibility when conjugated with Au@WT. Mirkin and co-workers[20] have shown that the hybridization of ssDNA on the Au surface with short sequences extends the non hybridized bases of ssDNA, making them more accessible to the incoming target sequence. The results of the study suggest an analogous scenario in which the target, instead of the probe, undergoes a conformational change. The assay shows high selectivity toward single base mutation. It has been shown[21,22] that the discrimination of single base mutations is related to the stability of the target molecule. In other words, longer targets are less discriminative with respect to point defects than shorter ones. It should be also mentioned that a point defect in sequences containing 70 or 140 bases represents only 1.5% or 0.7% of the complete sequence, respectively, making our assay a convenient strategy for detection of the mutation in long sequences. Finally, to evaluate the sensitivity of the assay, aggregation experiments were performed for 70 bases target (match and mismatch) at the following concentrations: 5, 1, 0.1, and 0.01 nM. **Figure 3.5** shows the discrimination of SNP in the target containing 70 bases down to 0.1 nM. At 10 pM of target concentration no differentiation between match and mismatch is observed.

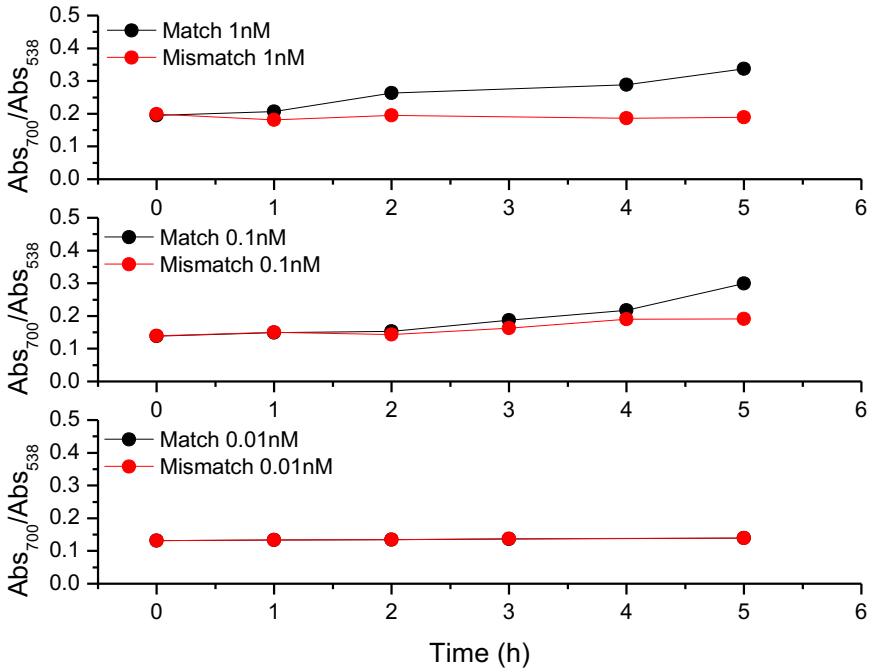

Figure 3.5. Selective discrimination of single base mutation for a 70 bases target, in a concentration range from 1 nM to 0.01 nM.

As it is shown in Figure 3.5, the preincubation step allows the detection and discrimination of single nucleotide polymorphism in long DNA sequences at low concentrations, 0.1 nM. However, longer detection times are required: 5h in the case of 0.1 nM detection.

To further determine to what extend the target molecules hybridize with WT or MUT during the preincubation step, a DLS analysis was carried out (**Figure 3.6**). Upon mixing of Au@WT with the match sequence, the hydrodynamic diameter increased from 93 to 104 and 106 nm for 70 and 140 bases, respectively, after 1 h of incubation. On the other hand, the hydrodynamic diameter of Au@MUT increased from 86 to 89 nm (70 bases) and to 91 nm (140 bases). Note that the initial hydrodynamic diameter of Au@MUT was 7 nm smaller as compared to Au@WT, owing to the different length and conformation of both sequences (see **Figure 3.1**c). The difference in the increase of hydrodynamic diameter for Au@WT (11 nm) and Au@MUT (2 nm) upon incubation with the target sequence suggests that binding events on Au@DNA are sequence-dependent. Note that the incubation of either Au@WT or Au@MUT with a non target sequence of 70 bases had no effect on the hydrodynamic diameter of the nanoparticles (**Figure 3.6**). MUT and WT are complementary to different areas of the target (**Figure 3.1**) that initially can form a variety of secondary structures with multiple loops and hairpins. Upon hybridization, WT on AuNPs unbinds the secondary structure of the target, allowing the tail sequence to point toward the solution, thereby increasing the hydrodynamic diameter. In the case of MUT, the same target molecule binds in the opposite direction, forcing the tail sequence to point toward the nanoparticles (**Figure 3.6**).

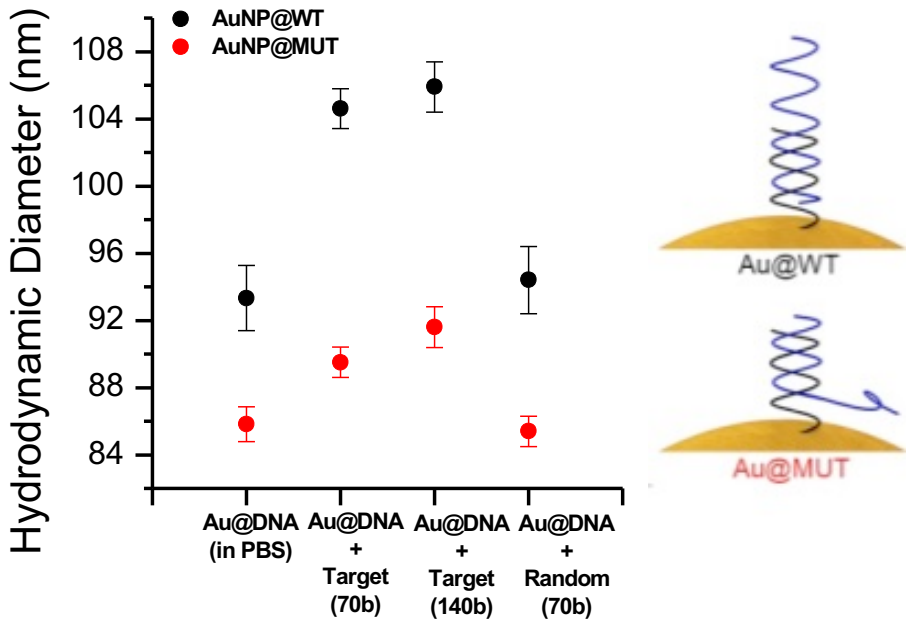

Figure 3.6. Hydrodynamic diameter, obtained by DLS, of either Au@WT or Au@MUT before and after incubation with the target sequences. The right-hand panel provides a schematic representation of the effect of pre-incubation on the increase in hydrodynamic diameter.

Both the DLS analysis and the experiments of reversed premixing (Au@MUT + target) suggest that the preincubation step disrupts the secondary structure. This reasoning is a basis for the statement that a preincubation step is crucial to open and stabilize the target molecules[23], making the sequences more accessible toward binding events with Au@MUT in the second batch, thus facilitating the formation of the sandwich architecture[20]. In contrast, the target DNA exposed to both types of particles (standard assay) is unable to selectively bridge the two particle types within a reasonable time-scale. The competitive interaction of Au@WT and Au@MUT for the same target molecules sterically constrains the target in a stable coiled conformation[24].

3.4 Conclusions

This Chapter described a methodology to discriminate single base mutation in long DNA sequences containing 70 or 140 bases. Preincubation of the target sequence with only one type of Au@DNA facilitated the formation of a sandwich structure upon addition of the second type of Au@DNA and discriminate single base mutation within 1 h. This approach shed a light on the capability of spherical nucleic acids to disturb the secondary structure of long DNA sequences, making feasible the detection of relevant mutations in biological targets.

3.5 References

(1) Sorenson, G. D.; Pribish, D. M.; Valone, F. H.; Memoli, V. A.; Bzik, D. J.; Yao, S. L. Soluble Normal and Mutated DNA Sequences from Single-Copy Genes in Human Blood. *Cancer Epidemiol. Prev. Biomark.* **1994**, *3* (1), 67–71.

(2) Freidin, M. B.; Freydina, D. V.; Leung, M.; Fernandez, A. M.; Nicholson, A. G.; Lim, E. Circulating Tumor DNA Outperforms Circulating Tumor Cells for KRAS Mutation Detection in Thoracic Malignancies. *Clin. Chem.* **2015**, *61* (10), 1299–1304.

(3) Qiu, M.; Wang, J.; Xu, Y.; Ding, X.; Li, M.; Jiang, F.; Xu, L.; Yin, R. Circulating Tumor DNA Is Effective for the Detection of EGFR Mutation in Non–Small Cell Lung Cancer: A Meta-Analysis. *Cancer Epidemiol. Prev. Biomark.* **2015**, *24* (1), 206–212.

(4) Chan, K. C. A.; Jiang, P.; Chan, C. W. M.; Sun, K.; Wong, J.; Hui, E. P.; Chan, S. L.; Chan, W. C.; Hui, D. S. C.; Ng, S. S. M.; Chan, H. L. Y.; Wong, C. S. C.; Ma, B. B. Y.; Chan, A. T. C.; Lai, P. B. S.; Sun, H.; Chiu, R. W. K.; Lo, Y. M. D. Noninvasive Detection of Cancer-Associated Genome-Wide Hypomethylation and Copy Number Aberrations by Plasma DNA Bisulfite Sequencing. *Proc. Natl. Acad. Sci.* **2013**, *110* (47), 18761–18768.

(5) Chimonidou, M.; Kallergi, G.; Georgoulias, V.; Welch, D. R.; Lianidou, E. S. Breast Cancer Metastasis Suppressor-1 Promoter Methylation in Primary Breast Tumors and Corresponding Circulating Tumor Cells. *Mol. Cancer Res. MCR* **2013**, *11* (10).

(6) Campitelli, M.; Jeannot, E.; Peter, M.; Lappartient, E.; Saada, S.; de la Rochefordière, A.; Fourchotte, V.; Alran, S.; Petrow, P.; Cottu, P.; Pierga, J.-Y.; Lantz, O.; Couturier, J.; Sastre-Garau, X. Human Papillomavirus Mutational Insertion: Specific Marker of Circulating Tumor DNA in Cervical Cancer Patients. *PLoS ONE* **2012**, *7* (8).

(7) Wu, Z.; Jiang, P.; Zulqarnain, H.; Gao, H.; Zhang, W. Relationship between Single-Nucleotide Polymorphism of Matrix Metalloproteinase-2 Gene and Colorectal Cancer and Gastric Cancer Susceptibility: A Meta-Analysis. *OncoTargets Ther.* **2015**, *8*, 861–869.

(8) Antoniou, A. C.; Casadei, S.; Heikkinen, T.; Barrowdale, D.; Pylkäs, K.; Roberts, J.; Lee, A.; Subramanian, D.; De Leeneer, K.; Fostira, F.; Tomiak, E.; Neuhausen, S. L.; Teo, Z. L.; Khan, S.; Aittomäki, K.; Moilanen, J. S.; Turnbull, C.; Seal, S.; Mannermaa, A.; Kallioniemi, A.; Lindeman, G. J.; Buys, S. S.; Andrulis, I. L.; Radice, P.; Tondini, C.; Manoukian, S.; Toland, A. E.; Miron, P.; Weitzel, J. N.; Domchek, S. M.; Poppe, B.; Claes, K. B. M.; Yannoukakos, D.; Concannon, P.; Bernstein, J. L.; James, P. A.; Easton, D. F.; Goldgar, D. E.; Hopper, J. L.; Rahman, N.; Peterlongo, P.; Nevanlinna, H.; King, M.-C.; Couch, F. J.; Southey, M. C.; Winqvist, R.; Foulkes, W. D.; Tischkowitz, M. Breast-Cancer Risk in Families with Mutations in PALB2. *N. Engl. J. Med.* **2014**, *371* (6), 497–506.

(9) Figl, A.; Scherer, D.; Nagore, E.; Bermejo, J. L.; Dickes, E.; Thirumaran, R. K.; Gast, A.; Hemminki, K.; Kumar, R.; Schadendorf, D. Single Nucleotide Polymorphisms in DNA Repair Genes XRCC1 and APEX1 in Progression and Survival of Primary Cutaneous Melanoma Patients. *Mutat. Res. Mol. Mech. Mutagen.* **2009**, *661* (1–2), 78–84.

(10) Guo, L.; Xu, Y.; Ferhan, A. R.; Chen, G.; Kim, D.-H. Oriented Gold Nanoparticle Aggregation for Colorimetric Sensors with Surprisingly High Analytical Figures of Merit. *J. Am. Chem. Soc.* **2013**, *135* (33), 12338–12345.

(11) Hu, Y.; Zhang, L.; Zhang, Y.; Wang, B.; Wang, Y.; Fan, Q.; Huang, W.; Wang, L. Plasmonic Nanobiosensor Based on Hairpin DNA for Detection of Trace Oligonucleotides Biomarker in Cancers. *ACS Appl. Mater. Interfaces* **2015**, *7* (4), 2459–2466.

(12) Underhill, H. R.; Kitzman, J. O.; Hellwig, S.; Welker, N. C.; Daza, R.; Baker, D. N.; Gligorich, K. M.; Rostomily, R. C.; Bronner, M. P.; Shendure, J. Fragment Length of Circulating Tumor DNA. *PLOS Genet.* **2016**, *12* (7), e1006162.

(13) Jain, P. K.; Huang, W.; El-Sayed, M. A. On the Universal Scaling Behavior of the Distance Decay of Plasmon Coupling in Metal Nanoparticle Pairs: A Plasmon Ruler Equation. *Nano Lett.* **2007**, *7* (7), 2080–2088.

(14) Rao, A. N.; Grainger, D. W. Biophysical Properties of Nucleic Acids at Surfaces Relevant to Microarray Performance. *Biomater. Sci.* **2014**, *2* (4), 436–471.

(15) Hurst, S. J.; Lytton-Jean, A. K. R.; Mirkin, C. A. Maximizing DNA Loading on a Range of Gold Nanoparticle Sizes. *Anal. Chem.* **2006**, *78* (24), 8313–8318.

(16) Turkevich, J.; Stevenson, P. C.; Hillier, J. A Study of the Nucleation and Growth Processes in the Synthesis of Colloidal Gold. *Discuss. Faraday Soc.* **1951**, *11* (0), 55–75.

(17) Bastús, N. G.; Comenge, J.; Puntes, V. Kinetically Controlled Seeded Growth Synthesis of Citrate-Stabilized Gold Nanoparticles of up to 200 Nm: Size Focusing versus Ostwald Ripening. *Langmuir* **2011**, *27* (17), 11098–11105.

(18) Scarabelli, L.; Grzelczak, M.; Liz-Marzán, L. M. Tuning Gold Nanorod Synthesis through Prereduction with Salicylic Acid. *Chem. Mater.* **2013**, *25* (21), 4232–4238.

(19) Sharma, S. V.; Bell, D. W.; Settleman, J.; Haber, D. A. Epidermal Growth Factor Receptor Mutations in Lung Cancer. *Nat. Rev. Cancer* **2007**, *7* (3), 169–181.

(20) Prigodich, A. E.; Lee, O.-S.; Daniel, W. L.; Seferos, D. S.; Schatz, G. C.; Mirkin, C. A. Tailoring DNA Structure To Increase Target Hybridization Kinetics on Surfaces. *J. Am. Chem. Soc.* **2010**, *132* (31), 10638–10641.

(21) Naiser, T.; Ehler, O.; Kayser, J.; Mai, T.; Michel, W.; Ott, A. Impact of Point-Mutations on the Hybridization Affinity of Surface-Bound DNA/DNA and RNA/DNA Oligonucleotide-Duplexes: Comparison of Single Base Mismatches and Base Bulges. *BMC Biotechnol.* **2008**, *8*, 48.

(22) Suzuki, S.; Ono, N.; Furusawa, C.; Kashiwagi, A.; Yomo, T. Experimental Optimization of Probe Length to Increase the Sequence Specificity of High-Density Oligonucleotide Microarrays. *BMC Genomics* **2007**, *8*, 373.

(23) Chen, C.; Wang, W.; Ge, J.; Zhao, X. S. Kinetics and Thermodynamics of DNA Hybridization on Gold Nanoparticles. *Nucleic Acids Res.* **2009**, *37* (11), 3756–3765.

(24) Zinchenko, A.; Tsumoto, K.; Murata, S.; Yoshikawa, K. Crowding by Anionic Nanoparticles Causes DNA Double-Strand Instability and Compaction. *J. Phys. Chem. B* **2014**, *118* (5), 1256–1262.

Chapter 4. Blocking Strategy for the Colorimetric Detection of Single Nucleotide Polymorphism in Long Double-Stranded DNA Sequences

Abstract

As mentioned in previous chapters, the rapid detection of single nucleotide mutations in circulating tumor DNA has become an attractive strategy for early cancer diagnosis. However, specificity remains a major challenge as the mutated sequence typically comprises only a small fraction (<1%) compared to the wild-type sequence. Furthermore, the use of hybridization based techniques requires the separation of dsDNA into ssDNA for efficient binding of probes. In the present chapter, it is proposed an amplification-free assay for discrimination of single nucleotide polymorphism in a binary mixture containing wild-type and mutated dsDNA, by using the aggregation of gold nanoparticles (AuNPs) as the only transducer. The method is based on the combination of high-temperature denaturation and selective blocking of the denatured strands, so that the aggregation of AuNPs becomes highly specific. It was possible to discriminate SNP in long dsDNA containing up to 140 bases and differentiate 5% of mutated dsDNA in a binary mixture containing both perfect match and mismatch sequences for dsDNA of 70 bases.

4.1 Introduction

The discovery of circulating cell free DNA by Mandel and Metais in 1948 has opened the possibilities for non-invasive monitoring of cancer[1]. But not earlier than in mid-90s,thefirst evidences that tumor cells release DNA – known today as circulating tumor DNA (ctDNA) werereported[2,3]. Since then, the methodologies for cfDNA detection evolved drastically to enable the development of liquid biopsies in the clinical field. Circulating tumor DNA is released from tumor cells into biological fluids such as blood, and can provide a useful source of cancer-associated biomarkers, for example as mutated sequences such as single nucleotide polymorphism[4–8] or methylation changes[9,10]. The difficulty in the detection of mutations and particularly single nucleotide mutations in ctDNA relates to the length of circulating genetic fragments (~140 base pairs) and their low concentration (from few to 10^4 units per mL). On top of that, a given mutation (single-base) is hindered in the double-stranded DNA (dsDNA),[11] and the fraction of mutated ctDNA is very low (<1 %) as compared to the wild-type sequence. Therefore, chemical complexity of the analyte biomolecule, inaccessibility of mutated base, as well as low concentration, require sophisticated detection methodologies.

Although Polymerase Chain Reaction (PCR)[12–14] is a technique that enables fast screening of mutations in DNA, its complexity and time-consuming analysis hinders implementation within point-of-care devices.[15] PCR, however, offers a conceptual framework for the development of assays relying on its principle, i.e. thermal annealing of dsDNA, splitting complementary strands, and discrimination of mutated sequences through a given signal transduction method. To detect dsDNA a thermal treatment it is required to denature the double helix. To avoid the rehybridization of sense and the antisense strand upon cooling, a blocking strategy is typically implemented, which is based on the use of short DNA sequences (complementary to the antisense DNA sequence),as presented shown in **Figure 4.1**[16]. This methodology is based on the strategy of asymmetric PCR, in which the reaction preferentially amplifies one DNA strand in a dsDNA template.

Several approaches have been proposed that benefit from the blocking strategy used in PCR.The most relevant one is probably the approach reported by Kelley and coworkers,[17,18] who proposed an electrochemical clamp assay to detect mutated dsDNA in serum with no need for enzymatic amplification. The core design involves the use of clutch probes (here blocking probes), which prevent reassociation of denatured DNA strands after thermal annealing. This conceptual development indicates that detection of single-nucleotide polymorphism in dsDNA is indeed possible, but other strategies, in particular colorimetric assays in colloidal phase, could facilitate detection.

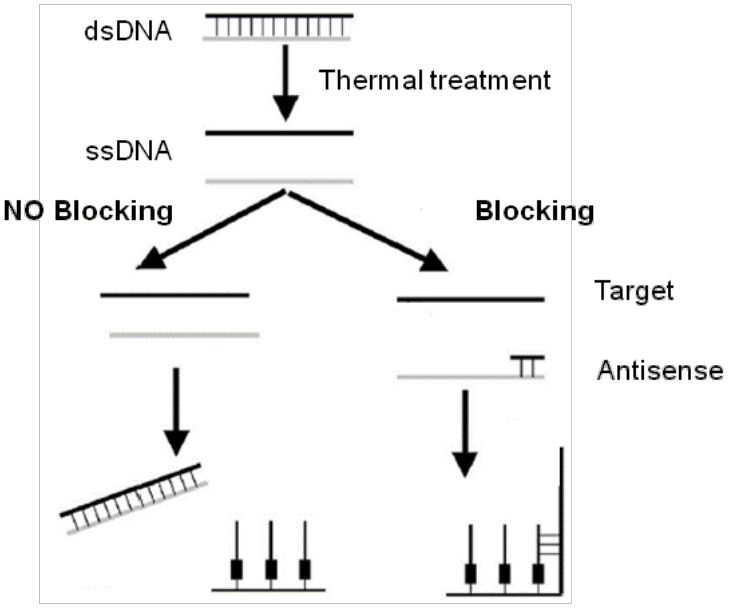

Figure 4.1. Methodology to dissociate the double-stranded DNA. Thermal treatment (95 ºC for 15 min) with and without blocking strategy. Adapted from [16].

As conclude in Chapter 2, the sensitivity of plasmon-assisted SNP detection in single-stranded DNA can be improved by the use of larger AuNPs – 63 nm in diameter.[19] Larger diameter of the AuNPs allowed a reduction of their concentration in the assay, which was critical to maximize the ratio between analyte DNA and AuNPs. It has been also exploited in Chapter 3 that assay based on large nanoparticles serve for the detection of single base mutation in long ssDNA sequences, up to 140 bases,[20] showing that DNA-functionalized nanoparticles can disrupt the secondary structure of ssDNA. This Chapter deals with a conceptually new strategy for the colorimetric

discrimination of SNP in binary mixtures of double-stranded DNA containing both wild-type and mutated sequences. The novelty of the strategy involves the implementation of thermal annealing and the use of two short ssDNA – blocking probes (BPs) – in the solution containing the target dsDNA (70 and 140 base pairs) and DNA-functionalized AuNPs (63 nm) (**Figure 4.2**).

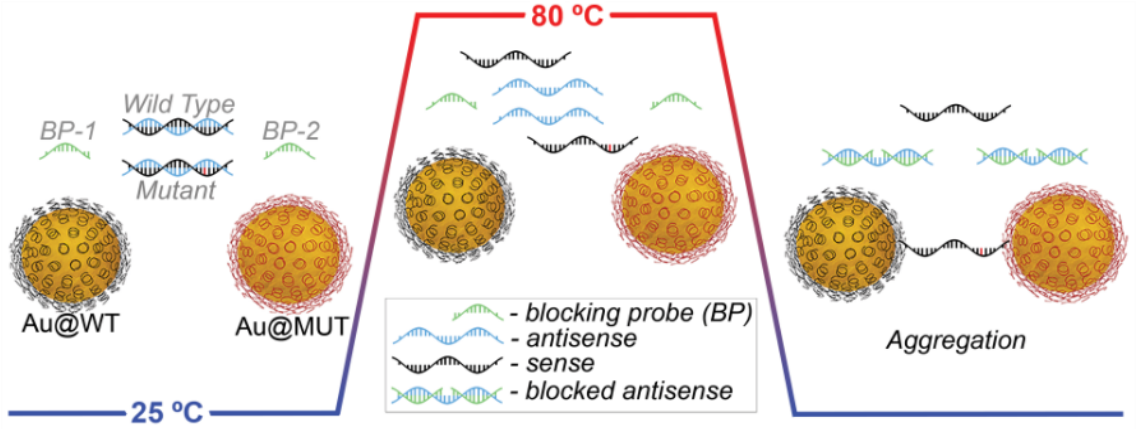

Figure 4.2. Detection strategy. The starting mixture (left) containing two types of nanoparticles, blocking probes and analyte dsDNA is annealed at 80 ºC for 10 minutes (middle), followed by cooling and signal readout (right). Blocking probes bind to the antisense sequence of the analyte DNA, preventing reannealing upon cooling. The target sequence that remains as ssDNA is recognized by the capture probes, leading to selective nanoparticle aggregation.

As shown in Figure 4.1, whereas annealing of the solution at 80 ºC leads to denaturation of the dsDNA, the cooling process allows for selective binding of blocking probes to the antisense strand, at a position that is complementary to the capture probe. As such, reannealing of dsDNA strands is minimized, and colorimetric detection is possible by selective AuNPs aggregation. Such approach is presumably the first colorimetric colloidal assay capable of differentiating <5% of mutated sequence in a binary mixture (5 nM) of mutated and wild type sequence dsDNA, without the need for enzymatic signal amplification.

4.2 Experimental Part

4.2.1 Chemicals

$HAuCl_4 \cdot 3H_2O$ was purchased from Alfa Aesar. Sodium dodecyl sulfate (SDS) (98%), sodium chloride (NaCl) (99.5%), sodium citrate tribasic dihydrate (98%), and phosphate buffer (PB) 1 M, pH 7.4, were purchased from Sigma-Aldrich. Phosphate buffered saline (PBS) 0.01 M, pH 7.4, containing 0.138 M NaCl and 2.7 mM KCl (Sigma-Aldrich) was used to mimic physiological conditions. DNA targets and thiolated oligonucleotides (**Table 4.1**) were purchased from Biomers (Germany). To quantify the concentration of DNA loaded on NPs, the Quant-iT Oli Green ssDNA Kit from Thermo Fisher Scientific was employed.

Name	Oligonucleotide Sequence
Probe DNA conjugated on NPs	
WT	HS-3'-C6-TTT-TTT-TTT-TGT-GTC-TAA-AA-5'
MUT	HS-5'-C6-TTT-TTT-TTT-TGT-TTG-GCC-CGC-CC-3'
Target DNA for hybridization	
Match 23mer	5'-AGA-TCA-CAG-ATT-TTG-GGC-***G***GG-CCA-AAC-TGC-TGG-GT-3'
Antisense 23mer	5'-GTT-TGG-CCC-GCC-CAA-AAT-CTG-TG-3'
Match 70mer	5'-GGT-GAA-AAC-ACC-GCA-GCA-TGT-CAA-GAT-CAC-AGA-TTT-TGG-GC***G***-GGC-CAA-ACT-GCT-GGG-TGC-GGA-AGA-GAA-A-3'
Mismatch 70mer	5'-GGT-GAA-AAC-ACC-GCA-GCA-TGT-CAA-GAT-CAC-AGA-TTT-TGG-GC***T***-GGC-CAA-ACT-GCT-GGG-TGC-GGA-AGA-GAA-A-3'
Antisense 70mer	5'-TTT-CTC-TTC-CGC-ACC-CAG-CAG-TTT-GGC-CCG-CCC-AAA-ATC-TGT-GAT-CTT-GAC-ATG-CTG-CGG-TGT-TTT-CAC-C-3'
Match 140mer	5'-GGT-GAA-AAC-ACC-GCA-GCA-TGT-CAA-GAT-CAC-AGA-TTT-TGG-GC***G***-GGC-CAA-ACT-GCT-GGG-TGC-GGA-AGA-GAA-AGA-ATA-CCA-TGC-AGA-AGG-AGG-CAA-AGT-GCC-TAT-CAA-GTG-GAT-GGC-ATT-GGA-ATC-AAT-TTT-ACA-CAG-AAT-CT-3'
Mismatch 140mer	5'-GGT-GAA-AAC-ACC-GCA-GCA-TGT-CAA-GAT-CAC-AGA-TTT-TGG-GC***T***-GGC-CAA-ACT-GCT-GGG-TGC-GGA-AGA-GAA-AGA-ATA-CCA-TGC-AGA-AGG-AGG-CAA-AGT-GCC-TAT-CAA-GTG-GAT-GGC-ATT-GGA-ATC-AAT-TTT-ACA-CAG-AAT-CT-3'
Antisense 140mer	5'-AGA-TTC-TGT-GTA-AAA-TTG-ATT-CCA-ATG-CCA-TCC-ACT-TGA-TAG-GCA-CTT-TGC-CTC-CTT-CTG-CAT-GGT-ATT-CTT-TCT-CTT-CCG-CAC-CCA-GCA-GTT-TGG-CCC-GCC-CAA-AAT-CTG-TGA-TCT-TGA-CAT-GCT-GCG-GTG-TTT-TCA-CC-3'
Blocking Sequences	
BP1	5'-GCG-GGC-CAA-AC-3'
BP2	5'-CAC-AGA-TTT-TGG-3'

Table 4.1. DNA sequences related to EGFR mutation detection.

4.2.2 Instrumentation

UV–Vis spectra were measured at room temperature on an Agilent 8453 UV–vis spectrophotometer, using UV Micro cuvettes with 1.0 cm optical path length. Transmission electron microscopy (TEM) was measured in a JEOL JEM-1400 PLUS, operating at 120 kV. Dynamic light scattering (DLS) measurements were carried out in a Malvern NanoSizer. Fluorescence measurements were performed in a MicroPlate Reader. A ThermoBath was used for the thermal treatment of the samples.

4.2.3 Synthesis and functionalization of Gold Nanoparticles (AuNPs, 63 nm)

AuNPs were synthesized following a previously reported seeded growth method[21].The particles were then functionalized with thiolated oligonucleotides (MUT and WT), according to the method reported by Hurst et al.[22]Briefly, to the AuNPs colloid (1.11 mL) containing SDS (0.1%) and PBS (0.01 M) was added a solution of oligonucleotides to reach a final concentration of 1 OD/mL. An excess of oligonucleotides was used in all the samples. The mixture of oligonucleotides and AuNPs was incubated at room temperature for 20 min. To improve oligonucleotide binding, a salt aging process was carried out. A solution containing NaCl (2 M), SDS (0.01%), and PBS (0.01 M) was gradually added to the mixture containing AuNPs and oligonucleotides, in the following aliquots: 5, 5, 15, 25, and 50 µL, reaching a final NaCl concentration of 0.2 M. Each salt aging step was alternated with sonication (10 s) and incubation (20 min), followed by incubation for 12 h. To remove excess oligonucleotides, the solutions were centrifuged (8500 rpm, 10 min, 3 times), each time redispersed in SDS (1 mL, 0.01%). The final concentration of nanoparticles was 0.4 mM in terms of metallic gold, for all the samples.

4.2.4 Quantification of Oligonucleotides Loaded on Gold Nanoparticles

To determine the number of oligonucleotides per particle, the concentration of NPs was first determined by UV-Vis spectroscopy.[23] Then, the oligonucleotide molecules were detached from the NPs surface using DTT using equal volumes of Au@DNA and DTT. After incubation (1 hour) the gold precipitate was separated by centrifugation and discarded. The supernatant (25 µL) was added to TE buffer (75 µL), followed by the addition of OliGreen reagent (100 µL) and incubated for 5 minutes at room temperature, protected from light. Fluorescence was measured and compared to a standard curve. For fluorescence measurements, the fluorophore was excited at 485 nm and the emission was recorded at 535 nm. The amount of DNA per NP was calculated dividing the concentration of oligonucleotides by the concentration of NPs.

4.2.5 Hybridization of AuNP-DNA Probes and Detection of Short ssDNA Targets – Blocking Strategy in Non-Competitive Assay

Blocking DNA was combined with the solution containing antisense strands in PBS (x1, 325 µL), and left undisturbed for 1h, followed by the addition of a mixture (50 µL) containing PB (0.01 M) and NaCl (2 M). Next, a solution containing sense strand was added to the above mixture, and left undisturbed for 15 min. The above solution was transferred to a UV-Vis mikro cuvette containing two batches of DNA-coated NPs (62.5 µL each). The final volume of the mixture was 0.5 mL, the concentrations of blocking, antisense and sense strands were 5 nM and the final concentration of NPs was 13 pM. UV−Vis spectra were measured at room temperature during 30 minutes.

4.2.6 Hybridization of AuNP-DNA Probes and Detection of Short ssDNA Targets – Blocking Strategy in Competitive Assay

Blocking DNA was combined with the solution containing sense strands in PBS (x1, 325 µL), followed by the addition of a mixture (50 µL) containing PB (0.01 M) and NaCl (2 M). Next, a solution containing antisense strand was added to the above mixture. The solution was transferred to a UV-Vis mikro cuvette containing two batches of DNA-coated NPs (62.5 µL each). The final volume of the mixture was 0.5 mL, the concentrations of blocking, antisense and sense strands were 5 nM and the final concentration of NPs was 13 pM. UV−Vis spectra were measured at room temperature during 30 minutes.

4.2.7 Hybridization of AuNP-DNA Probes and Detection of Long dsDNA Targets – Blocking Strategy

Equal volumes (62.5 µL) of two batches of NPs (Au@WT and Au@MUT) were combined into an Eppendorf tube, followed by addition of PBS (325 µL). To this solution we added 50 µL of a mixture containing PB (0.01 M) and NaCl (2 M), to reach the final volume of 0.5 mL. Equal volumes of BP-1 and BP-2 (2.5 µL) were added to the solution, reaching a concentration of 5 nM for each BP. Finally, an aliquot of 70 or 140 bases target dsDNA (either match or mismatch), at a concentration of 5 nM, was added to the solution. The temperature of the mixture was then increased from 25 ºC to 80 ºC in a ThermoBath and maintained for 10 min. The mixture was removed from

the ThermoBath and cooled down to room temperature (10 ºC/min), and then monitored by UV-Vis measurements every hour. Similarly, DLS measurements were performed to monitor aggregation.

4.2.8 Hybridization of AuNP-DNA Probes and Detection of Long dsDNA Targets in Binary Mixtures

Equal volumes (62.5 µL) of two batches of NPs (Au@WT and Au@MUT) were combined into an Eppendorf tube, followed by addition of PBS (325 µL). To this solution we added 50 µL of a mixture containing PB (0.01 M) and NaCl (2 M), to reach the final volume of 0.5 mL. Equal volumes of BP1 and BP2 (2.5 µL) were added to the mixture to reach the final concentration of 5 nM for each BP. Finally, a binary mixture of target dsDNA (70 bases, total concentration = 5 nM), containing match and mismatch sequences in different molar ratios, was added to the solution. The temperature of the mixture was increased from 25 ºC to 80 ºC in a ThermoBath and maintained for 10 min. The mixture was removed from the ThermoBath and cooled down to room temperature (10 ºC/min), then monitored by UV-Vis measurement every hour. Alternatively, the mixture was left in ThermoBath once the thermal treatment was finished, slowing the rate of cooling process down to 1 ºC/min. UV-Vis spectra were recorded each hour, once the temperature reached 25 ºC.

4.2.9 Dynamic Light Scattering Measurements

The conditions for the DLS experiments were: 6 measurements with 5 runs of 5 s each. The study was carried out at 25 ºC with an equilibration time of the sample of 30s.

4.3 Results and Discussion

The proposed strategy for SNP discrimination in a binary mixture of dsDNA involves the following steps:

1) Preparation of a stable mixture containing both types of nanoparticles, namely Au@WT (complementary to the wild type sequence) and Au@MUT (complementary to the mutated sequence), two types of blocking probes, BP1 (11 bases) and BP2 (12 bases), and analyte dsDNA of mutated and wild type sequences;
2) Thermal treatment of the mixture for 10 min at 80 ºC followed by cooling down to room temperature;
3) Signal readout by UV-Vis spectroscopy, using the unitless magnitude R = Abs_{700}/Abs_{540}, as a measure of the degree of aggregation.[24]

To evaluate the performance of the assay, double-stranded DNA sequences of 70 bp (as a first approach) and 140 bp were used as analyte, which is comparable to the length of ctDNA in a real scenario. In addition, it proposed to detect L858R mutation, which occurs in the Epidermal Growth Factor Receptor (EGFR) gene, a point mutation found in the tumors of 10-120% of non small cell lung cancer (NSCLC) patients.[25]The selection of this specific biomarker was based on its clinical importance, as the presence of this mutation in NSCLC patients is an FDA-approved biomarker for the administration of tyrosine kinase inhibitors. Since the key parameters in the assay are the presence of blocking probes and thermal treatment, a systematic study to identify the optimal BP concentrations and cooling rate were performed.

Since the blocking probes are complementary to the antisense of the analyte DNA, they are also complementary to the capture probes stabilizing the AuNPs. Therefore, step 1) in the assay leads to spontaneous association of blocking probes to the captures probes on the nanoparticles surface. Maeda and co-workers[26,27] have shown that the transition from ssDNA to dsDNA on the particles surface leads to non-specific aggregation of AuNPs by the decrease of steric repulsion and increase of van

der Waals attraction, resulting in aggregation; a process that is particularly relevant in the present case because we use unusually larger particles.

The non-specific aggregation of AuNPs through blocking probes can potentially induce a false positive. Thus, it was aimed at finding an optimal concentration of BPs, below which no aggregation of AuNPs would take place. For this reason, a stability experiments were performed using a wide range of BP concentrations **(Figure 4.3).** A typical mixture (0.5 mL) contained both types of NPs (13 pM) and different concentrations of both blocking probes: 1, 5, 10, 20, 40, 80, and 100 nM. As depicted in **Figure 4.4a**, the non-specific aggregation of AuNPs is enhanced by increasing BP concentration.

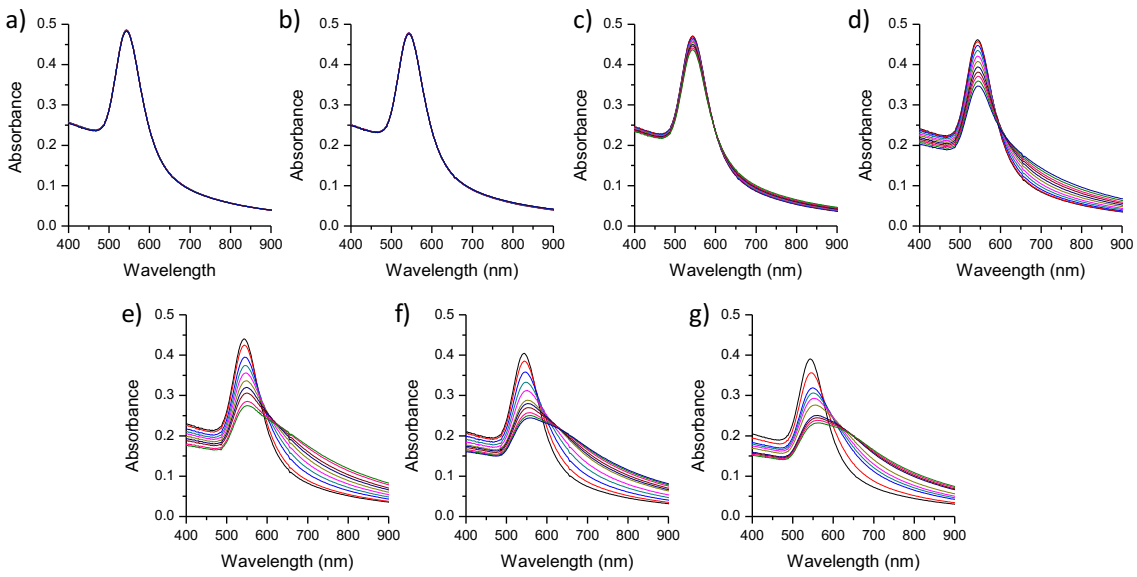

Figure 4.3. UV-Vis spectra of both types of AuNPs in the presence of blocking probe sequences in different concentrations: a) 1 nM, b) 5 nM, c) 10 nM, d) 20 nM, e) 40 nM, f) 80 nM and g) 100 nM.

The formation of dsDNA on the surface was further confirmed by plotting R@10min vs [BP], showing that the inflection point of the aggregation rate falls at a BP concentration of 20 nM (**Figure 4.4**). Fluorescence assays revealed that each particle carries ~1500 capture probes. Considering the number of DNA molecules on the

surface of the particles and the concentration of AuNPs (13 pM) in 0.5 mL of solution, the total concentration of capture probe in the solution was 19.5 nM. Therefore, the inflection point at 20 nM of BPs corresponds to the total value of the capture probe on the particles surface, indicating full coverage of the nanoparticles with BPs at this concentration. Above 20 nM, aggregation was even faster, eventually reaching a plateau at 80 nM. A relevant observation is that, below 5 nM BP non-specific aggregation of AuNPs is barely observed (**Figure 4.4b – red area**). Thus, the concentration of BP used in the following experiments is within a narrow concentration window, < 5 nM.

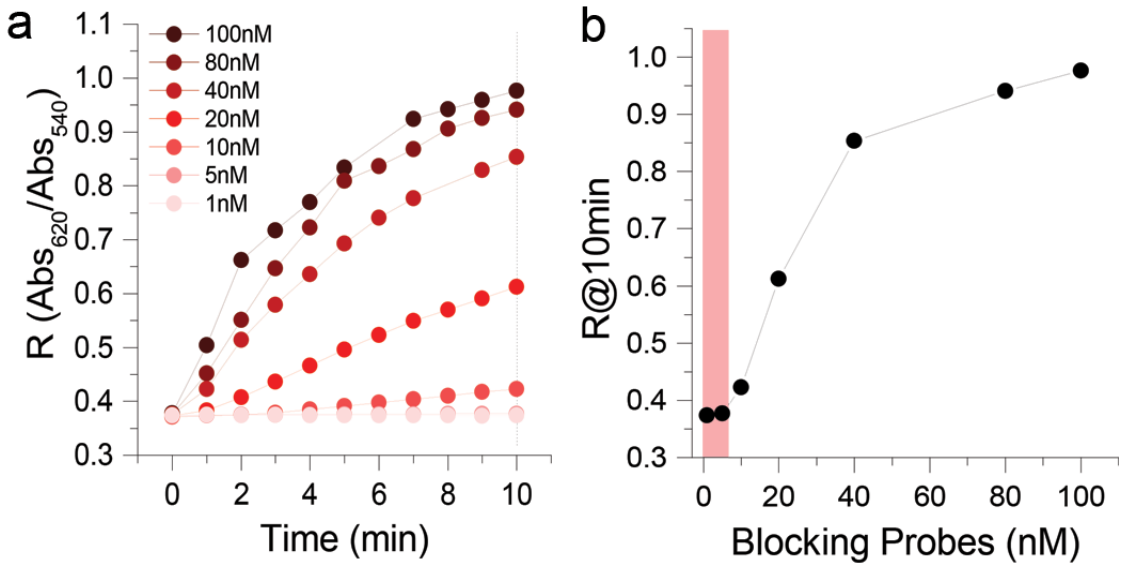

Figure 4.4. Stability of AuNPs in the presence of blocking probe sequences and the absence of dsDNA analyte. a) Kinetic study for 10 min, for various concentrations of blocking sequences, between 1 and 100 nM. b) Degree of aggregation at 10 min, for the different BP concentrations.

To understand the role of blocking probes, the experiments were performed related to the DNA-triggered aggregation of gold nanoparticles, using short targets of 23 bases. The reason of using shorter target sequences is that they exhibit fast binding kinetics. Note, that these short 23 bases sequences are shorter fragment of the long sequences comprising 70 and 140 base pairs. In addition, no thermal treatment is implemented since no dsDNA is used. **Figure 4.5** shows different strategies for

noncompetitive assay by mixing sense and antisense sequences with different blocking probes. The maximum aggregation degree was observed for the mixture containing nanoparticles and sense sequences (**Figure 4.5**e). In contrast, the minimum aggregation rate was observed in the case of the mixture containing gold nanoparticles together with sense and antisense couple, since the double strands comprising sense and antisense excluded the bridging of the nanoparticles with the sense sequence (**Figure 4.5**a).An important observation was that the aggregation rate correlated with blocking ability. To test the blocking probe efficiencies the antisense strands with premixed with different blocking probes: BP1, BP2 and the combination of both. The use of two blocking probes (BP1 and BP2) inhibited the hybridization of the sense and antisense sequences (**Figure 4.5**d), allowing the sense sequence to bridge the nanoparticles, hence increasing the aggregation rate. Comparative experiments showed that BP2 blocks improve the formation of double strand (sense-antisense) than BP1. The aggregation rate for BP2 was almost double as compared to the case of BP1 (compare **Figure 4.5**c and b). These noncompetitive assays confirmed the efficiencies of the blocking probes.

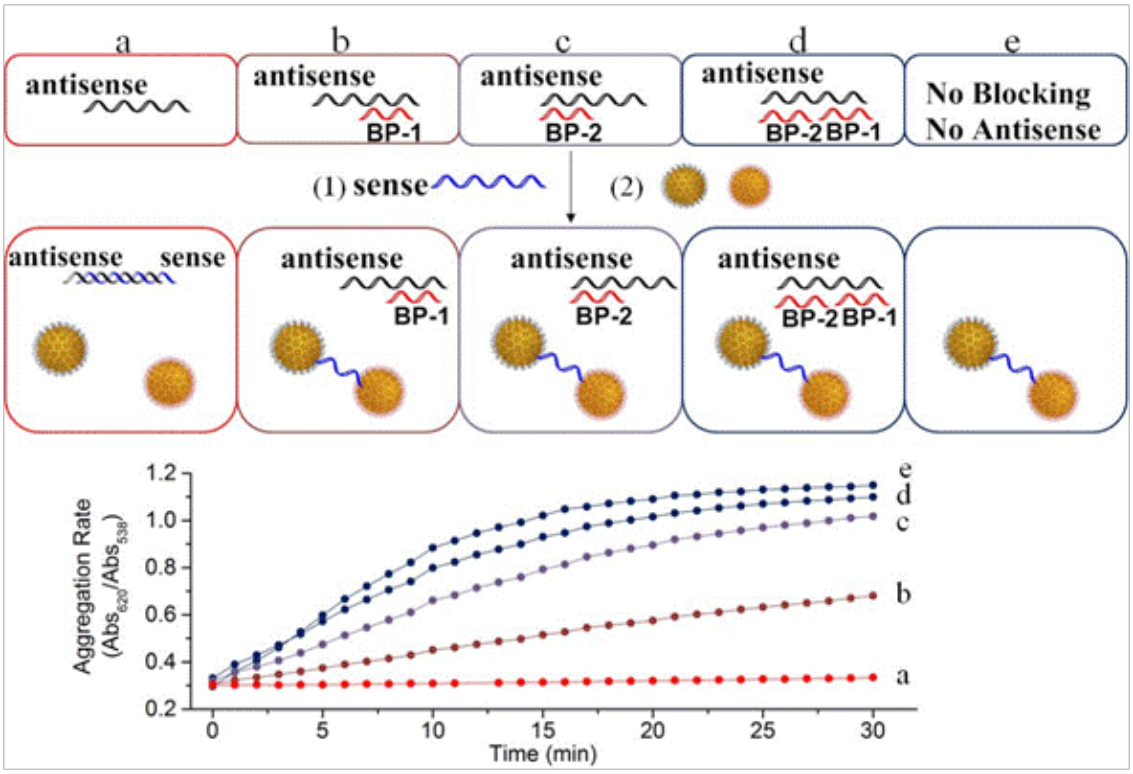

Figure 4.5. Efficiency of blocking probes in the selective aggregation of Au nanoparticles. (Upper) Schematic diagrams of the performed experiments. Antisense sequences were mixed with the corresponding blocking probes and subsequently subjected to the sense sequence and colloidal solution of gold nanoparticles. (a, e) Control experiments, (b, c, d) blocking of antisense by BP1, BP2, and the mixture of BP1 and BP2. (Lower) Aggregation rate vs. aggregation time for different blocking probes and control experiments.

To further evaluate if the action of blocking probes in competitive assay, the mixture of sense sequence and blocking probes (no interaction) were mixed with the antisense sequence and nanoparticles. These experiments allowed to evaluate the competition between BPs and sense strand toward the hybridization with the antisense sequence in a competitive manner (**Figure 4.6**). By plotting the aggregation degree vs time for different blocking scenario, one can observe that the best blocking efficiency is achieved when both blocking probes are used, instead of each blocking independently. It is noteworthy that in this competitive assay, the aggregation degree (0.8 after 30 min) was lower than in the case of non competitive assay (1.2 after 30 min), using the same two-blocking scenario. A possible explanation is that a small

fraction of sense strands hybridizes with the antisense sequence forming the double stranded DNA, instead of hybridizes with the capture probes on the surface of the nanoparticles.

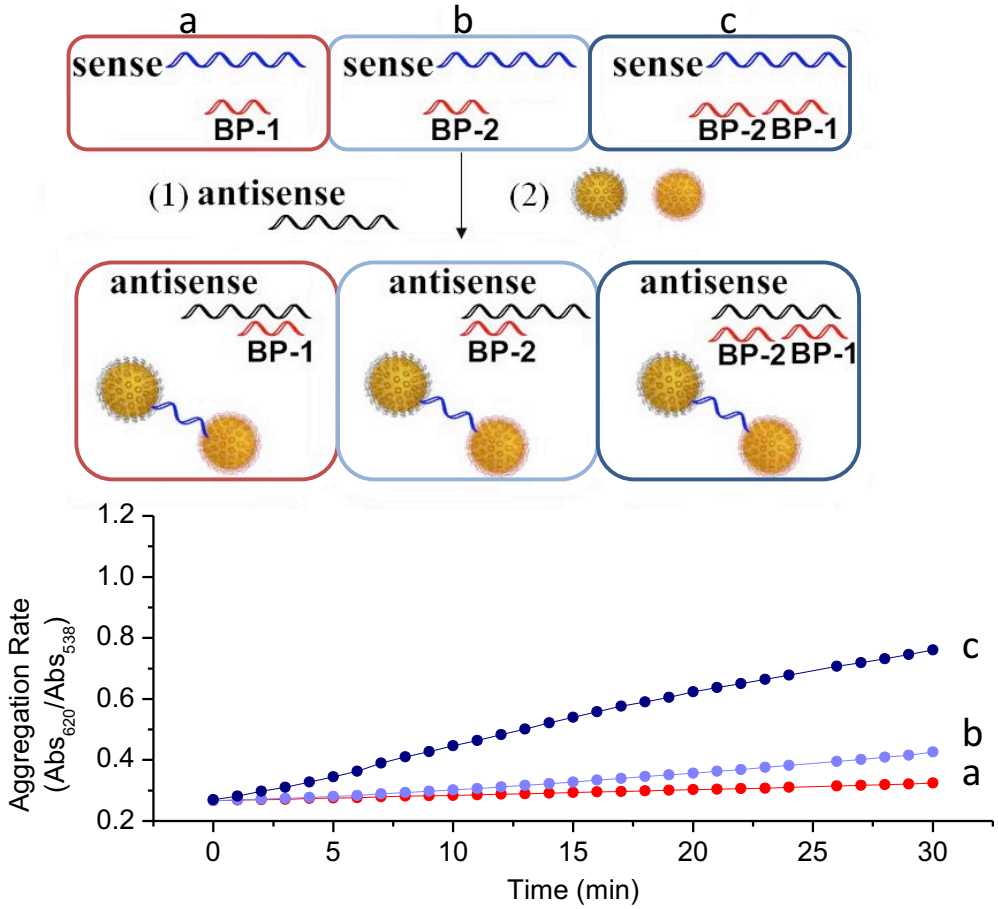

Figure 4.6. Efficiency of blocking probes in the selective aggregation of Au nanoparticles. (Upper) Schematic diagrams of the performed experiments. Sense sequences were mixed with the blocking probes and subsequently subjected to the antisense sequence and colloidal solution of gold nanoparticles. (a, b, c) blocking of antisense by BP1, BP2, and the mixture of BP1 and BP2. (Lower) Aggregation rate vs. aggregation time for different blocking probes.

By gaining the knowledge on blocking scenario, a series of experiments were performed in which different blocking scenarios were screened for longer sequences of 70 and 140 base pairs. In analogous manner to previous experiments of short

sequences, BP1 and BP2 were used separately, mixed together (BP1 + BP2), as well as no BP. Since, in the following experiments, the aggregation of AuNPs was monitored in the presence of dsDNA (match or mismatch, 70 and 140 bases, 5 nM), the thermal treatment step was implemented as shown on Figure 4.2. It has been accordingly found that the scenario involving two blocking probes led to more pronounced aggregation – higher blocking power – as compared to the use of one single blocking probe **(Figure 4.7a**).

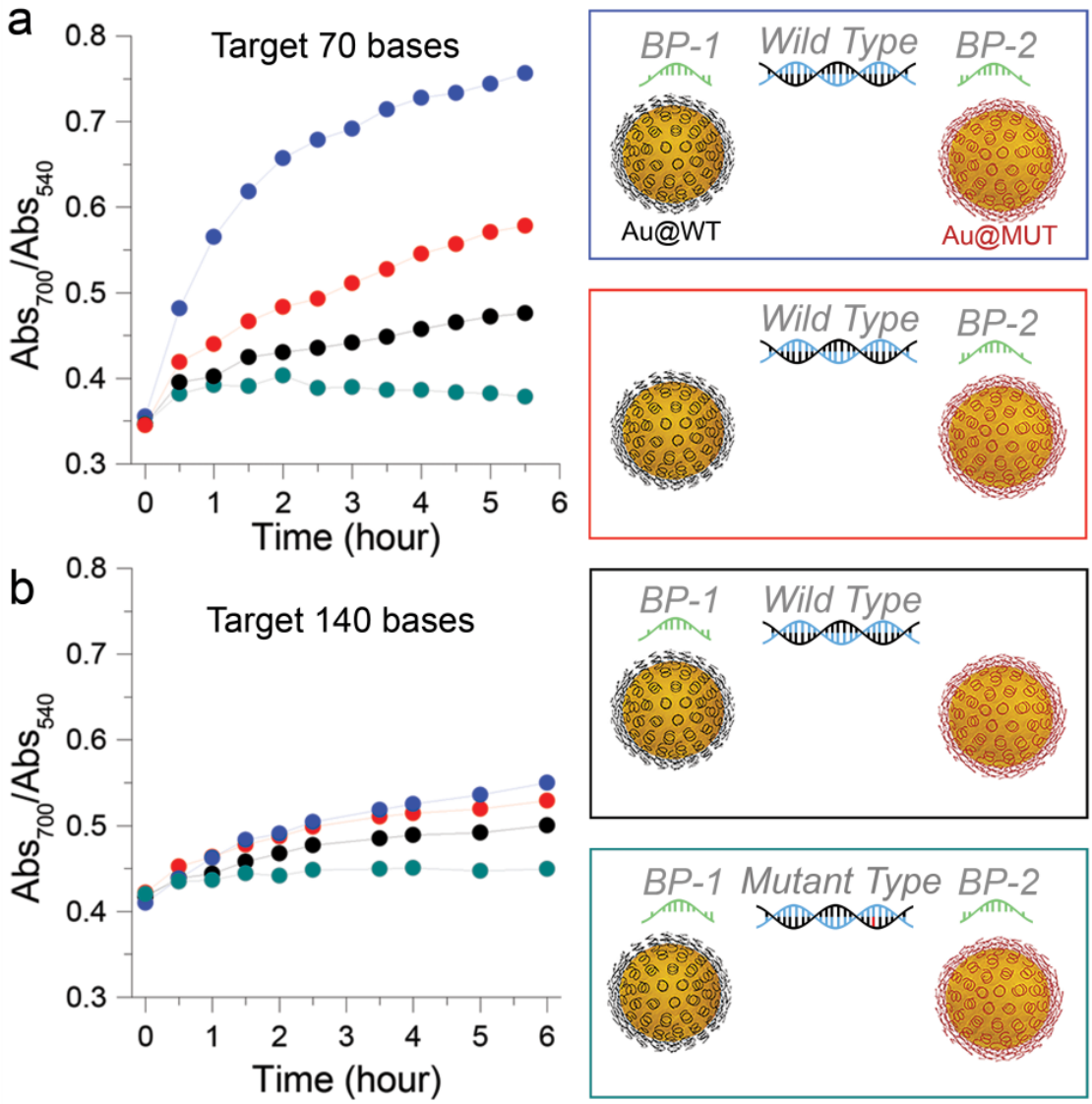

Figure 4.7. Kinetic study for different blocking strategies (two-BPs, only BP2, only BP1), for dsDNA match and mismatch analyte of a) 70 bases and b) 140 bases. In both cases, blocking probes and target concentrations were kept constant (5 nM).

Interestingly, BP2 exhibited better blocking performance than BP1, which can be explained by the high GC content in BP1 (72%), as compared to only 42% in BP2. Higher GC content increases the probability of self-dimerization, hindering the association of BP1 with target antisense sequence. Next, blocking strategy was evaluated for a long dsDNA comprising 140 bases (**Figure 4.7b**). As expected, the aggregation rate in the presence of long sequences (140 bases) was less pronounced, which is related to the longer interparticle distance.[20] Nevertheless, the superior performance of the assay involving two blocking probes is related to the fact that these small sequences hinder the nucleation of the complementary strands (sense and antisense). This nucleation process locates the middle of the strands[28] once the temperature drops below T_m, and is hindered due to the presence of blocking probes. The blocked antisense sequence releases the sense sequence, which can then be captured by the AuNPs, leading to selective aggregation, and hence signal transduction.

The performance of the two-blocking probes scenario, in the presence of perfect match sequence (**Figure 4.7** – blue, red and black), was also evaluated the discrimination of a single-base mutation in dsDNA. Indeed, the use of dsDNA carrying a mutation in the sense sequence prevented the aggregation of AuNPs (**Figure 4.7** – teal color). These data confirm that blocking the antisense sequence during thermal treatment allows for the selective aggregation of AuNPs, with the possibility of discriminating mutations in long sequences of clinical relevance. Importantly, simple naked-eye inspection allowed to differentiate between match and mismatch sequences. While the sample containing the perfect match turned purple, the sample containing the mismatch sequence retained the initial red color (data not shown).

A control experiment was carried out to confirm the need for using a BP. A typical experiment involved the use of no blocking probes, i.e. using a mixture containing Au@MUT and Au@WT, as well as dsDNA analyte carrying either perfect match or mismatch antisense sequences (**Figure 4.8**). Thermal treatment of the mixture (no BPs) caused more pronounced AuNPs aggregation in the presence of the

match sequences (70 or 140 bases), as compared to the mismatch sequence. In fact, the magnitude of the aggregation in the presence of match sequence was comparable to that in the presence of one blocking probe (BP2). Such a selective aggregation of AuNPs in the absence of BP is likely due to competitive interactions between sense-antisense and sense-capture probe during the cooling process. Although the capture probes have limited mobility (grafted on AuNPs surface), their population is ~4-fold higher than the antisense sequence. Note that the overall concentration of the capture probes is ~19 nM, while the sense sequence is only 5 nM. Thus, the kinetic effect might determine the selective aggregation of AuNPs in the absence of BPs.

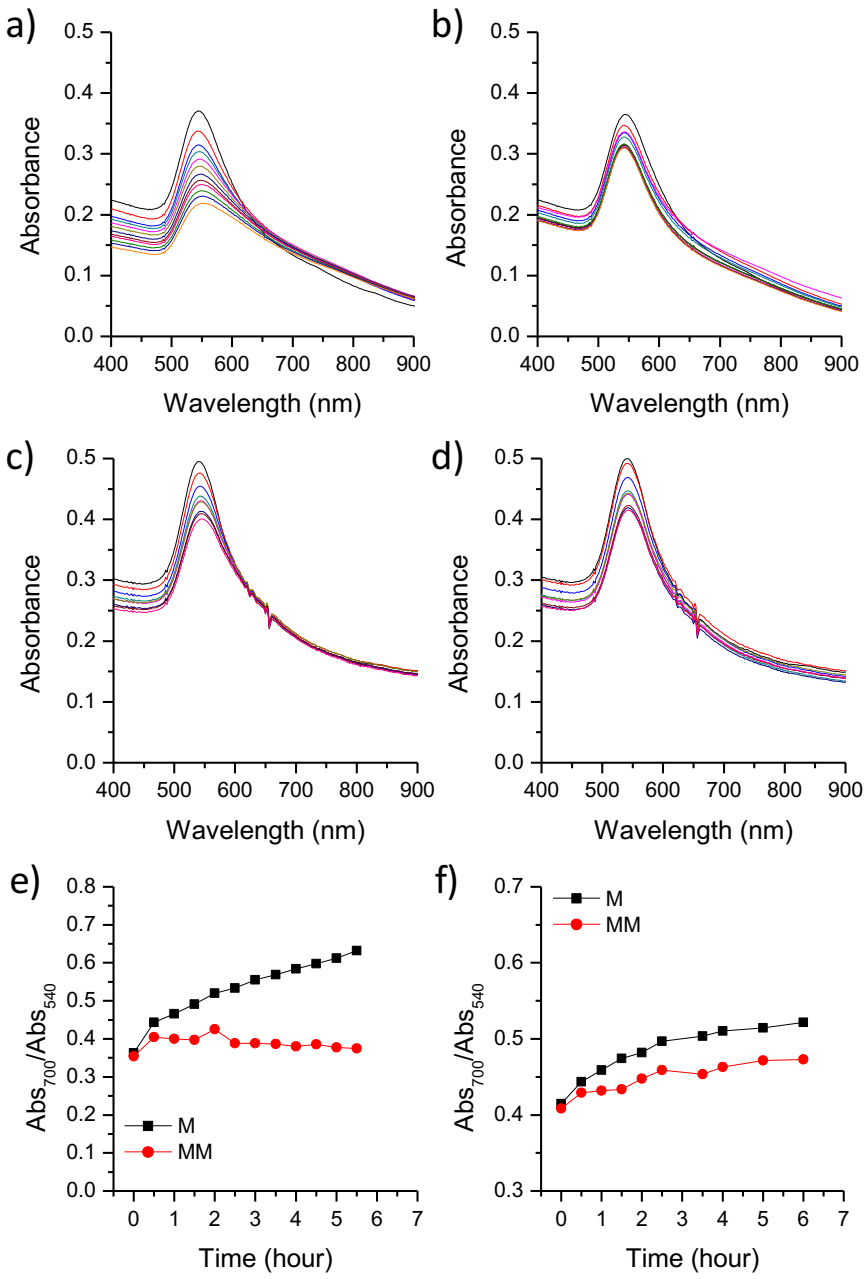

Figure 4.8. UV-Vis spectra for the detection of dsDNA a-b) 70 and c-d) 140 bases without blocking probes as control experiments, for match (a and c) and mismatch (b and d) sequences. Kinetic study for the detection of dsDNA e) 70 and f) 140 bases without blocking probes as control experiments.

Thermal treatment was equally important as the use of BP. In another control experiment, it was demonstrated that keeping the mixture at room temperature did

not affect the optical properties and therefore the performance of the assay (**Figure 4.9**). Therefore, these experiments show that combination of thermal treatment and the two-BPs system is required to discriminate SNP in dsDNA with high selectivity.

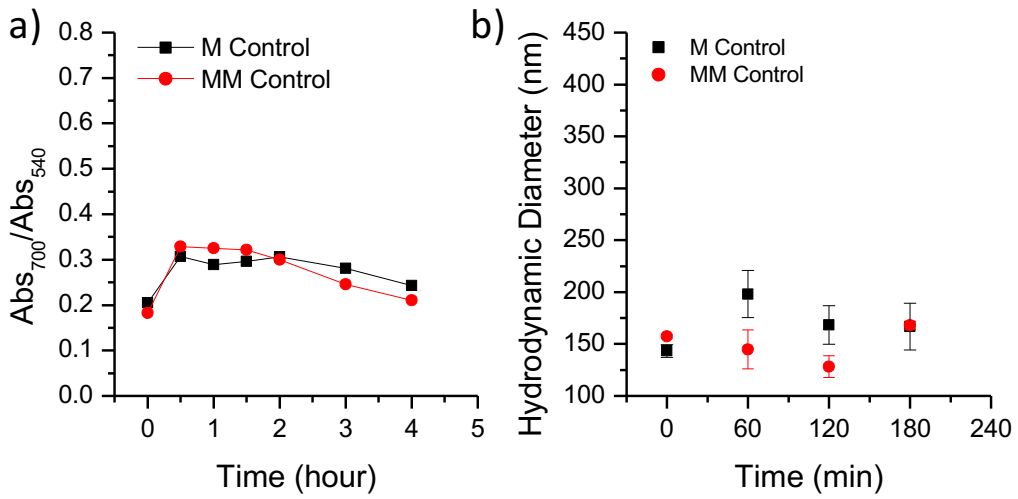

Figure 4.9. a) Aggregation degree of the control experiment without thermal treatment and without blocking probes. b) DLS characterization of the control experiment without thermal treatment and without blocking probes. M: match, MM: mismatch.

To further confirm the preferential aggregation of AuNPs in the presence of mismatch sequence, the assays comprising either two-BPs or no BPs was subjected toward the time-dependent dynamic light scattering measurements. Even when blocking probes were used, the AuNPs did not aggregate in the presence of dsDNA containing a single point mutation (**Figure 4.10 – red line**). On the contrary, for the dsDNA analyte with a perfect match, gradual aggregation was observed over a measurement time of 4 hours. (**Figure 10 – black line**). As expected, the presence of two blocking probes in the assay allowed for more pronounced clustering (400 nm), as compared to the assay with no blocking probe, for which clusters were limited to 300 nm in diameter (**Figure 4.10**).

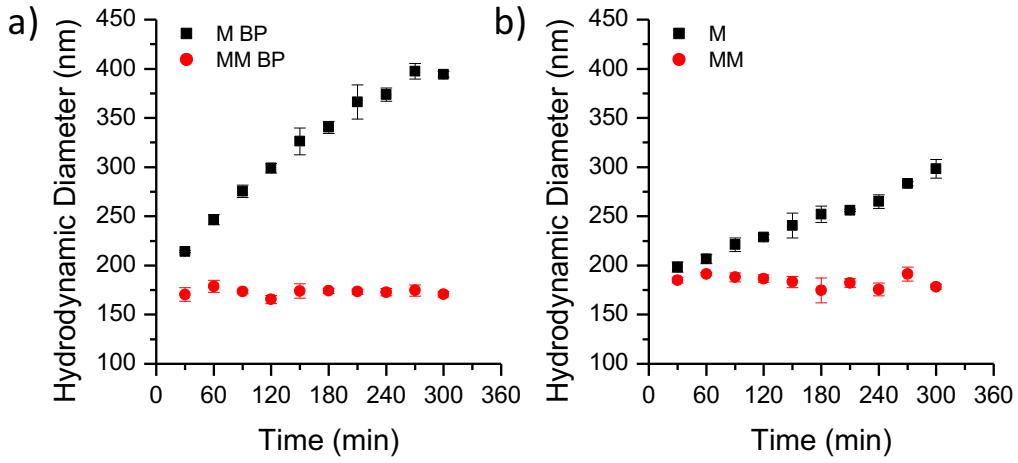

Figure 4.10. DLS monitoring of the aggregation process in the presence of match and mismatch sequence of 70 bases a) with BP1 and BP2 and b) without BP.

To bring assay closer to real-world conditions, the discrimination of SNP in a binary mixture of the match and mismatch dsDNA was evaluated by varying the relative target molar ratio and keeping constant its total concentration at 5 nM (**Figure 4.11).** These experiments limited to the use of sequence containing 70 bases. When increasing the concentration of mismatch dsDNA (from 0 to 5 nM), the aggregation rate was found to decrease, suggesting that the assay retains specificity toward single-base mutation in the binary mixture (**Figure 4.11**). Naked-eye inspection confirmed such trend (**Figure 4.11**). In the presence of 100% match dsDNA, the solution turned purple, accompanied by precipitation at extended times. With a gradual increase of the mismatch concentration, the solution preserved the initial color, showing that tiny changes of mismatch concentration affect the overall optical response.

Detailed analysis of the aggregation rate revealed a nearly linear relationship between R@4h and [Mismatch] in the binary mixture, over the entire range of analyte concentration (**Figure 4.11d**). However, differentiation of the mismatch at concentrations <1 nM, which corresponds to <20% of total dsDNA amount, was rather poor (**Figure 4.11d, red area, and Figure 4.12)**. (Note, that in a real sample the mismatch sequence constitutes <1% of the total cfDNA).

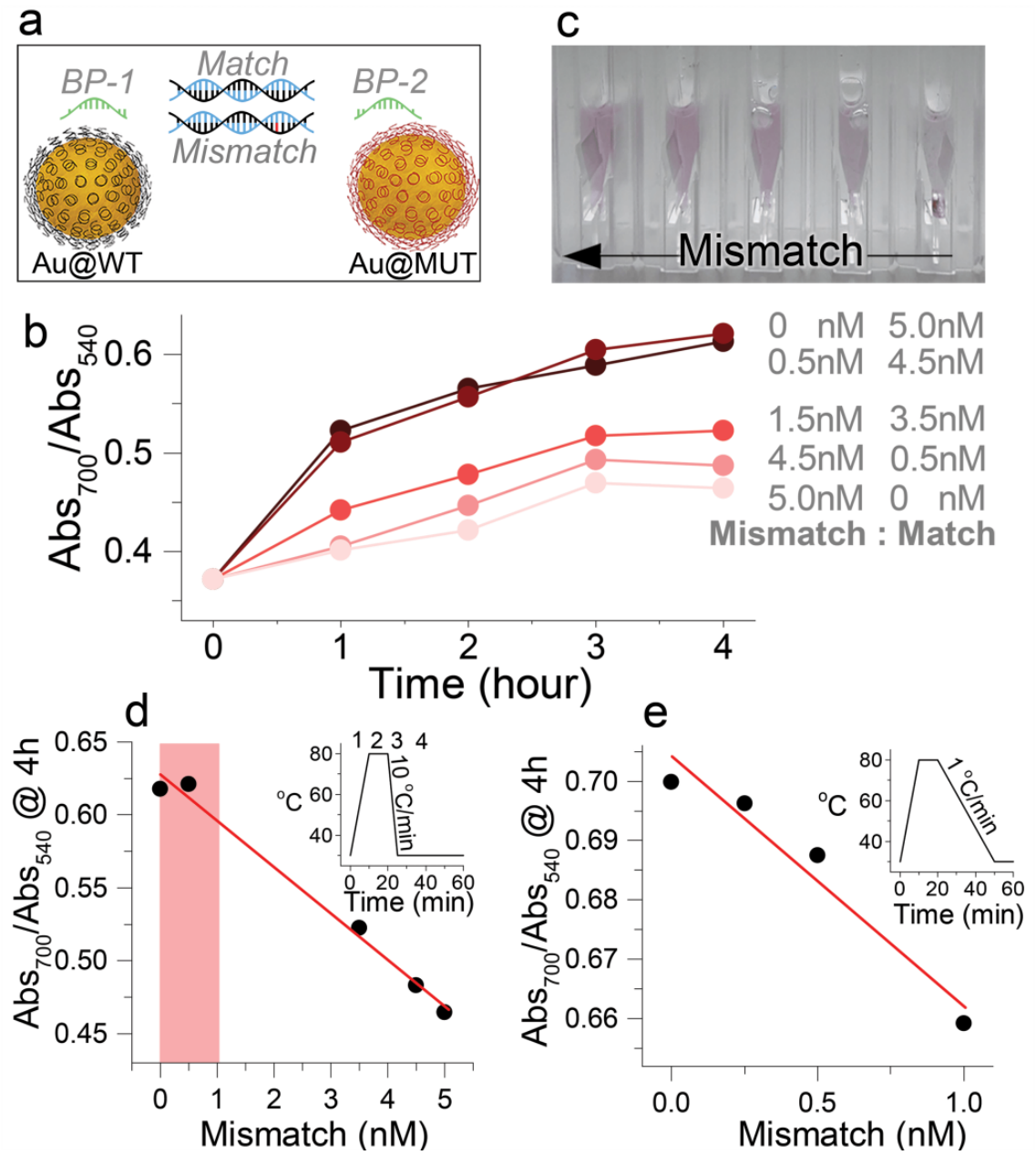

Figure 4.11. Differentiation of SNP in the binary mixture of match and mismatch dsDNA. a) Composition of the starting mixture. b) Time-dependent AuNPs aggregation at different mismatch:match molar ratios. c) Digital image of the corresponding solutions. d) Aggregation degree at 4h vs. mismatch concentration; the red solid line is a linear fit. Inset: temperature profile in the detection experiments with a cooling rate of 1 ºC/min. The numbers indicate different stages of the thermal cycle: 1 – heating up, 2 – annealing at 80 ºC, 3- cooling down, 4 – UV-Vis measurements at room temperature. e) Aggregation degree at mismatch concentrations below 1 nM (red area in d). Inset: temperature profile in the detection experiments Corresponding Author with cooling rate of 10 ºC/min.

The poor differentiation at low mismatch content was presumably related to the fast cooling process once thermal annealing is completed. In all experiments, the mixtures were cooled at a rate of 10 ºC/min prior to UV-Vis monitoring (**Figure 4.11d – inset**). In recent work by Mirkin and coworkers it has been showed that at a slow cooling rate the aggregation of Au@DNA is thermodynamically driven, thus favoring stable conformations by avoiding kinetically frozen states.[29,30] Following this reasoning, it is expected to assume that by avoiding kinetic traps at a slow cooling rate, the ssDNA sense sequence can bridge efficiently adjacent AuNPs, thereby improving the differentiation of SNP. To evaluate such statement, a series of differentiation experiments were performed in which the cooling rate was slowed down to 1 ºC/min and the range of mismatch concentration was kept constant, below 1 nM (**Figure 4.11e**). Importantly, during the cooling state, the solutions were left undisturbed, and UV-Vis monitoring commenced once the mixtures reached room temperature. As shown in **Figure 4.11e**, with increasing the relative amount of mismatch sequence in the assay, the aggregation rate gradually increased, suggesting an improved differentiation between match and mismatch sequences.

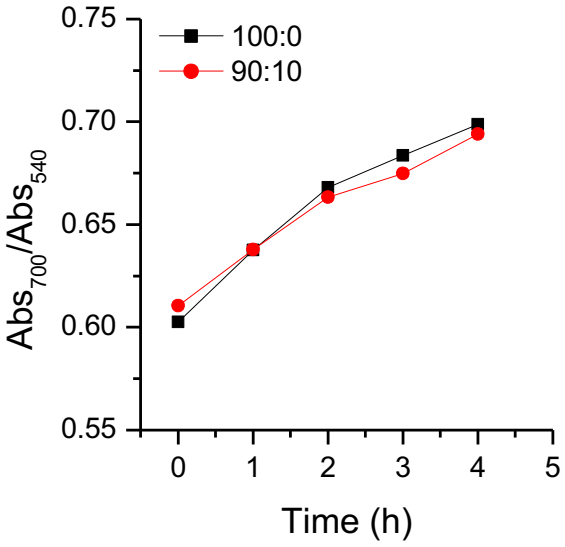

Figure 4.12. Aggregation degree for 2 different binary mixtures after a fast decrease of temperature.

4.4 Conclusions

This Chapter dealt with a plasmon-assisted colorimetric assay for discrimination of SNP in binary mixtures of dsDNA. Studied strategy involved the combination of heat-induced denaturation of the mixture and blockage of analyte reannealing using short sequences (blocking probes), to facilitate selective AuNPs aggregation. It was showed that the use of two blocking sequences was necessary to prevent reannealing of complementary DNA sequences after thermal treatment. With this methodology, it was possible to detect mutation in double-stranded DNA sequences up to 140 bases. Additionally, the selectivity of 5% toward SNP in the binary mixture (wild type and mutated dsDNA) was obtained at a slow cooling rate (1^{o} C/min), thereby favoring the thermodynamically most stable conformation.

4.5 References

(1) Mandel, P.; Metais, P. Les Acides Nucleiques Du Plasma Sanguin Chez L'homme. *C. R. Seances Soc. Biol. Fil.* **1948**, *142* (3–4), 241–243.

(2) Vasioukhin, V.; Anker, P.; Maurice, P.; Lyautey, J.; Lederrey, C.; Stroun, M. Point Mutations of the N-Ras Gene in the Blood Plasma DNA of Patients with Myelodysplastic Syndrome or Acute Myelogenous Leukaemia. *Br. J. Haematol.* **1994**, *86* (4), 774–779.

(3) Stroun, M.; Anker, P.; Maurice, P.; Lyautey, J.; Lederrey, C.; Beljanski, M. Neoplastic Characteristics of the DNA Found in the Plasma of Cancer Patients. *Oncology* **1989**, *46* (5), 318–322.

(4) Chan, K. C. A.; Jiang, P.; Zheng, Y. W. L.; Liao, G. J. W.; Sun, H.; Wong, J.; Siu, S. S. N.; Chan, W. C.; Chan, S. L.; Chan, A. T. C.; Lai, P. B. S.; Chiu, R. W. K.; Lo, Y. M. D. Cancer Genome Scanning in Plasma: Detection of Tumor-Associated Copy Number Aberrations, Single-Nucleotide Variants, and Tumoral Heterogeneity by Massively Parallel Sequencing. *Clin. Chem.* **2013**, *59* (1), 211–224.

(5) Yung, T. K. F.; Chan, K. C. A.; Mok, T. S. K.; Tong, J.; To, K.-F.; Lo, Y. M. D. Single-Molecule Detection of Epidermal Growth Factor Receptor Mutations in Plasma by Microfluidics Digital PCR in Non-Small Cell Lung Cancer Patients. *Clin. Cancer Res. Off. J. Am. Assoc. Cancer Res.* **2009**, *15* (6), 2076–2084.

(6) Diehl, F.; Li, M.; Dressman, D.; He, Y.; Shen, D.; Szabo, S.; Diaz, L. A.; Goodman, S. N.; David, K. A.; Juhl, H.; Kinzler, K. W.; Vogelstein, B. Detection and Quantification of Mutations in the Plasma of Patients with Colorectal Tumors. *Proc. Natl. Acad. Sci. U. S. A.* **2005**, *102* (45), 16368–16373.

(7) Qiu, M.; Wang, J.; Xu, Y.; Ding, X.; Li, M.; Jiang, F.; Xu, L.; Yin, R. Circulating Tumor DNA Is Effective for the Detection of EGFR Mutation in Non–Small Cell Lung Cancer: A Meta-Analysis. *Cancer Epidemiol. Prev. Biomark.* **2015**, *24* (1), 206–212.

(8) Freidin, M. B.; Freydina, D. V.; Leung, M.; Fernandez, A. M.; Nicholson, A. G.; Lim, E. Circulating Tumor DNA Outperforms Circulating Tumor Cells for KRAS Mutation Detection in Thoracic Malignancies. *Clin. Chem.* **2015**, *61* (10), 1299–1304.

(9) Chan, K. C. A.; Jiang, P.; Chan, C. W. M.; Sun, K.; Wong, J.; Hui, E. P.; Chan, S. L.; Chan, W. C.; Hui, D. S. C.; Ng, S. S. M.; Chan, H. L. Y.; Wong, C. S. C.; Ma, B. B. Y.; Chan, A. T. C.; Lai, P. B. S.; Sun, H.; Chiu, R. W. K.; Lo, Y. M. D. Noninvasive Detection of Cancer-Associated Genome-Wide Hypomethylation and Copy Number Aberrations by

Plasma DNA Bisulfite Sequencing. *Proc. Natl. Acad. Sci.* **2013**, *110* (47), 18761–18768.

(10) Balgkouranidou, I.; Chimonidou, M.; Milaki, G.; Tsarouxa, E. G.; Kakolyris, S.; Welch, D. R.; Georgoulias, V.; Lianidou, E. S. Breast Cancer Metastasis Suppressor-1 Promoter Methylation in Cell-Free DNA Provides Prognostic Information in Non-Small Cell Lung Cancer. *Br. J. Cancer* **2014**, *110* (8), 2054–2062.

(11) Wang, X.; Lim, H. J.; Son, A. Characterization of Denaturation and Renaturation of DNA for DNA Hybridization. *Environ. Health Toxicol.* **2014**, *29*.

(12) Grzelczak, M.; Pérez-Juste, J.; Mulvaney, P.; Liz-Marzán, L. M. Shape Control in Gold Nanoparticle Synthesis. *Chem. Soc. Rev.* **2008**, *37* (9), 1783–1791.

(13) Nath, N.; Chilkoti, A. A Colorimetric Gold Nanoparticle Sensor To Interrogate Biomolecular Interactions in Real Time on a Surface. *Anal. Chem.* **2002**, *74* (3), 504–509.

(14) Xue, C.; Li, Z.; Mirkin, C. A. Large-Scale Assembly of Single-Crystal Silver Nanoprism Monolayers. *Small* **2005**, *1* (5), 513–516.

(15) Kelley, S. O.; Mirkin, C. A.; Walt, D. R.; Ismagilov, R. F.; Toner, M.; Sargent, E. H. Advancing the Speed, Sensitivity and Accuracy of Biomolecular Detection Using Multi-Length-Scale Engineering. *Nat. Nanotechnol.* **2014**, *9* (12), 969–980.

(16) Minunni, M.; Mannelli, I.; Spiriti, M. M.; Tombelli, S.; Mascini, M. Detection of Highly Repeated Sequences in Non-Amplified Genomic DNA by Bulk Acoustic Wave (BAW) Affinity Biosensor. *Anal. Chim. Acta* **2004**, *526* (1), 19–25.

(17) Das, J.; Ivanov, I.; Montermini, L.; Rak, J.; Sargent, E. H.; Kelley, S. O. An Electrochemical Clamp Assay for Direct, Rapid Analysis of Circulating Nucleic Acids in Serum. *Nat. Chem.* **2015**, *7* (7), 569–575.

(18) Das, J.; Ivanov, I.; Sargent, E. H.; Kelley, S. O. DNA Clutch Probes for Circulating Tumor DNA Analysis. *J. Am. Chem. Soc.* **2016**, *138* (34), 11009–11016.

(19) Sanromán-Iglesias, M.; Lawrie, C. H.; Schäfer, T.; Grzelczak, M.; Liz-Marzán, L. M. Sensitivity Limit of Nanoparticle Biosensors in the Discrimination of Single Nucleotide Polymorphism. *ACS Sens.* **2016**, *1* (9), 1110–1116.

(20) Sanromán-Iglesias, M.; Lawrie, C. H.; Liz-Marzán, L. M.; Grzelczak, M. Nanoparticle-Based Discrimination of Single-Nucleotide Polymorphism in Long DNA Sequences. *Bioconjug. Chem.* **2017**, *28* (4), 903–906.

(21) Bastús, N. G.; Comenge, J.; Puntes, V. Kinetically Controlled Seeded Growth Synthesis of Citrate-Stabilized Gold Nanoparticles of up to 200 Nm: Size Focusing

versus Ostwald Ripening. *Langmuir* **2011**, *27* (17), 11098–11105.

(22) Hurst, S. J.; Lytton-Jean, A. K. R.; Mirkin, C. A. Maximizing DNA Loading on a Range of Gold Nanoparticle Sizes. *Anal. Chem.* **2006**, *78* (24), 8313–8318.

(23) Scarabelli, L.; Grzelczak, M.; Liz-Marzán, L. M. Tuning Gold Nanorod Synthesis through Prereduction with Salicylic Acid. *Chem. Mater.* **2013**, *25* (21), 4232–4238.

(24) Liu, Y.; Liu, Y.; Mernaugh, R. L.; Zeng, X. Single Chain Fragment Variable Recombinant Antibody Functionalized Gold Nanoparticles for a Highly Sensitive Colorimetric Immunoassay. *Biosens. Bioelectron.* **2009**, *24* (9), 2853–2857.

(25) Sharma, S. V.; Bell, D. W.; Settleman, J.; Haber, D. A. Epidermal Growth Factor Receptor Mutations in Lung Cancer. *Nat. Rev. Cancer* **2007**, *7* (3), 169–181.

(26) Sato, K.; Hosokawa, K.; Maeda, M. Rapid Aggregation of Gold Nanoparticles Induced by Non-Cross-Linking DNA Hybridization. *J. Am. Chem. Soc.* **2003**, *125* (27), 8102–8103.

(27) Akiyama, Y.; Shikagawa, H.; Kanayama, N.; Takarada, T.; Maeda, M. DNA Dangling-End-Induced Colloidal Stabilization of Gold Nanoparticles for Colorimetric Single-Nucleotide Polymorphism Genotyping. *Chem. – Eur. J.* **2014**, *20* (52), 17420–17425.

(28) Sedighi, A.; Li, P. C. H.; Pekcevik, I. C.; Gates, B. D. A Proposed Mechanism of the Influence of Gold Nanoparticles on DNA Hybridization. *ACS Nano* **2014**, *8* (7), 6765–6777.

(29) Auyeung, E.; Li, T. I. N. G.; Senesi, A. J.; Schmucker, A. L.; Pals, B. C.; de la Cruz, M. O.; Mirkin, C. A. DNA-Mediated Nanoparticle Crystallization into Wulff Polyhedra. *Nature* **2014**, *505* (7481), 73–77.

(30) Högberg, B.; Liedl, T.; Shih, W. M. Folding DNA Origami from a Double-Stranded Source of Scaffold. *J. Am. Chem. Soc.* **2009**, *131* (26), 9154–9155.

General Conclusions of the Thesis

Altogether this thesis represents a significant advancement in the development of plasmonic biosensors. Gold nanoparticles were successfully implemented for the detection of biomarkers, more precisely single nucleotide polymorphism, considered as relevant biomolecules related with breast and lung cancer.

In each chapter of this thesis, a different goal or parameter has been addressed which are important for the implementation of colorimetric biosensors in the detection of single nucleotide polymorphism. Different advances have been achieved in terms of sensitivity, selectivity and new approaches and strategies have been proposed for the detection of long single stranded DNA and long double-stranded DNA sequences.

Although specific conclusions have been presented along with each of the chapters of this thesis, we present here a compilation of those we consider more relevant, global conclusions of the work.

A) In Chapter 2 the effects of nanoparticle size on the sensitivity and selectivity of a colorimetric detection assay of the BRCA1 mutation were analyzed.
   1. At constant gold concentration and varying particle size, the best sensitivity was obtained when using larger particles of 63 nm. This trend was explained in terms of a higher target-to-particles ratio, as compared to smaller AuNPs.
   2. Using 63 nm particles we could differentiate the match from the mismatch sequences at concentrations down to 10 pM.
   3. Particle size was also found to affect the selectivity of the assay. Larger particles are more selective at lower target concentrations, but less selective at larger target concentrations, which is due to the lower surface curvature increasing the probability of multiple binding events.
   4. The results of our study show that colloidal biosensors based on AuNP aggregation have an intrinsic limitation, related to the number of target molecules per particle.

B) In Chapter 3 the effect of gold nanoparticles-DNA probes in the detection of long DNA sequences related with EGFR mutation was studied.
   1. 63 nm particles functionalized with DNA strands were used to discriminate single-base mutation in long single stranded DNA sequences containing 70 or 140 bases within 1 h.
   2. Preincubation of the target sequence with only one type of Au@DNA facilitated the formation of a sandwich structure upon addition of the second type of Au@DNA and discriminate single-base mutation within 1 h.
   3. Spherical nucleic acids can disturb the secondary structure of long DNA sequences, making feasible the detection of relevant mutations in biological targets.

C) In Chapter 4 a new methodology for the detection of single nucleotide polymorphism related with EGFR gene in double stranded DNA sequences was proposed.

1. Our strategy involved the combination of heat-induced denaturation of the mixture containing dsDNA analyte and blockage of analyte reannealing by the use of short sequences (blocking probes) to facilitate selective aggregation of the nanoparticles.
2. The use of two blocking sequences was necessary to prevent reannealing of complementary DNA sequences after the thermal treatment.
3. With this methodology, it was possible to detect double-stranded DNA sequences up to 140 bases with single nucleotide polymorphism.
4. The discrimination of SNP was also performed in binary mixtures of dsDNA containing different ratios of match and mismatch sequences.
5. The selectivity of the assay toward SNP in the binary mixture was improved by slowing down the rate of the cooling stage (1^{o}C/min), thereby favoring the thermodynamically most stable conformation.

Resumen

Con este resumen se pretende dar una visión global de la presente tesis, exponiendo los principales resultados y conclusiones de cada uno de los diferentes capítulos.

El tema principal de esta tesis se centra en el desarrollo de biosensores plasmónicos basados en la agregación de nanopartículas de oro funcionalizadas con diferentes secuencias de ADN. La aplicación de estos nanomateriales se centrará en la detección de un tipo concreto de biomarcadores, conocidos como polimorfismos de nucleótido único, relacionados con cáncer de pecho y de pulmón.

Además de la fabricación y caracterización de estos materiales a escala nanoscópica, también se ha llevado a cabo un exhaustivo trabajo en cuanto a la funcionalización superficial de las nanopartículas de oro con el fin de obtener la mejor estabilización posible y a la vez conseguir una cinética de detección lo más rápida posible.

El trabajo realizado ha requerido una buena base teórica en cuanto a los procesos relacionados con ADN y su hibridación, así como las propiedades de las diferentes secuencias de ADN tales como su estructura secundaria o sus puntos de fusión en función de la secuencia diseñada en cada estudio.

Además de intentar mejorar ciertos parámetros básicos en un biosensor como la sensibilidad y la selectividad, también se han abordado diferentes objetivos como la detección de largas secuencias de ADN de cadena simple clínicamente relevantes con la implementación de nuevas estrategias, o la detección de largas secuencias de ADN de cadena doble mediante la aplicación de un nuevo método basado en una combinación de tratamiento térmico más la adición de cadenas cortas de ADN.

1. Introducción

El cáncer es una de las principales causas de mortalidad el cual ha provocado aproximadamente unas 8.8 millones de muertes en el año 2015. Su origen está ligado a mutaciones genéticas que se acumulan poco a poco con el paso del tiempo, provocando una serie de procesos responsables de la carcinogeneis. Existen ciertas biomoléculas, denominadas biomarcadores, las cuales llevan información relevante para la diagnosis de cáncer. Un biomarcador se describe como una sustancia o actividad que puedes ser medida y evaluada como indicador de un proceso biológico normal, de un proceso patogénico o de una respuesta farmacológica. Los biomarcadores de cáncer están presentes en tejidos tumorales o serum y engloban una gran cantidad de moléculas como ADN, mARN, enzymas, metabolitos, factores de transcripción y receptores superficiales celulares.

El polimorfismo de nucleótido único (SNP) es una de las formas más comunes de variación genética en el genoma humano. El polimorfismo de nucleótido único es la variación de una sola base en una posición concreta de la secuencia de ADN. Esta variación ocurre con una frecuencia de 1 cada 1000 bases, aproximadamente y a día de hoy se conocen aproximadamente 1.42 millones de modificaciones de este tipo. Las variaciones en secuencias codificantes de los genes puede provocar modificaciones en los aminoácidos correspondientes y por lo tanto modificar la función de la proteína correspondiente. Teniendo esto en mente, los polimorfismos de nucleótido único han emergido como una nueva generación de biomarcadores e indicadores en el campo de diagnosis clínico y prognosis. En el contexto de esta tesis, nos centraremos principalmente en el estudio de dos polimorfismos de nucleótido único, uno relacionado con el cáncer de pulmón y otro relacionado con el cáncer de pecho. Los SNP relacionados con el cáncer de pulmón son considerados actualmente de gran relevancia debido a que el cáncer de pulmón es el que produce más muertes en el mundo. En concreto, la mutación que se estudiará relacionada con el cáncer de pulmón será L858R. Esta mutación aparece con una frecuencia del 43% en los pacientes con cáncer de pulmón relacionado con el receptor de factor de crecimiento epidérmico. Por otro lado nos hemos centrado en el cáncer de pecho ya que es la

principal causa de muerte de mujeres a nivel mundial. En este caso nos centraremos en el biomarcador relacionado con mutaciones en el gen BRCA1.

Por otra parte, las nanopartículas plasmónicas de oro han atraído una gran atención en diferentes campos, como biosensores, imagen, terapia, nanofotónica y catálisis debido a sus propiedades ópticas y electrónicas únicas. Este tipo de nanomaterials pueden exhibir fuertes colores en el rango de lo visible debido a resonancias plasmónicas superficiales localizadas. LSPR), mientras que sus agregados exhiben diferentes propiedades ópticas lineales y no lineales. Por lo que interacciones químicas entre el analito y la superficie de las nanopartículas conduciría a cambios graduales en las propiedades ópticas. Estos cambios podrían ser usados como métodos de detección, permitiendo un análisis cualitativo y en ciertos casos cuantitativo del analito en cuestión. Por lo tanto, los sensors plasmónicos basados en la agregación de nanopartículas ofrecen una detección selectiva, sensible y simple de diferentes tipos de analitos.

En cuanto al estado del arte en este campo, como se expone al final del capítulo 1, la mayoría de los métodos publicados emplean nanopartículas con un diámetro de 13 nm o desarrollan sistemas de detección de secuencias cortas de ADN, las cuales no guardan relación alguna con el escenario real. En este contexto, a lo largo de los siguientes capítulos se expone el desarrollo de un sistema de detección basado en la agregación de nanopartículas de oro de un diámetro de 63 nm las cuales conducen a un límite de detección más bajo. Además de optimizar este parámetro, también se han aplicado diferentes estrategias en la detección de secuencias largas de ADN tanto de cadena simple como doble.

2. Límite de Sensibilidad en Biosensores basados en Nanopartículas en la Discriminación de Polimorfismos de Nucleótido Único

En este capítulo se describe la detección de la mutación de polimorfismo de nucleótido único relacionado con el cáncer de pecho. Además se ha identificado la concentración límite de moléculas de analito necesarias para inducir cambios ópticos en la disolución coloidal, como función del tamaño de nanopartícula empleada. La agregación selectiva de nanopartículas proporciona una detección rápida y sencilla. El número de moléculas de analito disponibles es el factor principal que limita la sensibilidad de este tipo de sensores coloidales. El ratio entre el número de moléculas de analito y el número de nanopartículas es el cual induce la agregación de las partículas y por lo tanto transduce el evento en una señal óptica.

El tamaño de partícula es un factor muy importante a elegir en el diseño de los ensayos de detección ya que influye directamente en la modulación del ratio entre el número de moléculas de analito y el número de nanopartículas, manteniendo en todos los casos siempre la misma concentración de oro metal. Normalmente la elección del tamaño de partícula se omite en el diseño de los ensayos de detección debido a las dificultades en la síntesis y la funcionalización de nanopartículas de tamaños grandes.

En este capítulo se ha realizado un estudio sistemático de nanopartículas de oro de diferentes tamaños (13, 46 y 63 nm). Un aumento de hasta 5 veces en el tamaño de partícula ha conducido a una mejora del límite de detección de hasta 2 órdenes de magnitud: 5, 0.1 y 0.05 nM para partículas con diámetros de 13, 46 y 63 nm, respectivamente. De esta forma es posible detectar SNP hasta una concentración de 10 pM, es decir 11 fmol, en menos de 10 minutos (**Figura 1**).

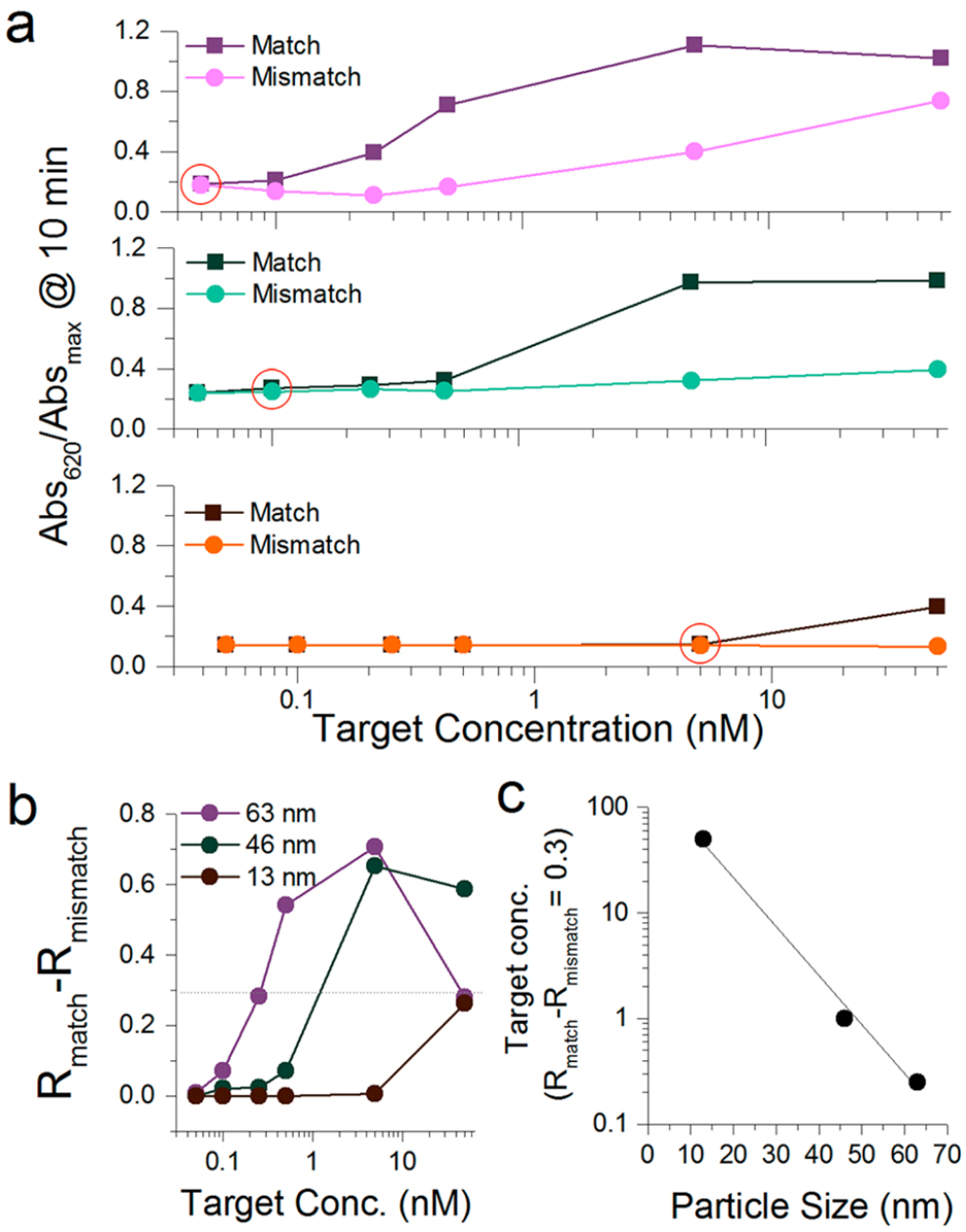

Figura 1. Selectividad entre las secuencias *match* y *mismatch* para diferentes concentraciones de analito, usando diferentes tamaños de AuNPs. a) Diferencias en el grado de agregación (Abs_{620}/Abs_{max}) para los diferentes tamaños de partícula, en un rango de concentración de analito entre 50 y 0.05 nM. Los círculos representan el límite de seletividad (*match/mismatch*) los cuales corresponden a un ratio analito/nanopartícula de 4. b) Diferencias entre los valres de R para *match* y *mismatch vs*. La concentración de analito, mostrando que la selectividad es mejor cuando se emplean partículas con un diámetro mayor. c) Concentración de analito a $R_{match} - R_{mismatch} = 0.3$ *vs* tamaño de partícula; mostrando una dependencia lineal en una escala logarítmica.

3. Discriminación basada en Nanopartículas de Polimorfismo de Nucleótido Único en Secuencias Largas de ADN

Como se discute en el Capítulo 1, las moléculas de ADN circulante y la detección de cáncer asociada a mutaciones mediante la realización de biopsias líquidas promete revolucionar la detección de cáncer. La principal dificultad, sin embargo, reside en la longitud de los fragmentos de ADN circulante que es aproximadamente de 140 bases. Debido a su longitud, normalmente tienen unas estructuras secundarias complejas las cuales pueden impedir la detección efectiva de estos analitos.

Este capítulo muestra un ensayo basado en nanopartículas de oro las cuales permiten discriminar polimorfismos de nucleótido único en secuencias clínicamente relevantes de 70 y 140 bases. El paso previo de preincubación con un solo tipo de nanopartículas es de crucial importancia ya que permite la hibridación secuencial entre Au@ADN y el analito (**Figura 2**), pudiendo diferenciar de esta forma el analito sano del analito con la mutación hasta una concentración de 100 pM.

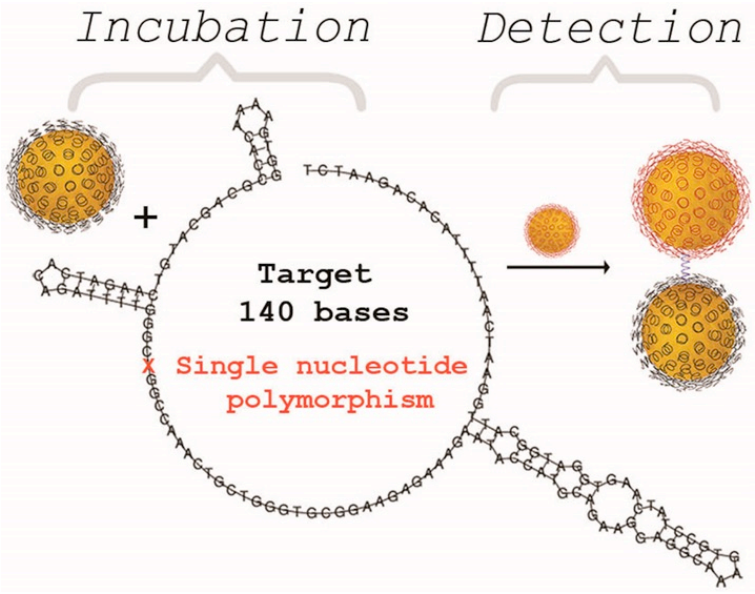

Figura 2. Descripción general del proceso de detección basado en un paso previo de preincubación entre el analito y uno de los tipos de nanopartículas funcionalizadas con ADN, y el posterior paso de adición del otro tipo de nanopartículas funcionalizadas, permitiendo la detección selectiva del analito.

4. Estrategia de Bloqueo para la Detección Colorimétrica de Polimorfismo de Nucleótido Único en Secuencias Largas de ADN de Doble Cadena

Como se menciona en capítulos anteriores, la rápida detección de mutaciones de nucleótido único en ADN circulante es de gran importancia en el campo clínico. Sin embargo, la especificidad en la detección es uno de los desafíos más grandes en el ámbito de la detección ya que la secuencia con la mutación representa una fracción muy pequeña (<1%) en comparación con la secuencia sin la mutación. Además de esto, el empleo de técnicas basadas en hibridación requiere la separación de la doble cadena de ADN en ADN de cadena simple.

En el presente capítulo, se propone un ensayo sin ningún tipo de amplificación en la detección de polimorfismo de nucleótido único en mezclas binarias de ADN de cadena doble de secuencias con y sin mutación mediante la agregación de nanopartículas de oro como transductores de señal del proceso de hibridación.

El método de detección se basa en la combinación de la desnaturalización térmica de la doble cadena de ADN y una estrategia de bloqueo selectivo de las cadenas desnaturalizadas, haciendo de este modo una detección más específica (**Figura 3**). De esta forma es posible discriminar polimorfismos de nucleótido único en ADN de cadena doble con hasta una total de 140 bases. Además, también ha sipo posible diferenciar un 5% de la secuencia con la mutación en mezclas binarias de ADN con 70 bases de longitud.

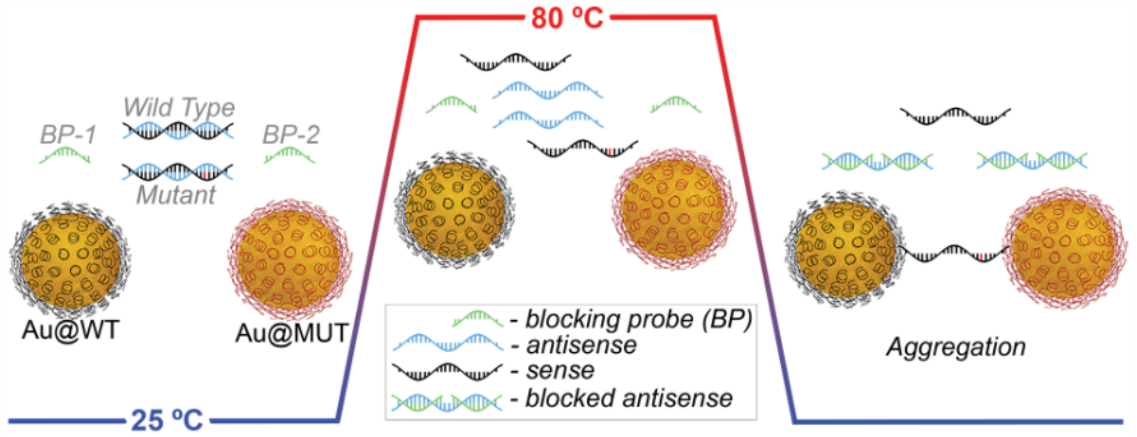

Figura 3. Esquema de la estrategia de detección. La disolución inicial (izquierda) contiene ambos tipos de nanopartículas, las secuencias cortas de bloqueo y ambos analitos de cadena doble con y sin la mutación. Esta solución es calentada durante 10 minutos a 80ºC (centro), seguido por un proceso de enfriamiento y lectura de la señal producida (derecha). Las secuencias cortas de bloqueo se unen a la secuencia *antisense* previniendo la rehibridación tras el proceso de enfriamiento. El analito que permanece como ADN de cadena simple tras el tratamiento térmico es reconocido por las secuencias de ADN en la superficie de las nanopartículas produciendo una agregación selectiva de las nanopartículas de oro debido a la presencia de la mutación.

List of Publications

The work described in this dissertation has given rise to the following publications:

Chapter 1: **Sanromán-Iglesias, M**.; Liz-Marzán, L. M.; Grzelczak, M. *Single Nucleotide Detection on Colloidal Nanoparticles*. (*in preparation*)

Chapter 2: **Sanromán-Iglesias, M**.; Lawrie, C. H.; Schäfer, T.; Grzelczak, M.; Liz-Marzán, L. M. *Sensitivity Limit of Nanoparticle Biosensors in the Discrimination of Single Nucleotide Polymorphism*. ACS Sens. **2016**, 1 (9), 1110–1116.

Chapter 3: **Sanromán-Iglesias, M**.; Lawrie, C. H.; Liz-Marzán, L. M.; Grzelczak, M. *Nanoparticle-Based Discrimination of Single-Nucleotide Polymorphism in Long DNA Sequences*. Bioconjug. Chem.**2017**, *28* (4), 903–906.

Chapter 4: **Sanromán-Iglesias, M**.; Lawrie, C. H.; Liz-Marzán, L. M.; Grzelczak, M. *Blocking Strategy for the Colorimetric Detection of Single Nucleotide Polymorphism in Long Double-Stranded DNA Sequences*. ACS Sensors **2017**, *submitted*.

Aboudzadeh, M. Ali.; **Sanromán-Iglesias, M**.; Lawrie, C. H.; Grzelczak, M.; Liz-Marzán, L. M.; T. Schäfer. *Enhancement of Detection of Single Nucleotide DNA Mutations by Short Blocking Probes: a Comparative Study in Solution and on the Surface.* Nanoscale **2017**, *accepted*.

Acknowledgments

En primer lugar quiero darles las gracias a mis directores de tesis, Marek Grzelczak y Luis M. Liz Marzán, por estos 3 años y por haberme dado la oportunidad de hacer esta tesis. A Marek por los ánimos que me has dado a lo largo de toda la tesis, por esas largas charlas y conversaciones sobre trabajo y sobre cualquier cosa que hiciera falta, por haber estado ahí cuando realmente lo necesitaba, y por los ánimos a empezar en el mundo del *running*. A Luis por haberme abierto las puertas hace 4 años a una experiencia como esta, de venir a Donostia y formar parte de un grupo tan increíble como este; además de haberme comprendido y entendido en los momentos que más me hacía falta. Gracias por estos años que me han enseñado tanto.

Obviamente, no me olvidaré nunca de toda la gente del laboratorio, de esos compañeros del día a día que han pasado a ser mi familia y que espero que lo sigan siendo por muchos años más. Susana, Eric, Isa, Ada, Dorleta, Ana, Javi, Rafaela, Marta, Jatish, Malou, Jesús, Ali, Christoph, Karolina, Judith, Malte, Ana Belén, Denis, Leo, Andrea, Marc, Guille, Juanjo, y a los que han pasado por el laboratorio, en especial a los *italianinis* Lucio y Gregorio por todos los buenos momentos y al alemán más fiestero que he conocido nunca, Stefan, sabes que nos quedan muchas fiestas pendientes en Hamburgo. Nunca os podré agradecer lo suficiente vuestro cariño. Mención especial merece Ada, creo que no podría explicarte lo importante que has sido y que eres para mí. Sé que hoy no estaría donde estoy si no fuera por ti. Siempre has estado ahí para escucharme, ayudarme, consolarme y darme infinidad de consejos; además de aguantar mis días malos y algún que otro enfado. Sencillamente … *Eskerrik asko* ¡!. Siempre vas a poder contar conmigo para lo que necesites. Rafaela … pan pipasssss ¡! xDDD ,,, gracias por todos los momentos y las largas conversaciones. Porque las 10 y las 13 en punto siempre serán nuestras horas de descanso. Gracias también por esas noches de fiesta y la ruta de bares por Donostia; además de la compañía en nuestra ruta por Bizkaia. Mucho ánimo en tu doctorado ¡! eres una de las personas más trabajadoras que he conocido así que no dejes que nadie te haga sentir lo contrario. Y ya sabes… al volver a Manchester a seguir manteniendo las buenas

costumbres de aquí. Ana, graciñas polas longas conversas no labo, polo apoio que sempre me deches en todo momento e sobre todo por ser coma unha nai que sempre preocupase por min, nunca che podrei agradecer o suficiente aquela conversa co meu pai. Grazas a ti hoxe estou onde estou. Además, no me quiero olvidar de mis compañeros de despacho: Unai, Mari Pili, Silvia, Susana, Ángel, Anabel … gracias por todos los buenos momentos, y por esos desayunos *fit*, Unai. Chunga, no creas que me olvido de ti, gracias por todas las risas que nos hemos echado juntas y por esos gifs de cabras. Al resto de gente de CIC biomaGUNE, gracias por hacer que mis años aquí hayan sido tan agradables.

A mi *kuadrilla Altafitera*, por descubrirme una Donostia que no conocía. Gracias a vosotras apareció la luz al final del túnel. Ainara y Argia, mis dos pilares más importantes, no os hacéis una idea de lo mucho que os quiero *nenisssss*. Al resto de gente también agradeceros los buenos momentos. Edu, el mejor *mendizale* y fotógrafo que he conocido; siempre serás importante para mí, quieras o no; y siempre estaré ahí para lo que necesites, quieras o no. Por hacerme entender un poco mejor lo de *Carpe diem* y por ayudarme a quererme un poco más, seguiré trabajando en ello. Al barraquero chachuno, señor Juan GurruCHaga, no olvidaré los picos de pan, esas llamadas a la 1 de la mañana, las noches de fiesta, esas horas y horas de conversaciones filosóficas, la montaña suiza, el kosmikar, … por ser el golpe de realidad que necesitaba, por ser *un mal que me hace bien… eta euskera ikasten laguntzeagatik.*

A mis amigas de toda la vida, las incondicionales de siempre, las que nunca me han fallado. Gracias de todo corazón. Natalia, Eva, Saray, Marta, Noemi, Paula … siempre presentes allá donde vaya. Mis compañeros de UVigo pero ante todo amigos: Rake, Juan, Silvia, Ana, Paula, Marta… 5 años que no olvidaré nunca.

A mis padres, para vosotros no hay palabras suficientes. *Maite zaituztet*! Siento todo lo que os he hecho pasar. Siento cada km y cada viaje que habeis hecho por mi culpa. Todo os lo debo a vosotros.

Eskerrik asko !!